IMPACT OF Nrf2 SIGNALING ON THIOL HOMEOSTASIS AND RENAL PHYSIOLOGY

by

Soma Jobbágy

B.S., University of Delaware, 2012

Submitted to the Graduate Faculty of

The University of Pittsburgh School of Medicine

in partial fulfillment of the requirements for the degree of

Doctor of Philosophy

In

Molecular Pharmacology

University of Pittsburgh

2018

UNIVERSITY OF PITTSBURGH

SCHOOL OF MEDICINE

This dissertation was presented

by

Soma Jobbágy

It was defended on

June 11, 2018

and approved by

Committee Chair: Thomas W. Kensler, PhD, Professor, Pharmacology & Chemical Biology

Bruce A. Freeman, PhD, Irwin Fridovich Distinguished Professor and Chair, Pharmacology & Chemical Biology

Bennet Van Houten, PhD, Professor, Pharmacology & Chemical Biology

Roderick J. Tan, MD PhD, Assistant Porfessor, Department of Medicine Renal-Electrolyte Division

Dissertation Advisor:

Francisco J. Schopfer, PhD MBA, Associate Professor, Pharmacology & Chemical Biology

IMPACT OF Nrf2 SIGNALING ON THIOL HOMEOSTASIS AND RENAL PHYSIOLOGY

Soma Jobbágy, B.S.

University of Pittsburgh, 2018

Cells evolved robust homeostatic mechanisms to protect against oxidation or alkylation by electrophilic species. Antioxidant signaling responses under control of the Kelch ECH associating protein 1 (Keap1)/nuclear factor erythroid 2-related factor 2(Nrf2) transcription factor were studied.

Glutathione (GSH) is the most abundant intracellular thiol and acts as the chief intracellular reduction-oxidation couple through oxidation to glutathione disulfide (GSSG) and subsequent enzymatic reduction back to GSH by glutathione reductase (GR). The fundamental effects of electrophilic Nrf2 activators on the GSH/GSSG antioxidant couple were studied in RAW264.7 macrophages. Electrophiles increased intracellular GSH through Nrf2-dependent transcription of GSH biosynthetic enzymes, yet paradoxically reduced the ratio of GSH to GSSG, which is commonly used as an index of oxidative stress.

GSH was found to regulate GR activity via product inhibition in an oxidative stress-independent manner, as determined by biochemistry studies, cell biology experiments, and kinetic modeling approaches. Additionally, inhibition of GR by electrophilic nitrated fatty acid (NO_2-FA) by covalent modification of Cys61 at the catalytic site was observed. Together, these results demonstrate that electrophiles differentially modulate the GSH/GSSG couple through two independent mechanisms, and electrophile-mediated increases in GSSG promote S-glutathionylation of cellular proteins.

Pharmacologic activators of Nrf2 are in preclinical and clinical development for treatment of a broad spectrum of renal disorders. To characterize the effects of this pathway on renal physiology a murine model of pharmacomimetic Nrf2 activation and primary human renal cortical epithelial cells in culture were studied. Nrf2 signaling was found to be constitutively high in the proximal tubule of the nephron and inducible in the distal convoluted tubule and collecting duct. Hyperactivation of Nrf2 was found to protect against polydipsia in lithium-induced nephrogenic diabetes insipidus (Li-NDI) without improving the urine concentrating defect due to down-regulation of aquaporin 2 (Aqp2). Nitric oxide-independent changes in vascular tone were observed in isolated resistance arteries as well as in conscious ambulatory animals. These effects were attributed to Nrf2-dependent downregulation of the vasodilatory autocoids prostacyclin and kynurenine. Together these findings suggest that Nrf2 protects against Li-NDI through alteration of tubuloglomerular feedback, and may offer a novel therapeutic approach for treatment of this condition.

TABLE OF CONTENTS

LIST OF TABLES

LIST OF FIGURES

PREFACE

Dedicated to friends and family who have supported me along this adventure.

1.0 INTRODUCTION

1.1 CELLULAR OXIDATIVE STRESS

Life in an oxidizing world began ~3 billion years ago with the evolution of photosynthetic prokaryotes, which oxygenated the atmosphere(1). Aerobic eukaryotes evolved to exploit chemical energy stored in carbon-carbon bonds, harnessing molecular oxygen as the terminal electron acceptor for mitochondrial electron transport. While controlled oxidation is a metabolic necessity for all aerobic organisms, the properties which make oxygen a favorable terminal electron acceptor, namely high electronegativity and large positive standard reduction potential, create unique challenges through off-target oxidation of cellular constituents by partially reduced oxygen species. Oxidation of cellular macromolecules can lead to deleterious loss- or gain-of function and compromise viability. Numerous complementary mechanisms have developed to maintain a reducing intracellular milieu and prevent oxidative damage. These mechanisms include low-molecular weight redox buffers, enzyme-catalyzed detoxification of reactive species, enzyme-mediated reduction of oxidized cellular macromolecules, and genetic programs that sense and respond to changes in oxidant exposure. The redox-sensitive thiol proteome translates oxidizing or alkylating signals into specific transcriptional responses, which are discussed in detail in the following sections.

1.2 KEAP1/NRF2 SIGNALING

1.2.1 The Redox-Sensitive Thiol Proteome

The redox-sensitive thiol proteome has evolved as a mechanism by which cells (1) detoxify ROS, (2) set in motion diverse compensatory programs, and (3) sense and respond to the metabolic and inflammatory status at the cellular, tissue, and organism level(2). The Kelch ECH associating protein 1 (Keap1) / nuclear factor erythroid 2-related factor 2 (NF2L2; Nrf2) complex is the chief apparatus which senses oxidizing or alkylating signals and translates them into cytoprotective signaling responses(3).

1.2.2 Nrf2

Nrf2 is basic leucine zipper (bZIP) transcription factor consisting of 605AA (human) or 597AA (mouse). Despite a predicted molecular weight of 68kDa, on electrophoresis the protein is detected at a 95-110kDa(4) due to the abundance of basic amino acids comprising the leucine zipper. The human and mouse proteins are 80.9% homologous. Nrf2 has 6 conserved functional Nrf2−ECH homology (Neh) domains, Neh1-7 (5–9). Neh1 contains the basic leucine zipper which mediates dimerization with small Maf chaperone proteins and facilitates DNA binding. Neh2 contains ETGE and DLG motifs, which are binding sites for the Nrf2 repressor Keap1. Hydrophilic lysine residues in Neh2 are the targets of Keap1/ Cullin 3 (Cul3)–RING (really interesting new gene)-box protein 1 (Rbx1) mediated ubiquitinylation(10). Neh3 is a C-terminal region that interacts with the helicase necessary for unwinding target DNA(11). Neh4-5 are transactivation domains located in the middle of the sequence. Neh6 is a degron required for removal of Nrf2 after

it has fulfilled its function in the nucleus. In concert with small musculoaponeurotic fibrosarcoma (Maf) proteins, nuclear Nrf2 binds to the antioxidant response element (ARE) as a dimer and induces transcription of specific target genes. Nrf2 is responsible for maintenance of redox homeostasis or phase II detoxification. Canonical Nrf2 targets include phase II enzymes responsible for detoxification such as heme oxygenase 1 (HO-1) and NAD(P)H-quinone dehydrogenase 1 (NQO1), xenobiotic exporters including multidrug resistance-associated protein (MRP) family members, and glutathione biosynthesis including cysteine import and catalytic and modulatory subunits of the rate limiting gamma-glutamyl-cysteinyl ligase (GCLC/GCLM) (12–18). A complete tabular summary of the genes positively regulated by Nrf2 in mouse and human is provided by Hayes *et al*(9).

1.2.3 Keap1

The broad spectrum of cytoprotective genetic programs initiated by Nrf2 likely makes its activation energetically expensive, and provides strong impetus for existence of an effective repressor system. Under non-stressed conditions Nrf2 is sequestered to the cytosol by Keap1 and targeted for rapid Cul3-Rbx1-mediated ubiquitin tagging and subsequent proteosomal degradation. In the presence of Keap1, the half-life of Nrf2 is approximately 20 min(19). The functional importance of Keap1 is validated by seminal studies showing that its genetic ablation result in Nrf2 hyperactivation in mouse and human cells(20, 21). Keap1 is a Broad complex, Tramtrack, and Bric-à-brac (BTB)-Kelch protein that functions as a dimer(10). The crystal structure of the Keap1 Kelch domain was recently solved, revealing a hexameric β-propeller(22). Binding of the Keap1 Kelch propeller to the Nrf2 Neh2 ETGE site occurs with high specificity and is followed sequentially by binding of the DLG (low-affinity) motifs of Nrf2. This process results in the Keap1

dimer shifting from an “open” to a “closed” conformation and promotes Cul3-Rbx1 association with the complex. The end result is sequestration of Nrf2 to the cytosol via interaction of the complex with actin cytoskeleton and ubiquitylation followed by proteosomal degradation of Nrf2(23). Human and mouse Keap1 have 27 and 25 cysteine residues, respectively, and these Cys residues are sensitive to oxidation and/or alkylation. Post-translational modification at Cys151, Cys273, or Cys288 play an important role in Nrf2 activation(24). Oxidation or alkylation of Keap1 cysteine residues stabilize the Keap1/Nrf2 protein complex, sequestering Keap1 and allowing newly synthesized Nrf2 to accumulate and translocate to the nucleus to activate transcription of hundreds of cytoprotective genes(3, 25, 26).

1.2.4 Murine models of genetic inhibition or activation of Nrf2

1.2.4.1 Knockout of Nrf2 inhibits antioxidant responses and sensitizes animals to tissue injury

To evaluate the physiologic significance of Keap1/Nrf2 signaling, several murine models have been developed. Knock-out of Nrf2 has been used to study the function of cytoprotective mechanisms under control of the ARE. Initial characterization of $Nrf2^{-/-}$ mice found them to be viable and showed no defects in erythropoiesis or development (27), however upon exposure to oxidative challenge in the form of dietary butylated hydroxyanisole, these animals demonstrated reduced Nrf2 target gene expression as compared to control mice(28). Further studies as well as our unpublished observations confirm reduced constitutive expression of phase 2 and cytoprotective enzymes under ARE control(29). Knockout of both Nrf1 and Nrf2 results in early embryonic lethality in mice and extensive oxidative stress with elevated ROS in cells(30).

Surprisingly, knockout of Nrf1 alone, but not Nrf2 alone, also results in embryonic lethality suggesting that Nrf2 is not functionally required but acts as a fine-tuning mechanism.

Multiple disease models reveal exacerbated pathology in $Nrf2^{-/-}$ mice. Aged $Nrf2^{-/-}$ mice display anemia with abnormal red cell morphology, splenomegaly, elevation of circulating immunoglobulins (Ig) and reduction in total serum GSH(31). Female $Nrf2^{-/-}$ mice developed symptoms of lupus nephritis as a consequence of aging, with vascular deposits of IgG, IgM, and complement C3 (32). Clinically, Nrf2 polymorphism predisposes to lupus nephritis in humans(33). Knockout of Nrf2 has also been shown to accelerate renal injury in models of streptozotocin-induced diabetes(34, 35). In a murine model of hepatic ischemia/reperfusion injury, $Nrf2^{-/-}$ mice displayed more severe liver pathology than wild-type counterparts (36). In experimental models of sepsis, Nrf2 was found to exacerbate endotoxin- and cecal puncture-induced septic shock(37). Ablation of Nrf2 sensitizes animals to DNA damage and chemical carcinogenesis(38, 39). Nrf2 has also been found to play a role in carcinogenesis and cancer chemoprevention, as reviewed in detail by Yu and Kensler(40).

1.2.4.2 Genetic ablation of Keap1 hyperactivates Nrf2 and provides tissue protection

Complete knockout of Keap1 causes post-natal lethality due to esophageal keratosis resulting in severe malnutrition(20). $Keap1^{flox/-}$ mice have hypomorphic expression of Keap1 and show Nrf2 activation without lethality, and are protected against acetaminophen (APAP) hepatotoxicity(41) as well as concanavalin A induced T cell-mediated acute liver injury(42) . Consistent with increased I/R injury in $Nrf2^{-/-}$ kidneys, I/R injury in a model of orthotopic liver transplant was reduced when donor livers had hepatocyte-specific knockout of Keap1(43). Keap1 inhibition reduces glomerulosclerosis in a NEP25/immunotoxin model(44) as well as tubular damage in an ischemia reperfusion model(45). Significantly, hyperactivation of Nrf2 in Keap1

hypomorphic mice also reduced adverse renal remodeling and fibrosis occurring 10 days after acute ischemic or obstructive injury(46). Until recently, studies of Keap1 knockout and hypomorphic animals focused on tissue protection in setting of disease processes characterized by oxidative stress. These important studies supported the preclinical development of pharmacologic Nrf2 activators.

1.2.4.3 Nrf2 hyperactivation may have deleterious renal effects

Genetic manipulation of the Keap1/Nrf2 signaling pathway has uncovered physiologic in addition to therapeutic effects. Mice with constitutive Nrf2 activation due to kidney epithelium-specific or whole-animal Keap1 knock-out displayed polyuria, hyposthenuria, and hydronephrosis(47, 48). While mechanistic insights remain sparse, in these studies Nrf2 hyperactivation appears to impair renal water reabsorption through down-regulation of Aqp2 at baseline, and abolish upregulation in response to vasopressin signaling. Interestingly, mice with kidney epithelium-specific deficiency in the E3 ubiquitin ligase Cullin 3 (Cul3) displayed not only hyperkalemic hypertension due to impaired kelch-like 3 (KLHL3)-mediated WNK kinase degradation and consequent hyperactivation of NCC and NKCC2, but also repression of Aqp2 and resultant polyuria (49). De-repression of Nrf2 by pharmacologic or genetic inhibition of the auxiliary Nrf2 chaperone glycogen synthase kinase 3 beta (GSK3β) was likewise found to impair urinary concentrating function after water deprivation or administration of the synthetic vasopressin analog dDAVP(50). These findings suggest that pharmacologic Nrf2 activation may have physiologic effects in addition to antioxidant, anti-inflammatory, and anti-fibrotic properties, and they may complement or synergize with diuretics to reduce circulating volume. However, studies designed to test this hypothesis explicitly have not been carried out.

1.3 ELECTROPHILES

Chemical (ie. non-biologic) therapeutics can be broadly divided into two classes based on mechanism of interaction with their targets. The majority of drug molecules interact with their targets via van der Waals and hydrogen bond interactions in the context of a sterically favorable binding pocket. This view encompasses the classical (albeit now defunct) lock-and-key paradigm postulated by Fisher, as well as the more contemporary idea of induced fit and electrostatic interactions within a conformationally constrained yet subtly mutable binding pocket. By contrast, other compounds can bind covalently to their targets. Electrophile comes from the Latin *electrum*, derived from the Greek *ḗlektron*, the amber resin which accumulates static charge when rubbed, and the Greek *phílos*, meaning dear or beloved. In strictly chemical terms, *electrophiles* are moieties (functional groups or compounds) that are attracted to and accept electrons from donors. The corresponding donors, termed *nucleophiles*, are electron-rich species attracted to centers of positive charge or electronegativity. In this section, the chemical basis of reactivity, endogenous formation, and signaling mechanisms of electrophiles will be discussed.

1.3.1 Electrophiles react with cellular constituents via Michael Addition

Electrophile/nucleophile interactions drive many different types of reactivity. The preferential reactivity of certain compounds can be partially explained by Pearson's qualitative hard/soft acid/base (HSAB) theory(51). In the conceptual framework of HSAB, hard acids and bases are small, have high oxidation states, low polarizability, and have an affinity for ionic bonding. Soft acids and bases by contrast are large, have low oxidation states, are highly polarizable, and preferentially undergo covalent bonding. In Michael addition, soft electrophiles

react with soft nucleophiles: the delocalized charge of alkene pi systems of electrophilic Michael acceptors (eg. α,β-unsaturated carbonyl compounds such as nitroalkenes) renders the β carbon electron-deficient and susceptible to nucleophilic attack by a Michael donor (eg. thiolate anions)(52). The pKa of free cysteine is high (~8.5), indicating that only a low percentage exists as the thiolate anion at physiologic pH (~7.2). However, reactivity can be increased by incorporation into proteins with neighboring basic lysine or arginine residues that stabilize the thiolate and confer selectivity(53). Thiol reactivity is further detailed in section 1.4.1. Soft Michael acceptors are emerging as effective endogenous signaling mediators and a promising category of therapeutic drug candidates due to their ability to engage specific cellular pathways encompassing redox homeostasis and inflammation, including activation of Nrf2. Comparison of pharmacologic and genetic activation of Nrf2 has revealed overlapping yet distinct gene expression profiles(54). Three specific families of these electrophiles, which are relevant to the experimental work performed for this thesis, are described below.

1.3.2 Nitrated fatty acids are endogenous electrophilic alkene derivatives

Nitrated fatty acids (NO_2-FA) are a family of endogenously-produced bioactive electrophiles formed by the nitration of dietary lipids during gastric digestion, or accompanying inflammatory processes(55, 56). Nitrogen dioxide ($^{\bullet}NO_2$) has for decades been known to react with unsaturated fatty acids(57). In biological systems $^{\bullet}NO_2$ is produced via multiple parallel mechanisms including nitric oxide ($^{\bullet}NO$) autooxidation, oxidation of nitrite (NO_2^-), disproportionation of HNO_2, and peroxynitrite ($ONOO^-$) homolysis. Lipids are preferential targets for biological nitration reactions, as $^{\bullet}NO$ and O_2 partition into hydrophobic lipid-containing membranes, resulting in a membrane-lens effect(58). Conjugated fatty acids (eg. conjugated

linoleic acid) are the main substrates of lipid nitration reactions, although other polyunsaturated fatty acids may also be nitrated. NO_2-FA are also present in plants and plant oils (eg. olive oil) and thus may be the active compounds conferring health benefits in the Mediterranean diet(59).

The biological activity of NO_2-FA is driven by their soft electrophilic nature. The -NO_2 functional group is the strongest electron-withdrawing moiety in biological systems. In unsaturated FA such as nitrated conjugated linoleic acid (NO_2-cLA), charge delocalizes across one or multiple pi-systems, rendering β or δ carbons with respect to the NO_2 electrophilic and targets for Michael addition. These properties make NO_2-FA activators of Nrf2 signaling through reaction with specific Keap1 cysteines. The reactivity and signaling activities of NO_2-FA are discussed in the following section.

Nitrated fatty acids have been identified *in vivo* in rodents (55, 60–62), and dietary supplementation with the substrates ^{15}N-labeled nitrite and conjugated linoleic acid (cLA) have been shown to increase formation of the $^{15}NO_2$-FA NO_2-cLA above basal levels(56, 63). In plasma from healthy humans, NO_2-FA are detected as free and esterified forms. Early studies suggested plasma levels of 1-500nM(64–67) however further study after with technical advances in the field has suggested that the actual values are closer to ~1nM for NO_2-oleic acid(68) and 1-3nM for NO_2-cLA(56, 63). NO_2-cLA formation can be increased to ~10nM by administration of the FA substrate conjugated linoleic acid (cLA) and nitrite/nitrate(63).

Excretion of electrophilic NO_2-FA is strikingly different from elimination of the parent fatty acid or non-electrophilic NO_2-FA. Fatty acids in plasma bind to albumin and fatty-acid binding proteins through hydrophobic and van der Waals interactions, and as such are not filtered at the glomerulus. By contrast, electrophilic NO_2-FA are capable of forming reversible covalent Michael adducts with low-molecular weight thiols such as GSH, N-acetylcysteine and cysteine,

yielding compounds that are significantly more hydrophilic than the parent fatty acid. Electrophilic NO_2-FA cysteine adducts, β-oxidation products, and derived dicarboxylates are detected in the urine of healthy human volunteers(63, 69, 70). It is not definitively known whether urinary NO_2-FA, its conjugates, and its metabolites are derived primarily from filtration or tubular secretion. However, other oxidized lipid mediators such as leukotrienes and prostaglandins are secreted into the tubular lumen as hydrophilic conjugates following Phase II metabolism(71, 72). These results suggest that NO_2-FA and NO_2-FA adducts may reach target cells in the kidney either from the apical or basolateral aspects.

1.3.2.1 Nitro-oleic acid

Nitro-oleic acid (NO_2-OA) is a promising therapeutic NO_2-FA consisting of an 18-carbon oleic acid nitrated at the 9 or 10 position. Like other NO_2-FA, NO_2-OA post-translationally modifies protein thiols through reversible Michael addition, exerting potent effects in diverse disease models(55, 73–77). While the precise mechanism of action remains unknown, NO_2-OA exerts anti-inflammatory actions by reducing LPS-induced pro-inflammatory cytokine secretion and tumor necrosis factor-α (TNF-α)-stimulated leukocyte margination and extravasation(60, 78). Recently, NO_2-OA was also found to inhibit LPS-TLR-4 induced leukocyte recruitment to vascular endothelium and downstream NF-kB driven inflammation(75, 79). In addition to its anti-inflammatory effects, NO_2-OA engages cytoprotective cellular mechanisms via activation of Nrf2. At the molecular level, specific NO_2-OA binding to Cys273/288 of the Nrf2-binding partner Keap1 via Michael addition stabilizes the Nrf2-Keap1 interaction, thus bypassing proteosomal degradation of Nrf2 and inducing transcription of antioxidant genes(80–83).

1.3.3 Triterpenoid electrophiles: targeted drug design meets traditional Chinese medicine

Oleanolic acid, a member of the saponin family of compounds which also encompasses cholesterol and phytosterols, has been used in traditional Chinese medicine(84). Electrophilic synthetic triterpenoid derivatives of oleanolic acid CDDO (2-cyano-3,12-dioxooleana-1,9(11)-dien-28-oic acid) and CDDO-imidazolide (1-[2-cyano-3-,12-dioxooleana-1,9(11)-dien-28-oyl]imidazole) were first synthesized and characterized as potent inhibitors of nitric oxide production, and found to also have anti-inflammatory and anti-proliferative effects (85, 86). At low micromolar concentrations, CDDO-Im was demonstrated to be thiol-reactive, depleting the mitochondrial GSH pool to induce apoptosis in a pancreatic cancer cell model (87). Surprisingly, potent induction of Nrf2/ARE signaling was a later discovery, but was demonstrated to be mediated by specific interaction between Nrf2 and the ARE, as mutation of the ARE prevented target gene activation(88). CDDO compounds are soft electrophile and react with Keap1 Cys151 in the BTB domain to inhibit recruitment of Cul3(89). Models of genetic Nrf2 activation caused by hypomorphism of Keap1 may be considered pharmacomimetic models for the CDDO-family of compounds. However differences in gene expression profiles do exist between genetic and CDDO-induced activation, likely due to pleiotropic effects of CDDO derivatives on other pathways including heat shock proteins, NFkB, and others(54, 90). CDDO and its derivatives have been studied in numerous chronic disease models, based on the premise that upregulation of Nrf2 activity may protect healthy cells from oxidative injury. In fact, the methyl ester CDDO-Me (trade name Bardoxolone) rapidly progressed from preclinical to clinical development for treatment of chronic kidney disease (CKD), as increases in glomerular filtration rate (GFR) were observed in rodent models(91). Clinical trials revealed increases in GFR in stage 4 CKD patients, but also unexpected increase in mortality due to adverse cardiovascular events, halting the trials (92–95).

Recently, a new clinical trial is investigating the efficacy of the drug in Alport syndrome, a genetic basement membrane disorder causing CKD in childhood or early adolescence (NIH ClinicalTrials.gov identifier NCT03019185).

1.3.4 Fumaric acid esters as therapeutic electrophiles

Fumarate, a simple four-carbon monounsaturated dicarboxylic acid, is a key intermediate of the citric acid cycle. In 1959, the German chemist W. Schwekendiek, who suffered from the dermatological disease psoriasis vulgaris, hypothesized that the disease was the result of disturbances in the citric acid cycle. Specifically, Schwekendiek believed that psoriasis was caused by depletion of fumarate, and undertook lengthy self-experimentation with fumaric acid and its derivatives. While fumaric acid had poor oral bioavailability and significant gastrointestinal side effects, empirical testing led him to discover that an orally-taken mixture of mono- and di-methyl fumaric acid esters (FAEs) demonstrated striking clinical efficacy(96). Schwekendiek's psoriasis cleared, and the mixture of mono- and dimethyl fumarate became the most commonly used systemic treatment for psoriasis in Germany. Strikingly, this drug was prepared exclusively by compounding pharmacies, without formal clinical evaluation, regulatory approval or a commercial pharmaceutical formulation. In 1994, a proprietary mixture of FAEs (Fumaderm®) was developed by the company Fumapharm AG and approved by the German FDA for treatment of moderate to severe plaque psoriasis. Fumaderm consists of dimethylfumarate, as well as methyl- and ethyl fumarate as salts of divalent cations (Ca^{++}, Zn^{++}, Mg^{++}). Esterases in the intestinal brush border metabolize the dimethyl-ester to monomethyl fumarate (MMF), the active metabolite which is identified in the plasma. Interestingly, despite the significant amounts of DMF administered, reaching into the hundreds of milligrams/day, only MMF can be identified in the plasma. As a

putative explanation, it has been shown that intestinal cells metabolize DMF to MMF completely, with only MMF found on the basolateral side(97).

In 2013, the U.S. Food and Drug Administration approved Tecfidera®, a proprietary formulation of dimethyl fumarate, for the treatment of relapsing remitting multiple sclerosis(98, 99). While the mechanism of Tecfidera is not precisely known, like other electrophiles it is thought to be pleiotropic, with complimentary components of immune modulation and Nrf2 activation through binding of Keap1 Cys151(100–102).

1.3.5 Signaling actions of electrophiles

1.3.5.1 Keap1/Nrf2

The mechanism by which Keap1 Cys residues react with endogenous and exogenous electrophiles, and the signaling cascade initiated by these interactions, were discussed in section 1.2. While an overabundance of reactive electrophilic species can cause damage, specific engagement of Keap1 at carefully titrated doses provides an opportunity to provide protection against a range of disorders through preconditioning(103).

1.3.5.2 NF-κB

In addition to engagement of Nrf2 signaling, diverse electrophiles including those discussed in this section have been observed to have potent anti-inflammatory effects. These effects are in part understood to be mediated by electrophile inhibition of nuclear factor kappa-light-chain-enhancer of activated B cells (NFκB) signaling. NF-κB is a transcription factor complex which controls expression of pro-inflammatory genes involved in cytokine, chemokine, and adhesion factor production(104, 105). The NF-kB family consists of 5 proteins sharing a Rel

homology domain(106), which form homo- and heterodimers. Phosphorylation of the inhibitor IkB by IkB kinase (IKK) leads to its proteolytic degradation and liberation of the NFkB p50/p65 dimer, allowing for nuclear translocation and target gene transcription. IkBα is an NF-kB target gene that serves as a negative feedback loop, suppressing NF-kB activity(104). NF-kB is known to be directly inhibited by electrophiles through covalent modification of the p65 subunit (107–109). However, this field is complicated by direct cross-talk between the Nrf2 and NF-kB signaling pathways(110).

1.4 THE GLUTATHIONE SYSTEM

1.4.1 Biological Scope and Significance of Thiols

The role of thiol chemistry in protecting against oxidative stress is underscored by the increased prevalence of cysteine (Cys) in organisms exposed to harsh environmental conditions, such as thermophiles(111). Many significant biological discoveries in the last hundred years have foundations in thiol chemistry, as underscored by the prevalent use of oxidizing agents such as iodine, alkylating agents including iodoacetamide or n-ethylmaleimide (NEM), reducing agents such as β-mercaptoethanol (BME), and thiol indicators such as Ellman's reagent (5,5′-dithiobis(2-nitrobenzoic acid), DTNB) in basic research and clinical chemistry alike(112).

Cys is one of the least abundant amino acids in proteins, and is underrepresented in the genome(113). Nonetheless, it contributes significantly to protein activity as a catalytic nucleophile in proteases, phosphatases, reductases, and other classes of enzymes. Cys is a non-essential amino acid, as it can be biosynthesized from the less-reactive thioether methionine. Cys is the only thiol-

containing amino acid, and its function is closely tied to the chemical properties of the thiolate anion $R\text{-}S^-$. The pKA of Cys sulfhydryl is relatively high (~8.5), indicating that 50% exists as the deprotonated thiolate at pH 8.5. From the Henderson-Hasselbach equation, it is apparent that under intracellular conditions of pH 7.2, only ~5% of solvent-exposed Cys is deprotonated. Due to the reactivity of the thiolate, however, most Cys residues are buried inside hydrophobic pockets to minimize solvent exposure. In fact, based on the localization of the majority of Cys residues, the (incorrect) conclusion of Cys hydrophobicity could be reached. The appearance of Cys in solvent-protected locations is instead likely due to strong evolutionary pressure favoring the minimization of indiscriminate thiol reactivity. In fact, burial of Cys within specialized protein structures affords specificity of reaction, as adjacent residues as well as intramolecular dipoles fine-tune the pKa of Cys to increase reactivity with desired substrates(114, 115).

Cys residues are highly conserved at regulatory, catalytic, or binding sites, indicating their functional importance(116). As the only amino acid containing a free thiol, replacement of Cys with any other amino acid would necessarily ablate any function based on thiol chemistry. Indeed, Cys conservation displays bimodal distribution, with >90% conservation at sites with known or postulated Cys function, and <10% conservation at degenerate sites containing “accidental” or non-essential Cys (117). Cys residues are also known to display clustering, suggesting that intramolecular reaction of Cys adjacent in sequence or in 3-dimensional structure may be biologically important(117). Indeed, many proteins which catalyze reduction-oxidation reactions use paired internal Cys which cycle between inter- and intra-molecular disulfides.

1.4.2 Glutathione

Glutathione (GSH) is the tripeptide γ-L-Glutamyl-L-cysteinylglycine and is the most abundant intracellular thiol. GSH was discovered first in 1888 by the French physician-scientist J. de Rey-Pailhade, using yeast extracts, and named philothion. It was rediscovered in the 1930s by F.G. Hopkins and received its current name, glutathione(112, 118). GSH acts as the chief intracellular reduction-oxidation (redox) couple by participating in enzymatic or non-enzymatic oxidation to glutathione disulfide (GSSG) and subsequent reduction back to GSH by glutathione reductase (GR). Although the pKa of the GSH Cys thiol is relatively high (8.94-9.42) (119, 120) suggesting low reactivity under cellular conditions, its redox buffering capacity stems from highly efficient synthesis, enzyme-catalyzed transfer and recycling pathways, as well as mass-action afforded by high intracellular concentrations. The intracellular concentration of GSH is accepted to be variable based on cell type but a commonly accepted value approximately ~10mM(121, 122). Total GSH levels are regulated by the expression of biosynthetic enzymes, with the Nrf2-regulated enzyme gamma-glutamyl-cysteinyl ligase (GCL; EC 6.3.2.2) catalyzing the rate-limiting step (3, 123). Knockout of GCL-catalytic subunit (GCLC) is embryonic lethal, and homozygotes ($GCLC^{+/-}$) demonstrate significant reduction in GSH levels(124). GSH detoxifies reactive species through multiple mechanisms. GSH can directly neutralize reactive oxygen and nitrogen species (ROS, RNS) as well as endogenous and exogenous electrophiles. GSH maintains pools of other chemical antioxidants such as ascorbic acid (vitamin C) and tocopherol (vitamin E), as well as directly reducing 1-Cys peroxiredoxins (Prdx) such as Prdx6, in reactions catalyzed by glutathione-S-transferases. GSH is also used as a cofactor by glutathione peroxidases (Gpx) and glutaredoxins (Grx). Gpx reduce H_2O_2 and lipid peroxides to H_2O and lipid alcohols respectively, using reducing equivalents from GSH. Grx couple with 2-cys Prdx (Prdx1-5) to reduce the peroxidatic cysteine

as the last step of the Prdx catalytic cycle. In addition, GSH and GSSG can both participate in post-translational modification of proteins through enzymatic and non-enzymatic conjugation reactions.

1.4.3 Opposing chemical and genetic effects of electrophiles on GSH

One of the main functions of GSH is detoxification of endogenous and exogenous electrophilic species. The nucleophilic thiolate GS^- can react with electrophiles, and adduction with DMF(125, 126), CDDO(87), and NO_2-OA(83, 127, 128) has been characterized *in vitro* and *in vivo.* However, the net effect of these compounds on intracellular GSH pools is not known, as activation of Nrf2 can both deplete GSH through chemical addition and induce GSH biosynthesis through upregulation of GCLM/GCLC as well as the X_c cysteine importer. The opposing (albeit temporally separated) effects of chemical reactivity and Nrf2 activation suggests that titration of electrophile dose and selectivity of reactivity with Keap1 Cys over GSH are required for prevalence of cytoprotection over GSH depletion.

1.4.4 Glutathione Reductase

Sacrificial oxidation of GSH produces glutathione disulfide (GSSG) which must be eliminated from cells or reduced back to GSH. Glutathione reductase (GR, EC 1.8.1.7) is a disulfide oxidoreductase responsible for reduction of GSSG to GSH (Reviewed (129)). GR was first characterized in wheat germ(130) and soon thereafter in mammalian tissue preparations in a seminal work in the laboratory of Albert Lehninger(131) as an enzyme capable of catalyzing the NADPH-mediated reduction of the GSSG disulfide. The biological significance of GR is underscored by high degree of conservation spanning prokaryota and eukaryota(118, 132). The

GR active site contains an internal disulfide, which undergoes reduction-oxidation cycling via a "ping-pong" or double-displacement mechanism(133): NADPH-mediated reduction of a proximal FAD cofactor is followed by formation of a charge-transfer complex which reduces the internal disulfide bond between Cys61 and Cys66 (S. cerevisiae) or Cys102 and Cys107 (H. sapiens) or Cys80 and Cys85 (M. musculus). The reduction of the disulfide yields a His- stabilized thiol which undergoes disulfide exchange with GSSG, resulting in release of one GSH and a mixed disulfide GS-S-GR. Re-formation of the internal disulfide liberates a second GSH and restores enzyme to the original form.

1.4.5 Glutathione:glutathione disulfide (GSH:GSSG) ratio

The ratio of GSH to GSSG has been widely promoted and extensively used as one of the most important markers of oxidative stress across the entire spectrum of human disease, including metabolic, cardiovascular, neurologic, and neoplastic disorders(134–137). As the most abundant thiol/disulfide pair in the cell, GSH:GSSG has been used as an indicator to quantify "oxidative stress". This concept has been further extended, with application of the Nernst equation to calculate the theoretical reduction potential of the GSH:GSSG couple, and find correlations of half-cell reduction potentials with specific cellular conditions(138). While creating a quantitative framework for the otherwise frequently qualtitative concept of "oxidative stress" is appealing, the limitations of such analyses and the numerous underlying assumptions should be considered with care(139). Specifically, it should be noted that cellular functions dependent on GSH are predominantly enzyme-catalyzed as opposed to thermodynamic equilibria, and have a kinetic dependence on [GSH] and not on $[GSH]^2$ as implied by the Nernst relation. Moreover, these processes, with the exception of S-glutathionylation, are generally independent of [GSSG].

Moreover, the ratio of GSH:GSSG may be considered an accurate reflection of redox state only if the total GSH pool is constant, and biosynthesis, export, and GSH regeneration are minimal.

1.4.1 Peroxiredoxins

Peroxiredoxins (Prdx; EC 1.11.1.15) are a large conserved class of peroxidases which reduce endogenous peroxides to prevent non-specific oxidation of cellular constituents(140). Peroxiredoxins are small (22-27 kDa) proteins and 6 isoforms have been identified in mammals(141). The cytosolic and mitochondrial 2-Cys peroxiredoxins, Prdx1 and 3 respectively, are highly reactive antioxidant enzymes that dimerize upon oxidation by hydrogen peroxide (H_2O_2) or peroxynitrite ($ONOO^-$) ($K \approx 10^5–10^7\ M^{-1}/s^{-1}$) (142–144). Changes in endogenous H_2O_2 levels are reflected by changes in the relative abundance of monomeric vs. dimerized Prdx, and the relative abundances of these speices can be followed by immunoblotting. The peroxidatic cysteine in typical 2-Cys peroxiredoxins can also be hyperoxidized to a $SO_{2/3}$ via a sulfenic acid intermediate(145).

1.5 OXIDATIVE STRESS IN THE KIDNEY

1.5.1 Structure and function of the kidney

Kidneys maintain the composition of extracellular fluid within tight parameters, ensuring that cells are continuously bathed in a solution of appropriate osmolarity, ionic composition, and pH, while minimizing exposure to metabolic and environmental wastes and toxins. This complex

task is achieved by nephrons, the functional units of the kidney. Despite constituting only ~0.5% of body weight, kidneys receive ~25% of cardiac output. Each day about ~180L of fluid are filtered, of which about 99% is reabsorbed to yield 1-2L of concentrated urine, in which metabolic waste and toxins are excreted. Each human kidney contains approximately one million nephrons, and each nephron is comprised of a glomerulus and a renal tubule. The glomerulus is a specialized structure consisting of capillaries and podocytes which act as the filter. The glomerulus performs the actual filtration of blood, after which the filtrate is directed through tubules which refine the composition of what will ultimately become the urine. Afferent arterioles supply the glomerulus with blood from the body, while a dense network of peritubular capillaries arise from the exiting efferent arterioles and surround the renal tubules. The proximal convoluted tubule reabsorbs sugars, amino acids, and the bulk of sodium (60-70%), potassium (65-70%), phosphate (85%), calcium (60-70%), and water (60-70%). The loop of Henle is a specialized structure with permeability to water along the descending limb, and passive and active permeability to salt but not to water in the ascending limb. This structure allows for establishment of an osmotic gradient with deeper interstitial spaces having higher osmolarity, through a mechanism termed the countercurrent multiplier system.

1.5.2 Significance of Keap1/Nrf2 signaling in kidney

The kidney has high energy requirements due to significant active transport mechanisms including Na^+/K^+ ATPases required for movement of solutes against their concentration gradients as well as the processes of detoxification of reactive compounds through conjugation and excretion. Indeed, despite their small size (0.5% body weight) the kidneys consume about 10% of

total oxygen used in cellular respiration. There is thought to be a gradient of glucose availability proceeding from renal cortex inwards, with the inner medulla thought to have relatively low O_2 tension and predominantly anaerobic metabolism(146).

Reactive species are formed continuously during aerobic respiration, and can diffuse from the mitochondria to impact both cytosolic and nuclear contents(147). In this context of high energy use and xenobiotic exposure, it is unsurprising that Keap1/Nrf2 signaling plays an important role in the kidney. Preclinical studies have demonstrated that pharmacologic or genetic activation of Nrf2 can protect against acute and chronic kidney diseases by protecting cells from oxidative injury. Rodent models of CKD have implicated Nrf2 deficiency as an important component of disease etiology(148–150). Mice with constitutive hyperactivation of Nrf2 activity induced by genetic hypomorphism of Keap1 are protected against obstructive and ischemic kidney injury(46). A comprehensive review of preclinical studies utilizing genetic modulation of Keap1/Nrf2 signaling, as well as clinical trials using pharmacologic Nrf2 activators, to protect against acute or chronic kidney injury was recently published by Nezu *et al.* (151). The pharmacologic potential of NO_2-OA in treating kidney disease was recently reviewed(152).

1.5.3 Lithium induced nephrogenic diabetes insipidus

For over 60 years lithium (Li) has been the gold-standard agent for prophylaxis and treatment of bipolar disorder, and has an established history of use for other CNS disorders as well. Complicating its beneficial mood altering properties, lithium exhibits a narrow therapeutic index and may cause cardiovascular, neurological, and renal sequelae(153). Development of nephrogenic diabetes insipidus (NDI) is among the most prevalent side effects of chronic Li administration, with over 50% of patients exhibiting hyposthenuria, and ~20% of patients

developing NDI with overt polyuria(154). Li-induced NDI discourages patient compliance as polydipsia and polyuria reduce quality of life, and in the long term poses more severe iatrogenic risk, as it has been found to increase the prevalence of chronic renal failure(155). Li has been demonstrated in murine models to target the epithelium lining the distal tubule (DT) and collecting duct (CD) of the nephron, where its uptake is mediated by the epithelial sodium channel (ENaC) and where it induces loss-of-function through uncoupling the effects of arginine vasopressin and down-regulating aquaporin 2 (AQP2) (156, 157). Tamoxifen-induced knockout of AQP2 in adult $AQP2^{flox/flox}$ mice has been shown to cause the NDI phenotype(158). These animals have a profound water-wasting phenotype, with polyuria and polydipsia approaching 1mL per gram body weight per day, and are unable to produce concentrated urine in response to water deprivation.

Several recent publications have implicated renal hyperactivation of Keap1/Nrf2 antioxidant signaling in development of NDI. Nrf2 is a basic leucine zipper transcription factor which controls transcriptional responses to oxidative and electrophilic insults through upregulation of cytoprotective gene expression. Under non-stressed conditions, Nrf2 is retained in the cytosol and rapidly targeted for proteasomal degradation by the Keap1/Cullin3 (Cul3) complex. Redox-sensitive cysteine thiols in Keap1 sense cellular exposure to oxidative or electrophilic insults through their propensity for oxidation or alkylation, and these post-translational modifications de-repress of Nrf2 transcriptional activity.

Specifically, genetic knockout of the Nrf2 suppressor Keap1 globally or in the kidney epithelium result in severe NDI with strong downregulation of AQP2(47, 48). Knockdown of the E3 ubiquitin ligase Cul3, which is responsible for regulating both NaCl reabsorption via WNK/SPAK signaling and Nrf2 signaling via Keap1, results not only in hyperkalemic hypertension via de-repression of WNK signaling, but also in nephrogenic diabetes insipidus with

loss of AQP2. In light of recent observations regarding NDI development in mice with genetic disruption of Keap1, ablation of Cul3 likely exerts this effect via concomitant activation of Nrf2(49). Finally, genetic ablation or pharmacologic inhibition of the accessory Nrf2 repressor glycogen synthase kinase 3 beta (GSK3β) down-regulate AQP2(50). The mechanistic link spurring this inquiry comes from *in vitro* observations showing that Li can inhibit GSK3β and consequently de-repress Nrf2(159–162).

2.0 MATERIALS AND METHODS

2.1 REAGENTS

Primary antibodies were purchased from the following suppliers: GR (Abcam, Cambridge, MA), GCLM (Proteintech, Chicago, IL), HO-1 (Cell Signaling, Beverly, MA), GAPDH (Trevigen, Gaithersburg, MD), Peroxiredoxin 1 (R&D Systems, Minneapolis, MN), Peroxiredoxin 3 (R&D Systems, Minneapolis, MN), Peroxiredoxin1-4 $SO_{2/3}$ (Abcam, Cambridge, MA), Anti-GSH (Virogen, Watertown, MA), Cyclooxygenase 1 (Cell Signaling, Beverly, MA), Cyclooxygenase 2 (ab15191 or ab179800, Abcam, Cambridge, MA), ENaC α/β/γ (StressMarq), NCC (Abcam, Cambridge, MA), phospho-NCC (T53; PhosphoSolutions, Aurora, CO) NKCC2 (Cell Signaling, Beverly, MA), Carbonic Anhydrase II (Abcam, Cambridge, MA), Aquaporin 2 (H7661; kind gift of Dr. Robert Fenton, Aarhus University, Denmark). Secondary antibodies were purchased from Santa Cruz Biotechnologies (Dallas, TX). LPS derived from E.coli 0127:B8, purified GR from S. cerevisiae, DMF, MMF, BSO, GSH, GSSG, $^{13}C^{15}N$ GSH was from Sigma-Aldrich (St. Louis, MO). Oleic acid was obtained from Nu-Check Prep, Inc. (Elysian, MN). NO_2-OA, biotin-NO_2-OA and NO_2-cLA were synthesized as previously reported(60). CDDO-Imidazol and CDDO-Methyl were from Toronto Research Chemicals (Toronto, Canada). Solvents were LC-MS quality and purchased from Burdick and Jackson (Morristown, NJ). Formic acid was purchased from Fisher Scientific (Pittsburgh, PA).

2.2 CELL CULTURE

RAW264.7 cells were obtained from American Type Culture Collection (ATCC, Manassas, VA) and grown per ATCC instructions in DMEM containing 4..5g/L glucose and supplemented with 10% fetal bovine serum and 1% penicillin/streptomycin.

2.3 TRANSGENIC MICE

Breeding pairs of homozygous $Keap1^{f/f}$ mice that are functionally Keap1 hypomorphs(41) and $Nrf2^{-/-}$ mice were kindly provided by Dr. Thomas Kensler at the University of Pittsburgh. Mice were bred in accordance with protocols approved by the University of Pittsburgh IACUC and males 8-12 weeks of age were used for experiments. Mice were genotyped using DNA extracted from tail snips and the oligonucleotide primers described previously(163, 164) and confirmed by immunoblotting for NQO1. The primers are shown in **Table 1** and an example of genotyping PCR results shown in **Figure 1.** Age-matched control mice of the C57BL/6J albino background (B6(Cg)-Tyrc-2J/J^{-}) were obtained from Jackson Laboratories and habituated in same vivarium as transgenic animals for at least one week prior to experiments.

5-cko-4int	GCACATCCTTCATCTCTCCGCACTGGGGAG
3-kp1-4Ex	CCTCCGTGTCAACATTGGCGCGACTAG
R379-EGFP	TCAGCTCGATGCGGTTCACC
Primer3Nrf2	TGGACGGGACTATTGAAGGCTG
3-1129-Nrf2	GCACTATCTAGCTCCTCCATTTCCGAGTC
Primer5Nrf2	GCGGATTGACCGTAATGGGATAGG

Table 1: Primers for genotyping Keap1$^{flox/flox}$ and Nrf2$^{-/-}$ mice

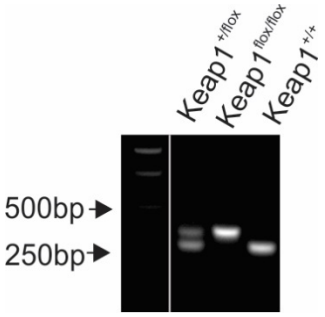

Figure 1: Representative PCR for genotyping Keap1$^{f/f}$ mice

2.4 ISOLATION AND CULTURE OF PRIMARY BONE-MARROW MACROPHAGES

Primary murine bone marrows from tibias and femurs of genotyped mice were obtained and differentiated into macrophages *in vitro* in the presence of 50 ng/ml of macrophage colony-stimulating factor (M-CSF, ThermoFisher)(165). Bone marrows were collected at age 10-16 weeks from Keap1$^{f/f}$ mice or from age matched wild-type C57BL/6J albino mice(41, 166).

2.5 BIOCHEMICAL ASSAY FOR GLUTATHIONE REDUCTASE ACTIVITY

GR activity was determined following the initial rates of dithionitrobenzoate (DTNB) reduction using an established biochemistry method adapted from Rahman *et al.*(167). Briefly, purified GR from S. cerevisiae (4mU-12mU; consistent within experiments) was incubated with vehicle or inhibitor in the presence of NADPH (150µM) or GSSG (1mM) and reaction was started with either GSSG or NADPH respectively. Consumption of NADPH ($\varepsilon_{\{340\}} = 6.22x10^3\ M^{-1}cm^{-1}$) or production of chromogenic TNB ($\varepsilon_{\{412\}} = 1.42x10^4 M^{-1}cm^{-1}$) were followed on a Agilent 8453 UV-Vis diode array spectrophotometer in kinetic mode.

2.6 PREPARATION OF $^{13}C_4{}^{15}N_2$ GSSG ISOTOPICALLY LABELED STANDARD

$^{13}C_2{}^{15}N$ (25µL 100mM) GSH in H_2O was incubated with 25µL 1M H_2O_2 for 30min at 37°C, followed by addition of 50µL 10mM KI(*aq*) and incubation 30min at 37°C to yield 25mM $^{13}C_4{}^{15}N_2$ GSSG. To confirm GSSG synthesis and absence of remaining free GSH, an aliquot of GSSG was incubated with 5-fold excess of N-ethylmaleimide (NEM) for 15min. The sample was diluted to a final concentration of 5µM in GSSG and spiked with 1µM $^{12}C_2{}^{14}N$ GS-NEM and $^{12}C_4{}^{14}N_2$ GSSG, followed by analysis by HPLC-MS/MS. The isotopic GSSG standard was only used in subsequent experiments if no labeled GSH or GS-NEM were detected.

2.7 DETERMINATION OF GLUTATHIONE AND GLUTATHIONE DISULFIDE

The method for simultaneous determination of GSH and GSSG was adapted from a previously published report(168). Briefly, RAW264.7 macrophages were seeded in 24-well plates at a density of 250,000 cells/well and were cultured overnight prior to treatments. Media was aspirated and cells were washed 2x with sterile PBS and incubated with PBS containing 25 mM NEM for 15 min at 37 °C. The PBS/NEM solution was aspirated and 550µL derivatizing solution (25 mM NEM, 40 mM HEPES/50 mM NaCl/1 mM EDTA) was added to each well and incubated for 15 min at room temperature. Cells were detached by scraping, and 500uL transferred to Eppendorf tube. Internal standards were added to achieve final concentration of 1 µM $^{13}C_2{}^{15}N$ GSH and 2 µM $^{13}C_4{}^{15}N_2$ GSSG, followed by 3 cycles of sonication in a 4°C water bath for 30 sec each. The lysate was cleared by centrifugation at 15,000 RPM for 10min at 4 °C. Protein content was assessed using the BCA assay. A 100µL aliquot was taken and proteins were precipitated by addition of 9 volumes of ethanol (200 proof), cooled to -80°C overnight, centrifuged (15,000 rpm, 4 °C, 10 min) and the supernatant dried under N_2 stream at room temperature. Samples were reconstituted in dH_2O (100 µL) and 20 µL were injected for analysis by LC-MS/MS.

2.8 REVERSED PHASE LIQUID CHROMATOGRAPHY – MASS SPECTROMETRY (LC-MS/MS) DETERMINATION OF GSH AND GSSG

Shimadzu HPLC (Columbia, MD) coupled to a Thermo Scientific CTC HTS PAL autosampler (Waltham, MA) and an AB Sciex (Framingham, MA) 5000 triple quadrupole mass spectrometer were used for the quantification of GSH adducts and GSSG. Samples (20 µL) were

chromatographically resolved on a Phenomenex C18 column (2.1 × 150 mm, 3.5 μm particle size) using the following solvent system A) aqueous 0.2% formic acid and B) 0.2% formic acid in acetonitrile:water (80:20) at a flow rate of 600μL /min. Chromatographic conditions were as follows: 1% solvent B for 0.1 min, followed by a linear gradient to 20.3% solvent B at 6 min, to then switch to 100% solvent B for 2 min and re-equilibration to return to the initial condition (1% solvent B) for 4 min. The following settings for the mass spectrometer were used: Source temperature 550 °C; ionization spray voltage 5500 V; CAD 4.0 arbitrary units; Curtain gas 40 arbitrary units; GS1 45 arbitrary units; GS2 50 arbitrary units; EP 5.00 V; CXP 10.00 V. Multiple reaction monitoring was performed with 65 ms dwell time and a declustering potential of 60 V using the following transitions in negative ion mode: GS-NEM (433.0/304.0, CE 38), $^{13}C_2{}^{15}N$ GS-NEM (436.0/307.0, CE 38), GSSG (613.2/355.2, CE 30), $^{13}C_4{}^{15}N_2$ GSSG (619.2/361.2, CE 30).

2.9 HPLC-MS/MS DETECTION AND ANALYSIS OF GR POST-TRANSLATIONAL MODIFICATIONS

Purified GR (S. cerevisiae; 10 μg) was incubated in the presence or absence of GSSG (2 mM), NADPH (3 mM), NO_2-OA (8 μM) for 30 min in 50 mM phosphate buffer, pH 7.4 and the reaction stopped by addition of iodoacetamide (10 mM final concentration, 10 min at room temperature). After alkylation, GR was digested using MS grade modified trypsin (trypsin/GR ratio of 1:50) for 16 h at 37 °C. The peptide digest was analyzed by LC-MS/MS for post-translational modifications using a Thermo Surveyor Plus HPLC coupled to an LTQ Orbitrap Velos mass spectrometer (Thermo Fisher Scientific). Peptides (3 μg on column) were loaded onto a Phenomenex C18 Luna SM (2.0 × 100 mm, 2.3 μm particle size; Torrance, CA) reverse-phase

column and resolved using a linear gradient of solvent A (0.1% formic acid in HPLC grade water) and solvent B (0.1% formic acid in acetonitrile) at a 650 µl/min flow rate. Chromatographic conditions were as follows: 5% solvent B for 2 min, followed by a linear gradient to 60% solvent B for 18 min, to then switch to 100% solvent B for 5 min and re-equilibration to return to the initial condition (5% solvent B) for 5 min. MS analysis was carried out in the positive ion mode with source parameters optimized for the detection of peptides containing nitroalkylated Cys. Instrument settings were as follows: source voltage, 3.75 kV; capillary temperature, 200 °C; source heater temperature, 450 °C; sheath gas flow and auxiliary gas flow, 25 arbitrary units; sweep gas flow, 20 arbitrary units; collision energy, 35 eV. MS/MS spectra was acquired using data-dependent acquisition in which one full MS spectrum was followed by MS/MS spectra of the top five ions. Peptide analysis was performed using Proteome Discoverer 2.0 (Thermo Fisher Scientific). MS/MS spectra (b and y ions) of detected modified peptides (presenting a 327.2410 atomic mass unit shift corresponding to NO_2-OA) were manually validated by comparing their fragmentation pattern with the native peptides (containing iodoacetamide alkylation in the case of Cys modifications).

2.10 QUANTIFICATION OF PROTEIN S-GLUTATHIONYLATION

The assay is based on the detection of protein adducts of GSH after sequentially 1) blocking free cellular GSH using N-methylmaleimide (NMM), 2) filtering the samples through two sequential 6 kDa cutoff size-exclusion gel columns to remove NMM, GS-NMM and GSSG, (3) reducing GS-S-protein mixed disulfides using an excess of BME, and finally (4) alkylating

released GSH using NEM in the presence of isotopically labeled GSH as internal standard. Protein-derived GS-NEM was quantified using the HPLC-MS/MS technique described in 2.8.

2.11 ISOLATION OF BONE-MARROW DERIVED MACROPHAGES

Primary murine bone marrows from tibias and femurs of genotyped mice were obtained and differentiated into macrophages *in vitro* in the presence of 50 ng/ml of macrophage colony-stimulating factor (M-CSF, ThermoFisher)(165) Bone marrows were collected at age 10-16 weeks from Keap1$^{f/f}$ mice or from age matched wild-type C57BL/6J albino mice.

2.12 IMMUNOBLOTTING

Cells were washed 2x with cold PBS and lysates were prepared in 4°C RIPA buffer with MiniTab protease inhibitor cocktail (Roche, Switzerland). For Prdx experiments, cells were incubated in alkylation buffer (40 mM HEPES, 50 mM NaCl, 1 mM EGTA, 1 mM EDTA, 100 mM NEM, pH 7.4) for 10 min at room temperature before lysing with Triton X-100 and protease inhibitor cocktail. Flash-frozen kidneys were homogenized in ice-cold RIPA buffer containing MiniTab protease and Phos-Stop phosphatase inhibitor cocktails (Roche, Switzerland). Cells were treated as indicated. At time of collection, cells were washed 2x with cold PBS and lysates were prepared in 4°C lysis buffer with MiniTab protease inhibitor cocktail and PhosStop phosphatase inhibitor cocktail (Roche, Switzerland). Lysates were cleared by centrifugation (15,000 rpm, 10min). Protein was quantified by BCA assay (Pierce, Waltham MA) and samples containing 15-

25µg total cellular protein were loaded on 4-12% Bis-Tris gel. Proteins were resolved by reducing or non-reducing SDS-PAGE, transferred to nitrocellulose membrane, blocked with 5% non-fat dry milk in TBS-0.1% Tween 20 for 1 hr. Primary and secondary antibodies were used at 1:1000 and 1:5000 dilutions unless otherwise indicated and visualized with Clarity ECL chemiluminescence kit and ChemiDoc imager (Bio-Rad, Hercules, CA).

2.13 IMMUNOHISTOCHEMISTRY

Immunohistochemistry was performed on 3 µm sections of formalin-fixed paraffin embedded kidneys. Sections were deparaffinized in xylenes (2x) and rehydrated in ethanol gradient (100-70%). Heat retrieval was performed using citrate pH 6 buffer (20min, 98°C, vegetable steamer). Rabbit anti-Cyclooxygenase-2 primary antibody was from Abcam (ab179800, 1:5000), and developed using Abcam Rabbit specific HRP-DAB kit (ab64261) following manufacturer's instructions.

2.14 IMMUNOFLUORESCENCE

Kidney cryostat sections (5 µm) were washed three times with phosphate buffered saline (PBS), followed by 3x washes with solution of 0.5% BSA in PBS. Sections were blocked with 5% normal goat serum in BSA solution for 45 minutes. The slides were incubated for 1 hour at room temperature (RT) with primary antibodies for rabbit anti NQ01 (ab34173, Abcam) at 1:500, and hamster anti MUC1(MA5-11202, Thermo) at 1:50 in .5% BSA solution. Slides were washed three

times with BSA solution and incubated for 1 hour at RT with Alexa 488 donkey anti mouse secondary antibody(A21202, Invitrogen) diluted 1:500, combined with goat anti rabbit CY5(111-605-003, Jackson Immuno) 1:1000, and goat anti hamster Cy3(127-165-160, Jackson) combined with 1:500 Alexa 488 phalloidin(A12379, Thermo) in BSA solution. Nuclei were stained with Hoechst dye(bisbenzamide 1mg/100ml water) for 30 seconds. After three rinses with PBS, sections were coverslipped with gelvatol mounting media. Images were captured with a Nikon A1 confocal microscope (NIS Elements 4.4)

2.15 MOUSE MODEL OF LITHIUM-INDUCED NEPHROGENIC DIABETES INSIPIDUS

Male C57BL6j/albino mice (JAX000058, Jackson Labs) at 8-12 weeks of age were habituated to individual housing for 4 days followed by randomization to receive control diet or diet containing 0.17% LiCl by weight (Teklad) ad libitum. Water was provided ad libitum. Mice were maintained on a 12h light/12h dark cycle. Mice and food were weighed daily. Water was supplied in 50mL conical with sipper tube as described (http://www.bio-protocol.org/e1822), and daily water intake was determined by weight. All experiments were performed with approval of the University of Pittsburgh's Institutional Animal Care and Use Committee.

2.16 BLOOD COLLECTION AND BLOOD CHEMISTRY ANALYSIS

Blood was collected from mice under deep isoflurane anesthesia using either retroorbital sampling or via cardiac puncture. Blood was collected in BD Microtainer tubes containing Lithium Heparin or K_2EDTA anticoagulant and inverted 10x to mix thoroughly. 150µL from LiHep anticoagulated sample was loaded onto Abbott iSTAT Chem8+ cartridge and analyzed immediately. Remaining sample was centrifuged at 500g for 10min at room temperature. Plasma was aliquoted and frozen in N_2(l) and stored -80°C.

2.17 TISSUE COLLECTION

After collection of urine and blood, a laparotomy and thoracotomy were performed. A hemostat was applied to the left renal vascular bundle and the left kidney was removed and flash-frozen in N_2(l). The vena cava was severed and whole-animal transcardial perfusion was performed with cold 2% PFA in PBS. The right kidney was removed, bisected lengthwise, and fixed in 2% PFA for 1.5h. Half of the kidney was further fixed in neutral buffered formalin and embedded in paraffin, and half by dehydration in 30% sucrose for 24h and freezing in OCT compound.

2.18 LITHIUM ASSAY

Plasma lithium was quantitated using Lithium Assay Kit (Colorimetric) from BioVision Inc., (Milpitas, CA, USA) using 10µL plasma and following manufacturer's instructions.

2.19 PLASMA RENIN CONCENTRATION ASSAY

Plasma Renin Concentration Assay: 30µL plasma was added to 270µL generation buffer (1.0M Tris 0.25M EDTA 1mM PMSF pH 5.5) containing 30µM tetradecapeptide renin substrate (Angiotensinogen 1-14, rat, DRVYIHPFHLLYYS, AnaSpec, Fremont CA) and the reaction was incubated at 37C. Aliquots (50µL) were removed at 0, 10, 20, and 30 min and quenched with 200µL MeOH containing 3% formic acid and $^{13}C/^{15}N$ labeled Angiotensin I internal standard (DR-V*-Y-I*-HPFHL, AnaSpec, Fremont CA, * = all $^{13}C/^{15}N$). The solution was chilled at -20°C and protein precipitates removed by centrifugation 13,000RPM for 10min. 20µL of supernatant were injected for HPLC-MS/MS analysis.

HPLC-MS/MS of angoitensin I and 14aa angiotensinogen substrate: A Shimadzu HPLC (Columbia, MD) coupled to a Thermo Scientific CTC HTS PAL autosampler (Waltham, MA) and an AB Sciex (Framingham, MA) 5000 triple quadrupole mass spectrometer was used for the quantification of AngI, isotopic AngI standard, and 14aa angiotensinogen substrate. Sample (20 µL) was separated on a Phenomenex Gemini C18 column (2.0 × 20 mm, 3 µ pore size). The solvent system employed 0.1% aqueous formic acid (A) and 0.1% formic acid in acetonitrile (B) at a flow rate of 850µl /min. Chromatographic conditions were as follows: 5% solvent B for 0.3 min, followed by a linear gradient to 45% solvent B at 2.5 min, to then move to 100% solvent B for 1

min and re-equilibration to return to the initial condition (5% solvent B) for 4.5 min. The triple quadrupole mass spectrometer was tuned in positive ion mode and the following settings were used: Source temperature 650°C; ionization spray voltage 5000V; CAD 5.0 arbitrary units; Curtain gas 40 arbitrary units; GS1 55 arbitrary units; GS2 55 arbitrary units; EP 10.00V; CXP 10.00V. Multiple reaction monitoring (75ms dwell time, declustering potential 100V, collision energy 30-37V) was performed using the following transitions: Ang I (Q1 433.20→Q3 110.20), isotopic Ang I (Q1 655.60→Q3 110.20), 14aa angiotensinogen substrate (Q1 608.50→Q3 269.20). Sample AngI was calculated based on area ratio and calibration curves prepared using commercially available AngI standards, and plasma renin concentration calculated from slope of AngI generated by each sample as function of time.

2.20 OSMOLALITY DETERMINATIONS

Spot urine was collected after spontaneous voiding on plastic wrap, or in case of terminal experiments, sampled from bladder after laparotomy under isoflurane anesthesia using 30G syringe. Urine osmolality measured in technical duplicate with Wescor 5500 Vapor Pressure Osmometer using 5µL urine. The instrument was calibrated on each day using standards of 0, 290, and 1000mOsm/kg and the average value of duplicates reported for each sample. For some samples, a 1:2 dilution in MilliQ Ultrapure water was necessary to remain within the dynamic range of the instrument.

2.21 PRIMARY HUMAN RENAL CORTICAL CELLS

Primary human distal tubule cells from human adult kidney were isolated and cultured as previously described (169). Confluent monolayers of cells were incubated with vehicle control, LiCl or CDDO-Im for 18 hr in serum-free hormonally defined media followed by preparation of lysates for immunoblotting. For confirmation of cell lineage, immunoblotting for CD10 and MUC1 was performed in each experiment.

2.22 REVERSED PHASE LIQUID CHROMATOGRAPHY – MASS SPECTROMETRY (LC-MS/MS) DETERMINATION OF PROSTAGLANDINS

Determination of 6-keto prostaglandin F1α:

Flash-frozen kidney samples were weighed on an analytical balance and transferred to chilled Eppendorf tubes containing an equivalent weight of zirconium oxide homogenization beads (NextAdvance, Troy NY). 380µL distilled water containing isotopically labeled standard 6-keto PGF1α-d4 (Cayman Chemical, Ann Arbor, MI) was added to each sample and homogenized at 4°C using Bullet Blender (NextAdvance, Troy, NY). The lysate was added to 1.6mL acetonitrile and centrifuged 15,000rpm for 15min at 4°C. The supernatant was transferred to a clean glass tube and dried under N_2(g) for 1hr. Samples were resuspended in 200µL MeOH and 10µL was injected for HPLC-MS/MS analysis. Analyte was quantified using 6-point calibration curve prepared for each experiment

For determination of 6-keto-PGF1α, chromatography was performed on Phenomenex Kinetex C18 2.1x50mm column (2.1 × 50 mm, 5µm particle size) using aqueous 0.1% ammonium

acetate (A) and 0.1% ammonium acetate in acetonitrile (B) at total flow of 0.25mL/min. 10% B was increased to 65% B over 20 min followed by 3 min wash with 100% B and return to 10% B for 2min for a total run time of 25 min. An AB Sciex API 5000 triple quadrupole mass spectrometer was tuned in negative ion mode and the following settings were used: Source temperature 650°C; ionization spray voltage 5000V; CAD 5.0 arbitrary units; Curtain gas 40 arbitrary units; GS1 55 arbitrary units; GS2 55 arbitrary units; EP -5.00V; CXP -18.40V. Multiple reaction monitoring was performed with 150ms dwell time, declustering potential -50V, collision energy -17V was performed using the following transitions: 6-keto PGF1α (Q1 369.10→Q3 245.00), 6-keto PGF1α-d4 (Q1 373.1→Q3 167.00).

2.23 MEASUREMENT OF GLOMERULAR FILTRATION RATE

Glomerular filtration rate was measured in unrestrained conscious rodents by following FITC-sinistrin elimination using MediBeacon transdermal device and software package (MediBeacon GmbH, Mannheim, Germany) following the manufacturer's instructions(170).

2.24 DETERMINATION OF PLASMA AND URINE NITRITE

1.0mL blood was collected into tubes containing 50µL acid citrate dextrose anticoagulant and immediately centrifuged for 10min at 500g to separate plasma. Plasma was aliquoted and stored -80°C until analysis. Urine was collected onto clean plastic sheet as described previously.

50µL sample was analyzed using GE Sievers NOA 280i following manufacturer's instructions. A calibration curve containing known amounts of sodium nitrite was prepared for quantification.

2.25 DETERMINATION OF PLASMA AMINO ACIDS

Plasma amino acids and kynurenine were measured using isotope-dilution HPLC-MS/MS following derivatization with phenylisothiocyanate (PITC) as previously described(171).

2.26 WIRE MYOGRAPHY

Endothelium-dependent and -independent relaxation responses of second order mesenteric or thoracodorsal arteries to cumulative doses of acetylcholine (Ach) and sodium nitroprusside (SNP) were evaluated using two-pin wire myography (Multiple Myograph Model 610 M, DMT; Denmark).

2.27 RADIOTELEMETRY

Blood pressure was analyzed in WT and Keap1$^{f/f}$ mice chronically instrumented with PA-C10 telemetry units (Data Sciences International) and fed 0.1% (normal sodium) or 0.01% NaCl (low-sodium) chow. Systolic, diastolic, and mean ABP and heart rate were sampled at 2 KHz and averaged for both day (10AM–4PM) and night (10PM-4AM) periods. Standard vivarium conditions, lights on 7 AM–7 PM, 25°C.

2.28 STATISTICAL ANALYSIS

Statistical analyses were performed using GraphPad Prism (La Jolla, CA. USA) version 7.01 by Student's t-test, one-way or two-way analysis of variance (ANOVA) and corrections for multiple comparisons as indicated in figure legends. P values less than 0.05 were statistically significant. In addition to statistical significance, magnitude of differences with regards to biological or physiological relevance was also considered in interpretation of results.

3.0 GLUTATHIONE REDUCTASE IS A GSH- AND ELECTROPHILE-SENSITIVE CONTROLLER OF INTRACELLULAR GSSG

3.1 INTRODUCTION

One of the most salient characteristics of electrophilic mediators is their pleiotropic signaling actions, a property afforded by the broad set of cellular targets that can be modified. These targets encompass nucleophilic residues including cysteines, histidines, and lysines, with signal transduction downstream of cysteine addition predominating. Previous reports have established the nonspecific reactivity of therapeutic electrophiles with cysteine residues, and the correlation between electrophilicity of parent compounds or their metabolites and idiosyncratic drug toxicity has been a provoking correlation leading to frequent exclusion of electrophilic compounds in the drug development pipeline(172). The nonspecific reactivity of many electrophiles has posed additional challenges for pharmacologists, as these compounds frequently give false positive results in screening assays(173, 174).

GSH depletion by electrophiles is a well-documented surrogate measurement reflective of cellular toxicity, and GSH depletion through inhibition of biosynthesis has been shown to potentiate adverse effects of arylating species such as electrophilic metabolites of acetyl-para-aminophenol (acetaminophen, APAP)(175).

While the pKa of cysteine thiol of glutathione is relatively high (8.94)(119), GSH reactivity is driven by the activity of glutathione-S-transferases, rapid turnover of oxidized GSSG by glutathione reductase and its high intracellular concentrations (~10mM). GS-NO_2-OA and GS-NO_2-cLA Michael adducts have been detected *in vitro* and *in vivo*, and suggest that reduction in

GSH levels could be a major cellular consequence of NO_2-FA exposure(83, 176). Similarly, CDDO-Imidazole and –Methyl have been found to adduct and in some cases deplete GSH(87, 177, 178).

In this context, the first half of this thesis sought to rigorously define the temporal effects of endogenous and pharmacological electrophilic molecules on GSH cycling, depletion, and biosynthesis. GSH and GSSG were measured in cell preparations after treatment with electrophiles or an inhibitor of GSH biosynthesis. Electrophiles were found to transiently decrease intracellular GSH, followed by induction of GSH biosynthesis and accumulation of GSH. Paradoxical accumulation of GSSG was observed, accompanied by increases in protein S-glutathionylation but without enhancement or suppression of peroxiredoxin dimerization or involvement of MRP1 exporters. Direct and indirect mechanisms by which electrophiles modulate GSSG cycling through GR were identified. Elevation in GSH and GSSG was accompanied by increases in protein S-glutathionylation. Finally, *in vitro* studies of immortalized and primary murine macrophages showed that TLR4-dependent macrophage activation is situated pharmacologically and genetically downstream of the redox sensitive thiol proteome, with specific tolerogenic function of Nrf2 derived from its effects on the GSH axis.

3.2 RESULTS

3.2.1 Lipid electrophiles upregulate GSH biosynthesis through induction of Nrf2 in RAW264.7 macrophages

To quantify intracellular concentration of GSH and GSSG, a method based on NEM derivatization previously developed by Harwood *et al.* (168) was implemented and validated (**Figure 2**). The method is described in detail in 2.6, 2.7, and 2.8.

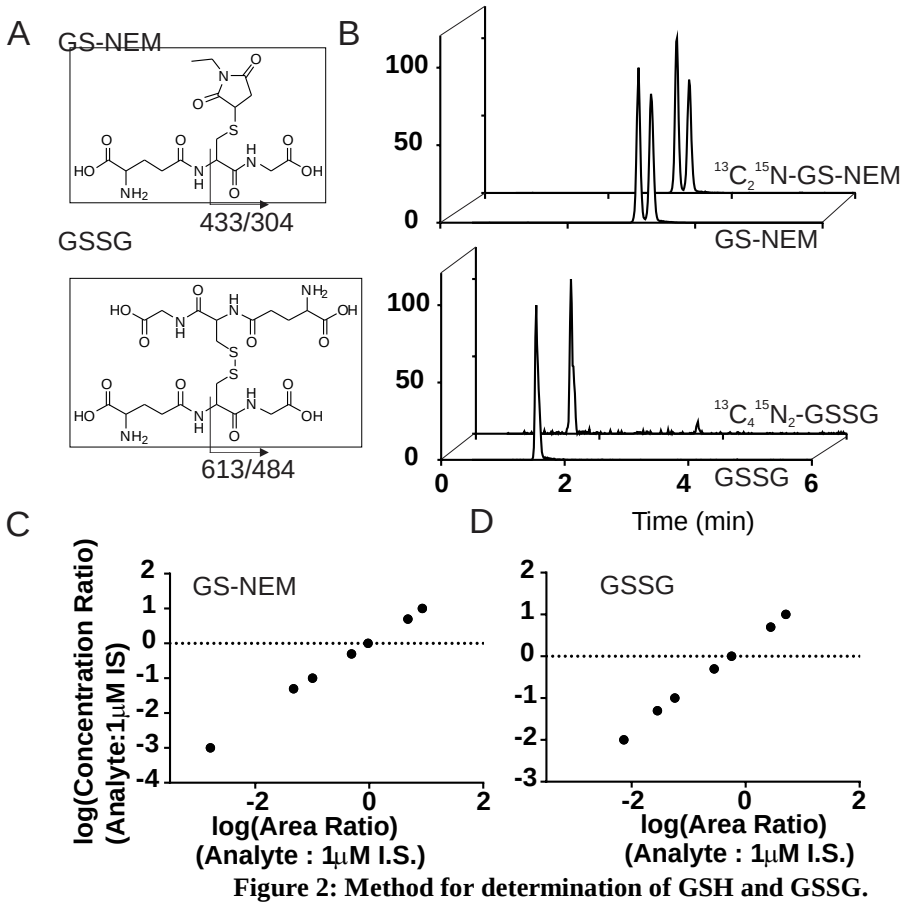

Figure 2: Method for determination of GSH and GSSG.

(A) Structures and MS fragmentation diagrams with multiple reaction monitoring transitions of GS-NEM and GSSG. (B) Representative HPLC-MS/MS traces of GS-NEM and GSSG co-eluting with their respective isotopic standards. (C) Representative log-log plots of calibration curves used for quantitation of GS-NEM and GSSG. Abscissa: log([GS-*]/[1μM $^{13}C_2{}^{15}N$-GS-*]). Ordinate: log((A.U.C. GS-*)/(A.U.C. 1μM $^{13}C_2{}^{15}N$-GS-*)). GS-* = GS-NEM or GS-SG. Calibration curves were prepared for each independent experiment using GSH, GSSG and their respective $^{13}C_2{}^{15}N$ isotopic standards. Calibration curves displayed linearity between instrument response and analyte concentration over 4 and 3 orders of magnitude for GS-NEM and GSSG respectively, allowing simultaneous determination of both species and LOQ for both GSH and GSSG was 10nM.

Intracellular GSH and GSSG were measured in cultured RAW264.7 macrophages and yielded a mean of 56.4±5.2 and 0.16±0.01 nmol/mg protein for GSH and GSSG respectively and an overall ratio of GSH/GSSG of 366±24 (n=3-6 from 5 independent experiments, mean ± standard error). Cells were then activated with LPS or either exposed to NO_2-OA or the GSH synthesis inhibitor buthionine sulfoximine (BSO) and the GSH pool evaluated. After 1 hr of exposure to 5μM electrophilic NO_2-OA, GSH levels were reduced by 23%, returned to baseline level by 3 hr and increased two-fold by 6 hr (Fig. 2A, red trace). Surprisingly, the GSSG levels did not significantly change under this initial mild GSH depletion but increased 8.3-fold at 6 hr (Fig. 2B, red trace). Both GSH and GSSG significantly decreased by 24 hr but remained elevated compared to baseline. Notably, although GSH levels significantly increased at 6 and 24 hr post-NO_2-OA exposure, a pronounced decrease in GSH/GSSG ratio was observed (Fig. 2C, red trace).

In contrast, LPS induced an initial decrease in GSH that recovered to initial levels by 6 hr while GSSG increased as a function of time, reaching a maximum over 10-fold above baseline at 24 hr. Next, the effects of GSH depletion were investigated in the absence of exogenous electrophilic or oxidative stimuli. To this end, the irreversible γ-glutamylcysteine synthetase inhibitor BSO was used. A linear reduction in intracellular GSH was observed over 24 hr, with an overall loss of 55% of the GSH pool (Fig. 2A, blue trace). Interestingly, the loss in GSH resulted in a more pronounced (87%) reduction in GSSG (Fig. 2B, blue trace) suggesting that the decrease in GSH was not associated to increased oxidative stress. We then evaluated the Nrf2-dependent responses of GSH biosynthesis to NO_2-OA treatment. The expression of the modulatory subunit of GCLM, which is the rate-limiting step in GSH biosynthesis, was increased at 6 hr and was at its highest at 24 hr. By comparison, the NO_2-OA modulated target HO-1 was upregulated between 3 and 6 hr but trending towards baseline levels by 24 hr. Finally, and despite the presence of

putative ARE sequences in its promoter sequence, GR expression was not modulated by NO_2-OA treatment(179) (Fig. 2D).

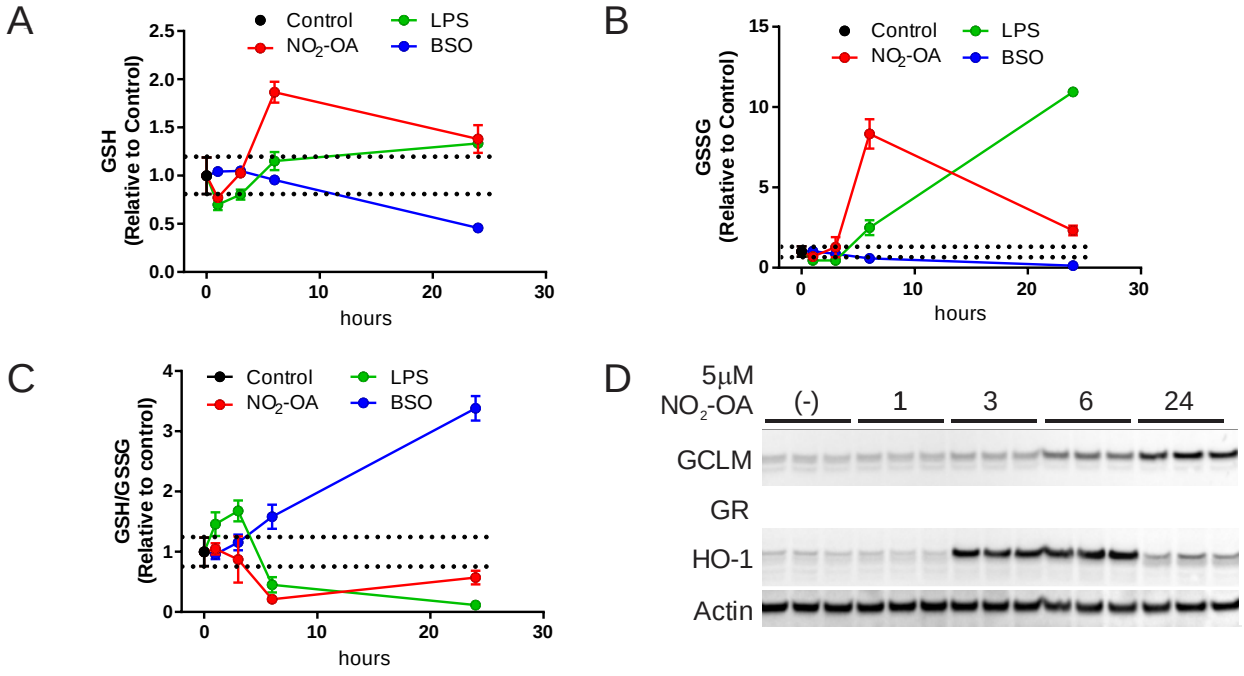

Figure 3: Modulation of GSH and GSSG levels by NO_2-OA, LPS and BSO

RAW264.7 cells were treated with 5μM NO_2-OA (red trace), 200 ng/mL LPS (green), or 20 μM BSO (blue trace) and GSH (A), GSSG (B) and the GSH/GSSG ratio (C) were determined. Results are expressed as mean ± standard error of 3 independent replicates for each condition. Results normalized to vehicle control (black, t=0 hr) ± standard error (dashed lines) of 6 replicates. (D) Time-dependent response of Nrf2 activation by NO_2-OA (5 μM) in RAW264.7 cells.

3.2.2 NO_2-OA induced upregulation of GSSG occurs independently of oxidative stress

I would like to acknowledge the significant contributions of Dr. Dario Vitturi, PhD, who helped perform experiments evaluating Prdx oxidation state.

The paradoxical increase in both intracellular GSH and GSSG in cells treated with NO_2-OA motivated testing whether the increase in GSSG correlated with increased oxidative stress markers within the same time-frame (Fig. 3). The cytosolic and mitochondrial 2-Cys peroxiredoxins, Prdx1 and 3 respectively, are highly reactive antioxidant enzymes that dimerize upon oxidation by hydrogen peroxide or peroxynitrite ($k \sim 10^5$ $M^{-1}s^{-1}$-10^7 $M^{-1}s^{-1}$)(142–145). As a result, any change in endogenous peroxide levels are reflected by changes in the relative abundances of monomeric vs. dimerized Prdx.

Under basal conditions, RAW264.7 macrophages presented ~35% of Prdx1 (**Figure 4A-B**) and ~60% Prdx3 covalently dimerized. It is tempting to speculate that the higher level of basal oxidation of Prdx3 compared to Prdx1 is a result of elevated ROS formation in the mitochondria. Treatment with NO_2-OA had no effect on the proportion of covalent Prdx dimers compared to controls, despite the elevation in intracellular GSSG (**Figure 4A-C**). In contrast, exposure to 50 µM H_2O_2 for 10 minutes resulted in oxidation of both Prdx1 and Prdx3, with ~98% of the Prdx proteins running as the disulfide-linked dimer (not shown). To model physiologic oxidative stress, macrophages were activated with LPS, which led to oxidation of Prdx1 and Prdx3 after 6hr (**Figure 4D**). To evaluate whether NO_2-OA affected Prdx function, RAW264.7 cells were incubated with 10µM H_2O_2 in the presence or absence of 5µM NO_2-OA. **Figure 4E** shows that both Prdx1 and 3 oxidized fully within 20 min of exposure regardless of the presence of NO_2-OA.

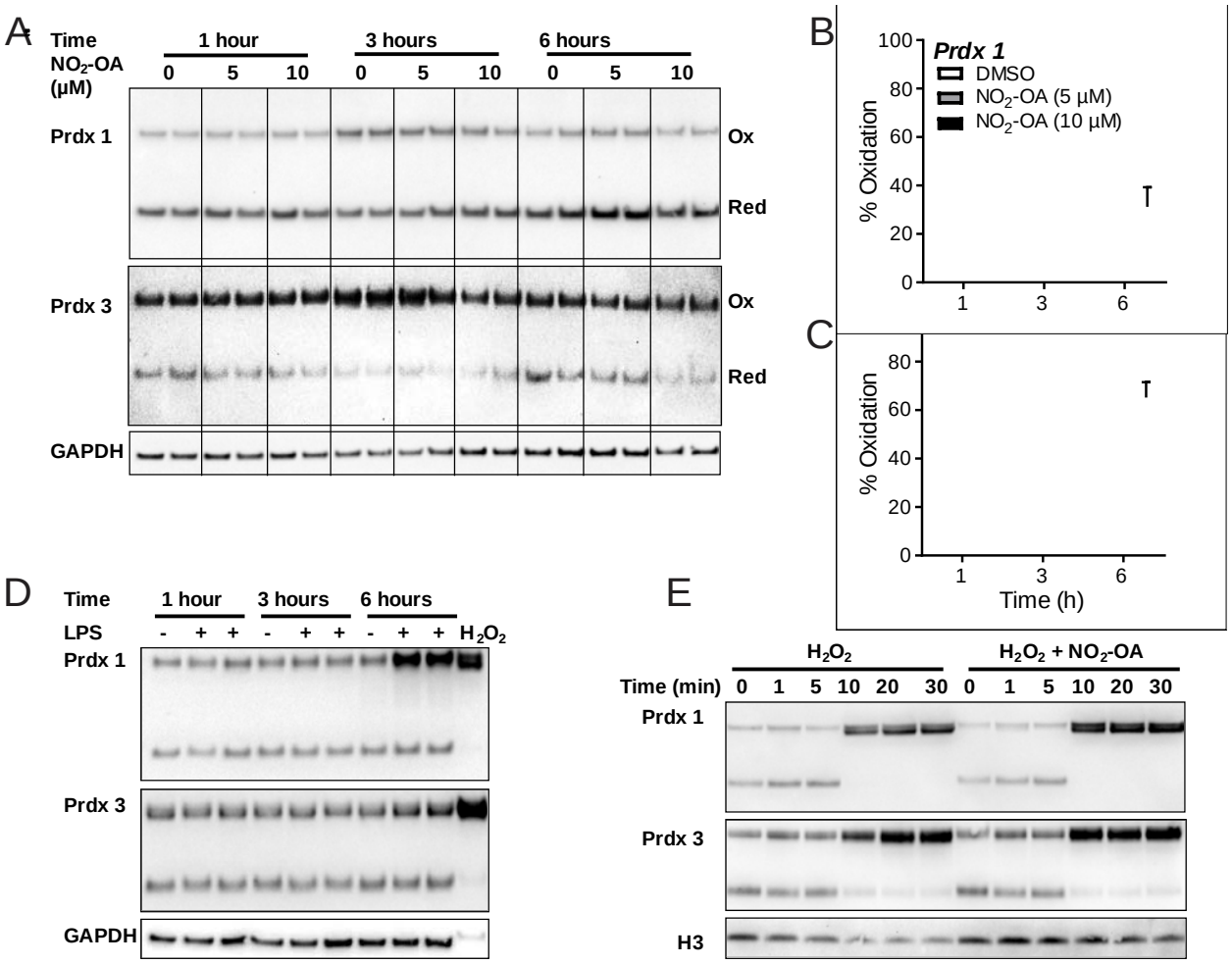

Figure 4: NO_2-OA does not affect oxidation of Prdx1/Prdx3

RAW264.7 macrophages were incubated for 1, 3 or 6h with DMSO vehicle or NO_2-OA (5μM and 10 μM). Dimerization of Prdx1 (A, B) and Prdx3 (A,C) was assessed by non-reducing gel electrophoresis followed by immunoblotting and densitometry. Representative immunoblot shown; vertical lines superimposed on blot to facilitate interpretation. Densitometry is expressed as mean ± standard deviation of 6 samples from 3 independent experiments. (D) Prdx1 and Prdx3 oxidation after macrophage activation with LPS for 0, 1, 3, or 6 hours. As positive control, cells were exposed to 400 μM H_2O_2 for 10 min, which fully oxidized both Prdx1 and Prdx3. (E) Prdx oxidation by 10 μM H_2O_2 occurs rapidly (within 10min) and is neither inhibited nor promoted by NO_2-OA.

The peroxidatic cysteine in typical 2-Cys peroxiredoxins can be hyperoxidized to $SO_{2/3}$ via a sulfenic acid intermediate(145). Hyperoxidation simultaneously inactivates the Prdx and

prevents protein dimerization, as the Cys-$SO_{2/3}$ is incapable of forming disulfide bonds. Thus, in the setting of pervasive oxidative stress, hyperoxidation could mask dimerization. Immunoblotting using a pan-Prdx1-4 $SO_{2/3}$ antibody revealed appearance of a hyperoxidized Prdx monomer after exposure to 400µM H_2O_2, while hyperoxidation was absent in NO_2-OA treated cells (**Figure 5**). Taken together these results support that the accumulation in intracellular GSSG is not associated with changes in steady-state oxidant exposure.

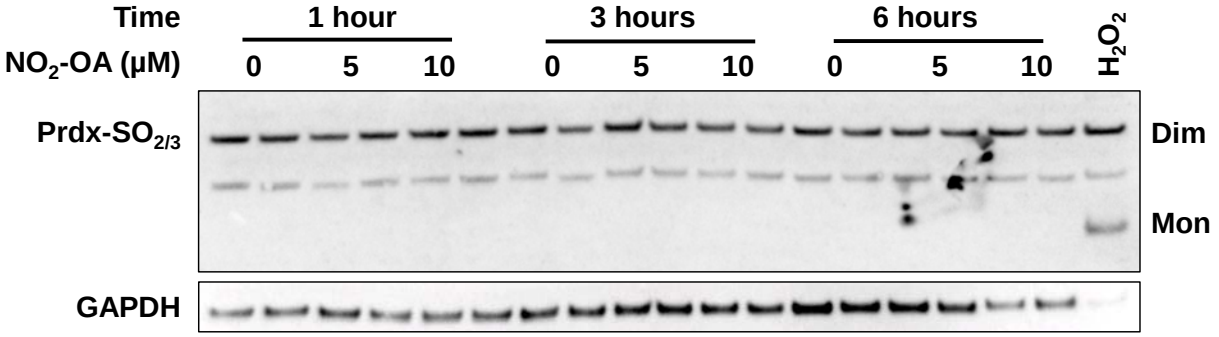

Figure 5: NO_2-OA does not induce hyperoxidation of Prdx.

Hyperoxidized Prdxs were detected using an antibody that reacts with PRX 1–4 when in the PRX-SO2/3 state. Incubation of RAW264.7 macrophages with 0, 5, or 10µM NO_2-OA for 1-6hr failed to induce hyperoxidation. Upon exposure to H_2O_2 (400µM) for 10min the appearance of hyperoxidized Prdx-$SO_{2/3}$ monomer is seen.

3.2.3 Inhibition of MRP1 is insufficient to increase intracellular GSSG

Electrophilic compounds and their detoxified GSH conjugates, as well as GSSG are eliminated from cell via ATP-binding cassette (ABC) transporter class proteins including MRP1(180). It was postulated that covalent or competitive inhibition of MRP1 by NO_2-OA could lead to accumulation of intracellular GSSG. Incubation of RAW264.7 macrophages with the pan-MRP/organic anion transporter (OAT) inhibitor probenecid (250µM) or the MRP1-selective

inhibitor MK-571 (25μM) revealed that inhibition of these transporters did not lead to accumulation of intracellular GSSG (**Figure 6A-C**).

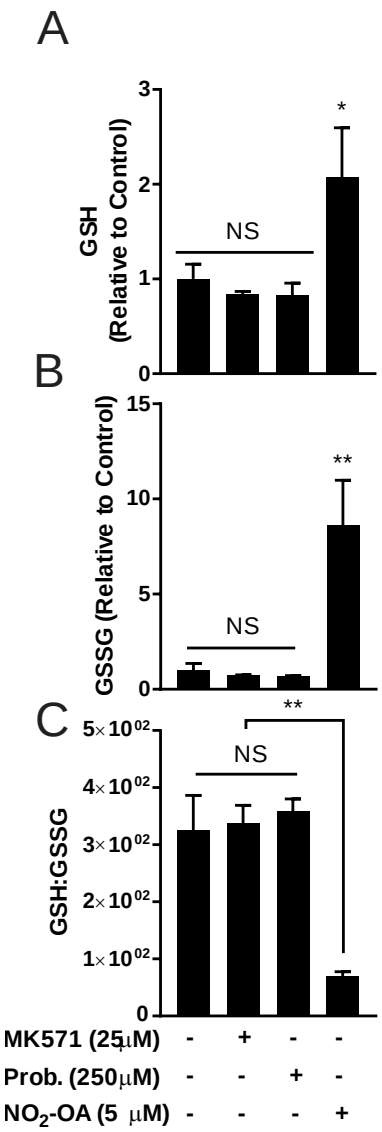

Figure 6: Inhibition of MRP1 does not increase intracellular GSSG.

Incubation of RAW264.7 macrophages with the specific MRP1 inhibitor MK571 (25μM) or the pan-MRP inhibitor probenecid (250μM) for 6 hr did not cause accumulation of intracellular GSSG. NO_2-OA was included as control. Results are expressed as mean ± standard error, n=3. *p<0.05; **p<0.01; Statistical analysis by one-way ANOVA with Tukey multiple comparison test.

3.2.4 NO_2-OA is a covalent reversible inhibitor of GR

Since NO_2-OA did not induce cellular oxidative stress (**Figure 4 and Figure 5**), and appreciating that Nrf2 activation upregulates GSH biosynthesis and NADPH production *in vivo*(181), it was hypothesized that NO_2-FA may inhibit GR, reducing GSH regeneration and increasing intracellular GSSG. The GR active site contains two critical cysteines that form an internal disulfide during the catalytic reduction-oxidation cycle of the enzyme. Both NO_2-OA and NO_2-conjugated linoleic acid (NO_2-cLA) inhibited *S. cerevisiae* GR activity, with NO_2-OA effecting a more pronounced inhibition (**Figure 7A**). Interestingly, whereas incubation of GR with 3μM NO_2-OA in the presence of NADPH resulted in a complete inhibition of GR activity upon GSSG addition, GR pre-incubation with 3μM NO_2-OA in the presence of GSSG but in the absence of NADPH did not immediately result in GR inhibition. The inhibition of GR only started to occur after NADPH addition (**Figure 7B**).

To further characterize the inhibition and reactivity of GR with NO_2-OA, rate constants were determined using pseudo-first-order conditions by stopped-flow (**Figure 7C**). A linear dependence was observed between the pseudo-first order rate constant (k_{obs}) and NO_2-OA concentration (**Figure 7D**).The forward second-order rate constant (k_{on}) was determined from the slope of the k_{obs} versus NO_2-OA concentration plot as $(3.45 \pm 0.04)x10^3\ M^{-1}s^{-1}$. The non-zero y-axis intercept indicates a reversible reaction with a $k_{off} = (4.4 \pm 0.4)x10^{-4}s^{-1}$. The equilibrium dissociation constant K_{eq} was then calculated by dividing k_{off} by k_{on} and its value was $(1.3\pm0.1)x10^{-7}$M (25°C, pH 7.4). No significant changes in the initial rate occurred in the absence of NO_2-OA. In order to compare the values obtained with other abundant thiol-containing intracellular enzymes, we kinetically characterized the reaction with glyceraldehyde-3-phosphate dehydrogenase (GAPDH), a known target for NO_2-OA (**Figure 7D**, inset)(83). The values

obtained were k_{on} = 389±64$M^{-1}s^{-1}$, k_{off} = (3.2±0.9)x10^{-3} s^{-1} and K_{eq} = (8±4)x10^{-6}M (25°C, pH 7.4) indicating that GR reacts ~10 times faster with NO_2-OA than GAPDH. In the case of GSH, the forward rate constant with NO_2-OA is 64±1 $M^{-1}s^{-1}$ (25°C, pH 7.4), ~50 times slower than GR(176). Thiol alkylation by NO_2-OA inhibits target proteins (e.g. GAPDH) and has been shown to be reversible(83). To confirm the reversibility of GR inhibition by NO_2-OA, GR was treated with NO_2-OA, and β-mercaptoethanol (BME) was added during the linear phase of the reaction. A rapid, complete recovery of GR enzymatic activity was achieved with 0.5 mM BME and the degree of reactivation was dose-dependent (**Figure 7E-F**).

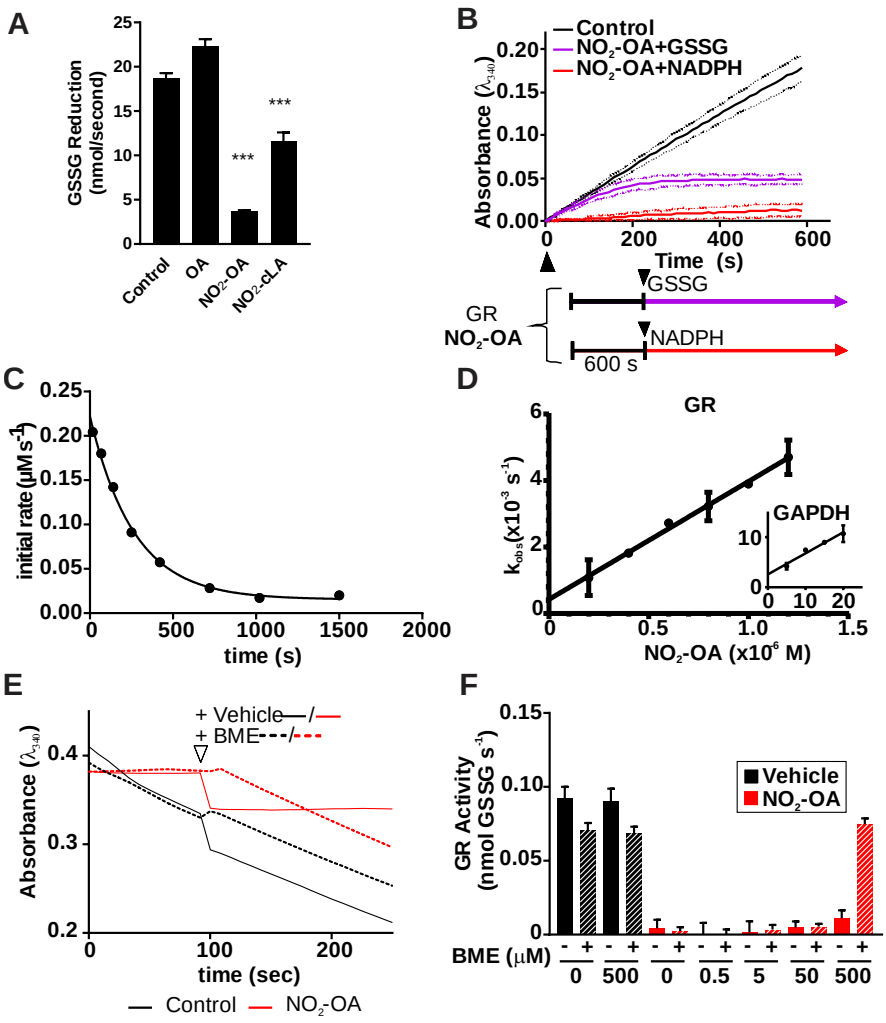

Figure 7: NO_2-OA is a reversible covalent inhibitor of GR.

A) Inhibition of GR activity by NO_2-OA, NO_2-cLA, or non-electrophilic OA (5 μM each) as measured by the DTNB-reduction assay after 10 min incubation. Results are mean ± SD from 3-5 independent experiments. *** $p<0.0001$ by one-way ANOVA vs control, using Tukey multiple comparison test. (B) TNB production by GR pre-incubated with vehicle control, NO_2-OA + GSSG (purple) or NO_2-OA + NADPH (red) for 10 min prior to addition of missing substrate. Results are summarized as mean ± SD from 3-5 independent experiments. (C) Reduced GR (2 nM) was incubated with 800 nM NO_2-OA. At increasing times, aliquots (1.6 nM) were mixed with 0.1 mM NADPH and 1 mM GSSG, and the initial rate of absorbance decay at 340nm and 25°C was measured. The solid line represents the best fit to a single exponential equation. (D) k_{obs} values at increasing concentrations of NO_2-OA (200-1200 nM) were determined from kinetic traces as in (A); k_{obs} values for the reaction between NO_2-OA and GAPDH. (E) Representative kinetic traces showing that addition of BME (5 mM) rapidly restores GR activity and NADPH

consumption of pre-inhibited GR. (F) GR activity restoration is dependent of BME concentration. Results are reported as mean ± SD. For some points, the error bars are shorter than the height of the symbol.

3.2.5 NO_2-OA binds Cys61 of GR

Next, we sought to evaluate whether the inhibition involved a covalent binding between GR and NO_2-OA using biotin-labeled NO_2-OA. GR contains 5 Cys and 15 His residues, all of which could be potential nucleophilic targets of NO_2-OA. To test the covalent reaction of GR with NO_2-OA, we decided to incubate GR with biotin-tagged NO_2-OA followed by immunoblotting with streptavidin. Since the derivatization of NO_2-OA carboxylic acid with biotin significantly impacts its size and charge, the inhibition of GR by biotin-NO_2-OA was first tested (**Figure 8**). Biotin-NO_2-OA did inhibit GR, albeit with lower potency than non-tagged NO_2-OA. Incubation of purified GR with a 100-fold molar excess of biotin-NO_2-OA in the absence of NADPH resulted in only low levels of adducted biotin-NO_2-OA detected by non-reducing immunoblot. The adducted level of NO_2-OA increased significantly in the presence of NADPH, suggesting Cys61 and Cys66 as potential targets (**Figure 9A**). Digestion of GR under native conditions (non-reduced) yielded 69% coverage of the primary sequence encompassing 5/5 Cys and 11/15 His residues, and displayed the expected disulfide between Cys61 and Cys66 (**Figure 9D, E**). When reduction was followed by alkylation with iodoacetamide, 81% sequence coverage was obtained, presenting stable carbamidomethyl-adducts at the active site dithiol (**Figure 9D, F**). Likewise, incubation of GR with a 100-fold molar excess of NO_2-OA followed by tryptic digestion yielded only the Cys61-Cys66 disulfide bridge without evidence of nitroalkylation of either catalytic Cys and only minor alkylation of other Cys and His (not shown). In contrast, incubation of GR with NADPH in the

presence of NO_2-OA permitted the identification of Cys61 as the specific nucleophilic target with 84% primary sequence coverage (**Figure 9D, G**).

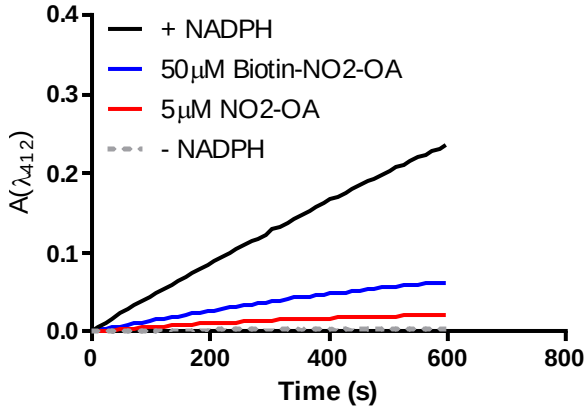

Figure 8: Biotin-NO_2-OA inhibits GR

GR was incubated with vehicle control, 5μM NO_2-OA or 50μM biotinylated NO_2-OA in the presence of NADPH and GSSG and DTNB were added. TNB absorbance at 412nm was recorded as a function of time. Like NO_2-OA (Fig. 6), biotin-NO_2-OA inhibited GR activity as compared to the vehicle control (+NADPH). GR did not reduce GSSG in the absence of NADPH (-NADPH).

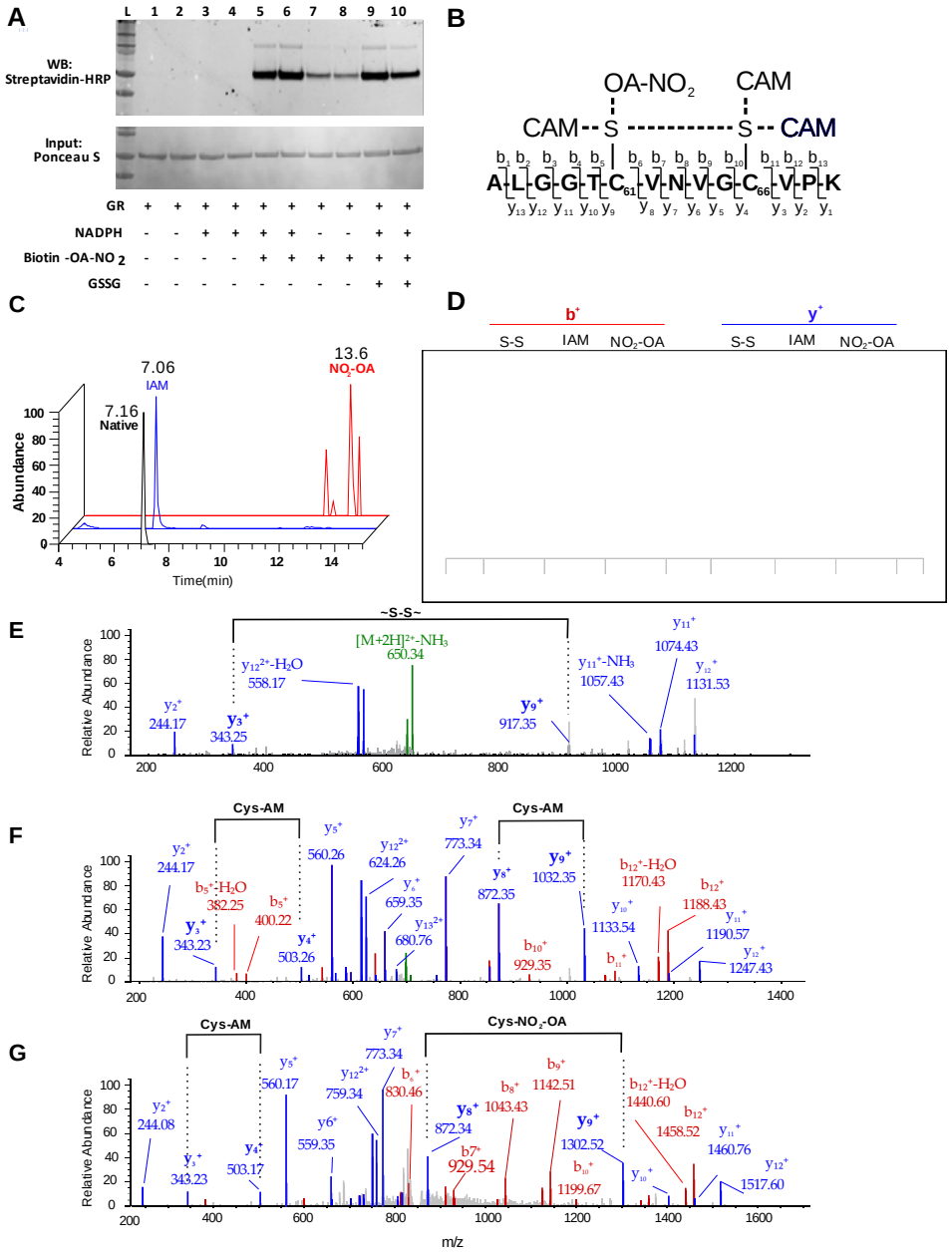

Figure 9: NO_2-OA inhibits GR via Cys61 modification

(A) Catalytic cysteines are a main target of NO_2-OA as assessed by 10 min incubation with biotinylated NO_2-OA (8µM) in the presence or absence of cofactor NADPH and GSSG (n=2). (B) Sequence of tryptic peptide encompassing the GR catalytic site ALGGTC_{61}VNVGC_{66}VPK with b^+ and y^+ fragmentation patterns and potential Cys modifications. (C) Elution profile of the native and alkylated peptides containing Cys61. (D) Tabular summary of calculated (black) and identified (blue/red) b^+ and y^+ ions, respectively. MS/MS spectra of the GR catalytic site peptide

obtained after (E) control, (F) IAM and (G) NO_2-OA treated GR showing native (E), carbamidomethylated (CAM) (F), and nitroalkylated (G) Cys61 peptide.

3.2.6 GSH noncovalently modulates GR activity

Thiol-reversibility of the covalent inhibition of GR by NO_2-OA was recapitulated with the endogenous thiol GSH. However, unlike BME, GSH elicited a hormetic response in which low concentrations partially restored GR activity but higher levels resulted in enzyme inhibition (**Figure 10A**). To test if GR exhibited product inhibition *in vitro,* GR activity was assayed as a function of [GSH] (**Figure 10B**). GR activity was inhibited by 50% above 10mM GSH suggesting that this mechanism is relevant at physiologic GSH concentrations and may affect GSH equilibria inside the cell. To test if functional tuning of GR activity was a generalizable effect among different classes of therapeutic electrophiles, the triterpenoid electrophile CDDO-imidazolide (CDDO-Im), the electrophilic prodrug dimethylfumarate (DMF) and the active DMF hydrolysis product monomethylfumarate (MMF) were evaluated. These species did not inhibit GR, indicating that this activity was specific for NO_2-FA and not a general characteristic of electrophilic species (**Figure 10C**). Based on the product inhibition observed with GSH, it was hypothesized that electrophiles which do not inhibit GR directly may nonetheless exert indirect inhibition and induce GSSG accumulation through upregulation of GSH. CDDO-Im activated Nrf2 and strongly upregulated GCLM (**Figure 10D**). To compare temporal effects of CDDO-Im and NO_2-OA, a time-course experiment was performed evaluating GSH and GSSG 0-24hr after electrophile exposure. Changes in GSH induced by CDDO-Im were comparable to those induced by NO_2-OA, and increased intracellular GSH 1.5-fold after 6hr. Notably, despite the lack of direct GR inhibition *in vitro*, CDDO-Im treatment significantly increased (3 fold) GSSG (**Figure 10E-F**). Treatment of

cells with DMF, CDDO-Im, CDDO-Methyl (CDDO-Me; a structural analog of CDDO-Im), or NO_2-OA for 6hr increased [GSH] 1.5-fold, and the extent of GSH upregulation was similar or identical between all compounds tested (**Figure 10G**). By contrast, [GSSG] was increased 3-4-fold by DMF, CDDO-Im and CDDO-Me, it was increased >20-fold by NO_2-OA (Fig. 9H). All 4 electrophiles paradoxically reduced the GSH:GSSG ratio, with NO_2-OA inducing the largest decrease (**Figure 10H**).The large increase in GSSG induced by NO_2-OA was found to be dose-dependent with respect to [NO_2-OA] (**Figure 11A-C**), indicating that NO_2-OA had a direct effect on GR activity in cells.

Strikingly, the increase in intracellular GSSG in response to CDDO-Im was not dose-dependent with respect to [CDDO-Im]. Four concentrations (50-400nM) of CDDO-Im tested, which were all within the range to activate Nrf2 and upregulate GSH, led to 50% increase in [GSH] and ~4-fold increases in GSSG (**Figure 11D-F**). In a separate experiment (**Figure 11G**), CDDO-Im (200nM) did not increase Prdx oxidation, suggesting that product inhibition by GSH and not oxidative stress was responsible for GSSG accumulation.

Together these results implicate two separate and specific mechanisms by which electrophiles induce the accumulation of intracellular GSSG: covalent inhibition at catalytic Cys61 in the case of NO_2-OA and product inhibition secondary to activation of Nrf2 and upregulation of GSH in the case of fumaric acid- and triterpenoid-derivatives which do do not directly inhibit GR.

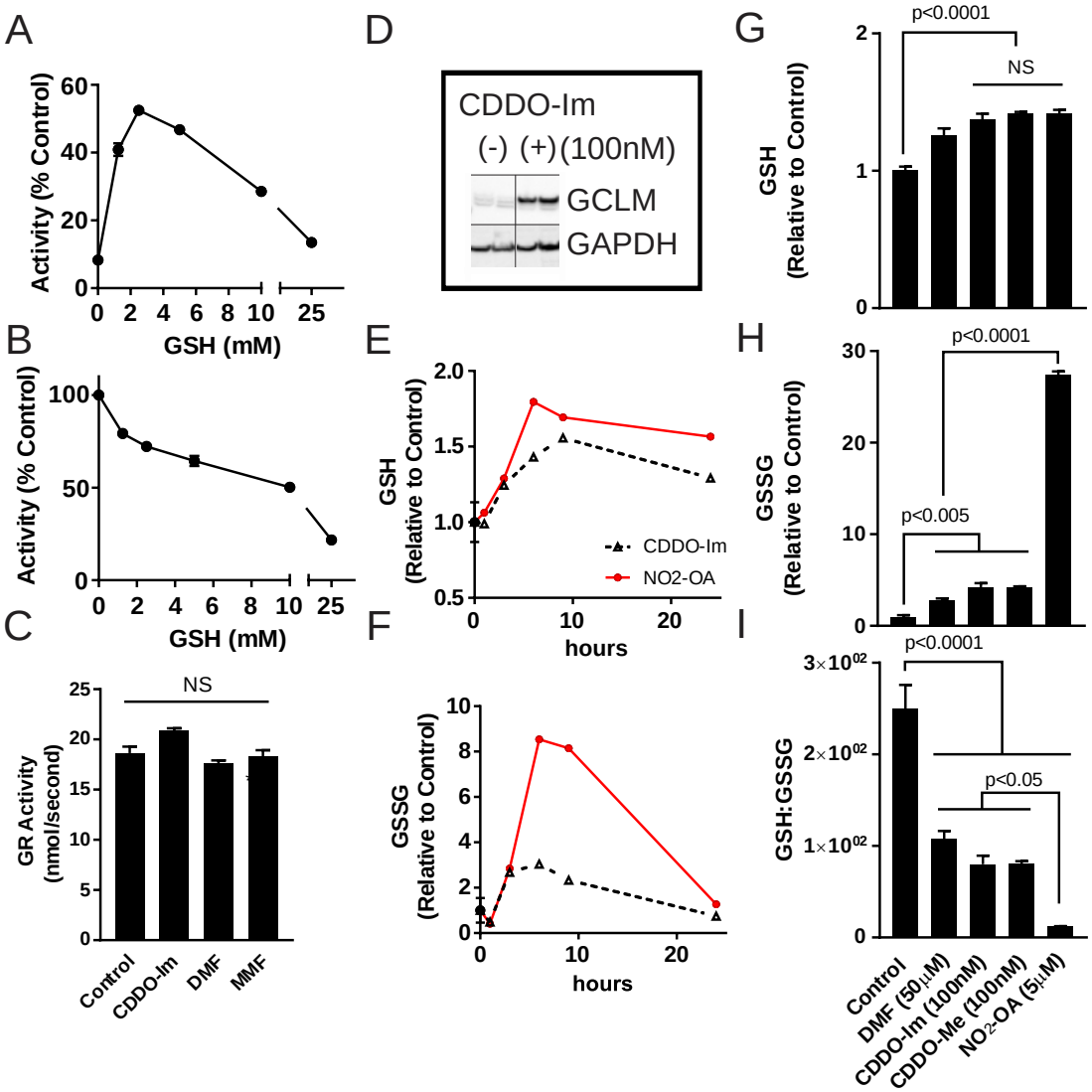

Figure 10: GR is sensitive to product inhibition in context of electrophile-induced upregulation of [GSH]

(A) Hormetic reversal of NO_2-OA inhibition of GR by GSH. GR inhibited with NO_2-OA was treated with increasing concentrations of GSH and activity was assayed. (B) GSH is an allosteric negative regulator of GR activity. GR rate was measured in absence or presence of physiologically relevant concentrations of GSH and displayed dose-dependent reduction in activity suggesting product inhibition. (C) Electrophiles CDDO-Im, DMF, and MMF do not inhibit GR activity *in vitro*. (A-C) For each experiment 3.36mU GR was incubated in 145µL 5µM NO_2-OA or vehicle control for 10min at ambient temperature. Rates are reported as % control ± SD (A-B) or nmol/sec GSSG (C) from 3-5 independent experiments; for some points, the error bars are shorter than the height of the symbol. (D) CDDO-Im (100 nM) induces GCLM expression in RAW264.7 macrophages. Vertical line indicates intervening lanes cropped to approximate non-adjacent bands from one blot showing two biological replicates. (E-I) Electrophiles that do not

inhibit GR *in vitro* nonetheless increase [GSSG]. Increased levels of GSH (E) and GSSG (F) in RAW264.7 macrophages following treatment with 5 μM NO_2-OA (red) or 100 nM CDDO-Im (dashed) for indicated times. (G) GSH, (H) GSSG, and the ratio of GSH:GSSG (I) in RAW264.7 cells after 6hr treatment with indicated electrophilic ligands. Statistical analysis by one-way ANOVA with Bonferroni correction for multiple comparisons; for some groups, error is less than thickness of the error bar.

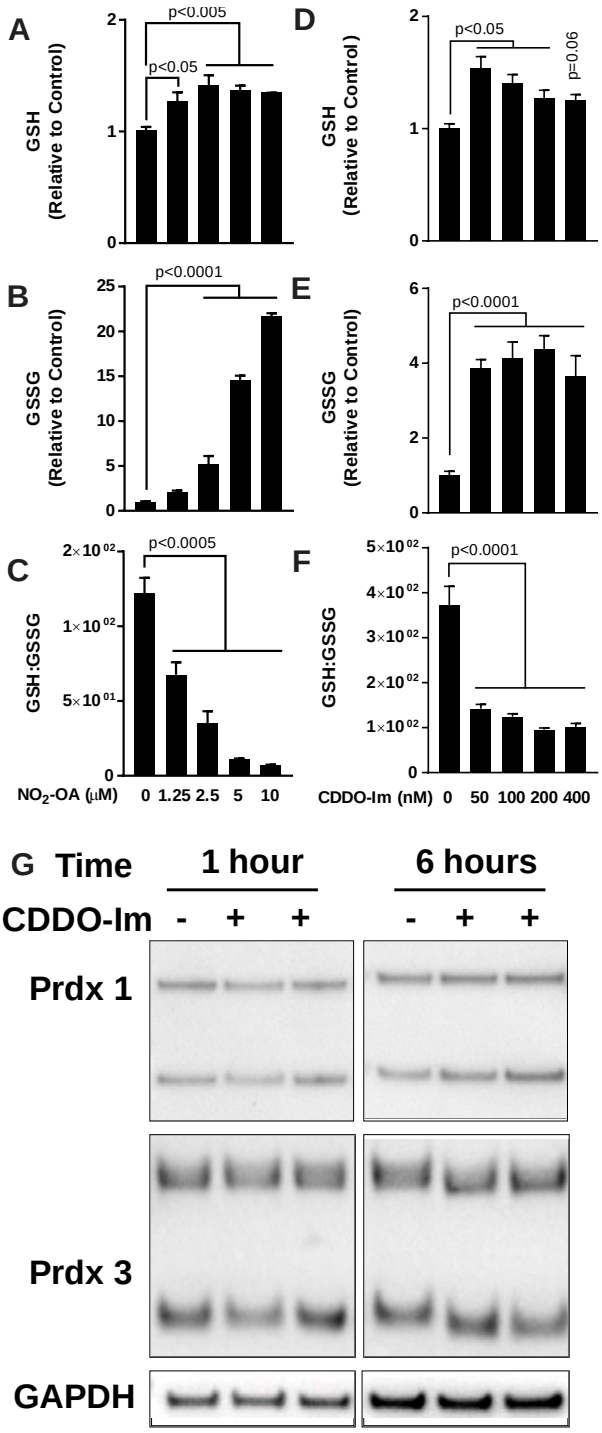

Figure 11: NO_2-OA but not CDDO-Im dose-dependently increases intracellular GSSG

RAW264.7 macrophages incubated with increasing concentrations of NO_2-OA (A-C) or CDDO-Im (D-F) for 6hr followed by measurement of (A, D) GSH, (B, E) GSSG, and calculation of GSH:GSSG ratio (C, F). Despite equivalent increase in GSH over baseline by all concentrations of NO_2-OA tested, a dose-dependent accumulation of GSSG was

observed, supporting that NO_2-OA inhibits GR in cells as well as *in vitro*. No dose-dependent accumulation of GSSG was observed in CDDO-Im treated cells, suggesting that CDDO-Im inhibits GR indirectly through upregulation of [GSH]. Immunoblotting for monomeric and dimeric Prdx1 and Prdx3 after 1 and 6hr treatment with 200nM CDDO-Im revealed no increase in cytosolic or mitochondrial Prdx oxidation. Statistical analysis by one-way ANOVA with Dunnett test, comparing treatment groups to control (DMSO).

3.2.7 Theoretical predictions of GSH/GSSG with GSH inhibition of GR based on published kinetic parameters

I would like to acknowledge the significant contributions of Dr. Jack Lancaster, PhD, who performed the computational modeling described in this section.

Spurred by the observation that electrophiles which do not covalently inhibit GR nonetheless increase [GSSG], we hypothesized that product inhibition may be a biochemically relevant phenomenon in cells. Examination of the relative cellular concentrations of GSH and GSSG when the total amount of glutathione (denoted as the concentration of glutamyl residue $[GS]_T$ = [GSH] + 2x [GSSG]) increases without changes in the oxidative conversion of GSH into GSSG provides a unique opportunity to gain insight into the enzymatic mechanisms that determine GSH homeostasis(182). Increasing $[GS]_T$ without change in the oxidative environment results in an apparent increase in [GSSG] relative to [GSH], and provides evidence suggesting that this may be a result of allosteric inhibition of GR by GSH, as reported previously for the isolated enzyme(183, 184). It is possible to kinetically model the cellular effects of this inhibition and to quantitatively compare our experimental results with theoretical predictions. Although kinetic modeling approaches have been applied previously to the GSH/GSSG system(185–195), to our knowledge the inhibition of GR by GSH has not been included. To perform this modeling a constant level of

cellular H_2O_2 of 1 µM was assumed where the major hydroperoxidase is selenocysteine-containing glutathione peroxidase (GPx)(187), with regeneration of GSH by GR. Regeneration of reduced GR by NADPH was assumed to be more rapid than these enzymatic reactions. **Figure 12** presents a simplified mechanism for metabolism of H_2O_2, GSH, and GSSG with v_1 and v_2 denoting the rates of GR and GPx respectively.

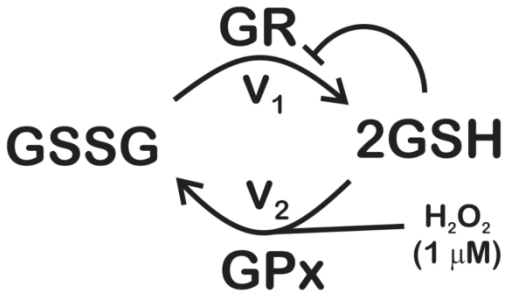

Figure 12: GSH cycling by GR and GPx

We assume that at steady-state the rate of GR (v_1, Equation 1: Steady-state rate of GR) is given by the Michaelis-Menten equation with uncompetitive inhibition by GSH, with K_m = 35 µM and K_i = 6.6 mM(184):

$$\upsilon_1 = \frac{V_{\max}[GSSG]}{\left(1+\frac{[GSH]}{K_3}+\frac{[GSH]^2}{K_3K_4}\right)K_m+\left(1+\frac{[GSH]}{K_5}+\frac{[GSH]^2}{K_5K_6}\right)[GSSG]}$$

Equation 1: Steady-state rate of GR

The steady-state rate of GPx (v_2, Equation 2) is given by the rate equation for the enzyme-substitution mechanism with constant [H_2O_2] incorporated in the k_3 term (16), as presented in **Figure 13**.

Elementary Reactions and Initial Conditions:

GR:

(1) $GR + GSSG \rightleftarrows GR{\bullet}GSSG$

(2) $GR{\bullet}GSSG \rightarrow GR + 2GSH$

$k_{1f} = 1\times10^{7}\,M^{-1}s^{-1}$

$k_{1r} = 8.692\times10^{2}\,s^{-1}$

$k_{2} = 10.8 s^{-1}$

$[GR]_o = 3\times10^{-5} M$

$[GSH]_o = [GSSG]_o / 2 = 2\times10^{-5} M$

$[GPx]_o = 2\times10^{-7} M$

$[GCL]_o = 1M$

Noncompetitive Parabolic GR Inhibition by GSH:

$k_{3f}, k_{4f}, k_{5f}, k_{6f} = 1\times10^{7}\,M^{-1}s^{-1}$

(3) $GSH + GR \rightleftarrows GRi1$

(4) $GSH + GRi1 \rightleftarrows GRi2$

(5) $GSH + GR{\bullet}GSSG \rightleftarrows GRi3$

(6) $GSH + GRi3 \rightleftarrows GRi4$

$k_{3r} = 4.8\times10^{4}\,s^{-1}; K_3 = 4.8\ mM$

$k_{4r} = 1.479\times10^{5}\,s^{-1}; K_4 = 14.79\ mM$

$k_{5r} = 3\times10^{4}\,s^{-1}; K_5 = 3\ mM$

$k_{6r} = 1.1\times10^{4}\,s^{-1}; K_6 = 1.1\ mM$

Gpx:

(7) $GPxR \rightarrow GPxO$

(8) $GSH + GPxO \rightarrow GPxG$

(9) $GPxG + GSH \rightarrow GPxR + GSSG$

$k_7 = 50 s^{-1}$

$k_8 = 1\times10^{7}\,M^{-1}s^{-1}$

$k_9 = 1\times10^{5}\,M^{-1}s^{-1}$

$k_7 = k_{7'}\times[H_2O_2]$

$k_{7'} = 5\times10^{7}\,M^{-1}s^{-1}$

$[H_2O_2] = 1\times10^{-6}\ M$

Increase in $[Glu]_T$:

(10) $GCL \rightarrow GSH$

$k_{10} = 5.6\times10^{-8}\,s^{-1}$

Figure 13: Rate constants used for steady-state calculations

$$v_2 = \frac{k_7[GPx]_T[GSH]}{\frac{k_7}{k_9} + [GSH]}$$

Equation 2: Steady-state rate of GPx

Numerical integration of the governing rate equations was performed to predict the relative concentrations of GSSG and GSH as the total $[GS]_T$ is increased (**Figure 14A**). As time is gradually increased, enzymatic instantaneous steady-state conditions for each time point are achieved by employing enzymatic rate constants that are much faster than the rate of increase in $[GS]_T$ (reaction (10) in Figure 13: Rate constants used for steady-state calculations). The values for K_3 and K_4 for noncompetitive parabolic inhibition are taken from published values for the rat

liver enzyme and the values for K_5, K_6, and V_{max} (for GR, v_1) and $[GPx]_o$ (for GPx, v_2) are set to achieve optimal fit to the data (steady-state [GSSG], [GSH]) for all electrophiles except NO_2-OA.

Figure 14B shows that steady-state is achieved very early during the calculation (within 5 sec) and the inset shows that the rates of each enzymatic reaction are equal ($v_1 = v_2$) at every point throughout the calculation, a requirement for steady-state. In addition, this shows that the calculated results are identical to the results predicted by the steady-state derivation (Eq. 1 and 2).

Figure 14C shows that the model accurately predicts the experimental results for [GSSG] and [GSH] for all electrophiles except NO_2-OA. It is clear that as the total $[GS]_T$ approaches 10 mM there is a dramatic increase in [GSSG] with only modest increases in [GSH].

To examine the mechanistic basis for this phenomenon, **Figure 14D** shows the distribution of GR between different forms as $[GS]_T$ is increased. The noncompetitive parabolic binding of GSH to both GR and GR-GSSG results in conversion of active enzyme (GR) into inactive GRi forms; however, the overall rate of GSSG reduction to GSH (v_1) remains relatively constant (**Figure** 14:**B** inset). This is because at [GSH] > 5 mM GPx is saturated ($K_m = k_7/k_9 = 0.5$ mM, Eq. 2) and so the rate v_2 is maximal and constant, equal to $k_7[GPx]_T$. Because of the steady-state condition $v_1 = v_2$ and so v_1 is also constant. Therefore, the only way to counteract loss of active enzyme (**Figure 14D**) is to increase substrate (GSSG) concentration for the remaining active enzyme. This illustrates the concept that major changes in the relative amounts of GSH and GSSG can occur independently of changes in oxidative conversion of GSH into GSSG (indeed, the rate of this conversion, v_2, is essentially unchanged, **Figure 14B** inset).

Figure 14E includes the NO_2-OA data in comparison to the other electrophiles and the model prediction. In contrast to the other electrophiles, the extent of [GSSG] increase (due to inhibition) is much more dependent on the NO_2-OA concentration and not on the GSH

concentration. This emphasizes our conclusion that the primary mechanism for NO_2-OA I by adduction rather than as result of increase of $[GS]_T$. Finally, in order to test how much tolerance there is in the values for the adjusted parameters K_3 and K_4, **Figure 15** shows that the model provides a reasonable fit to the data only when these values vary by no more than approx. ± 15%.

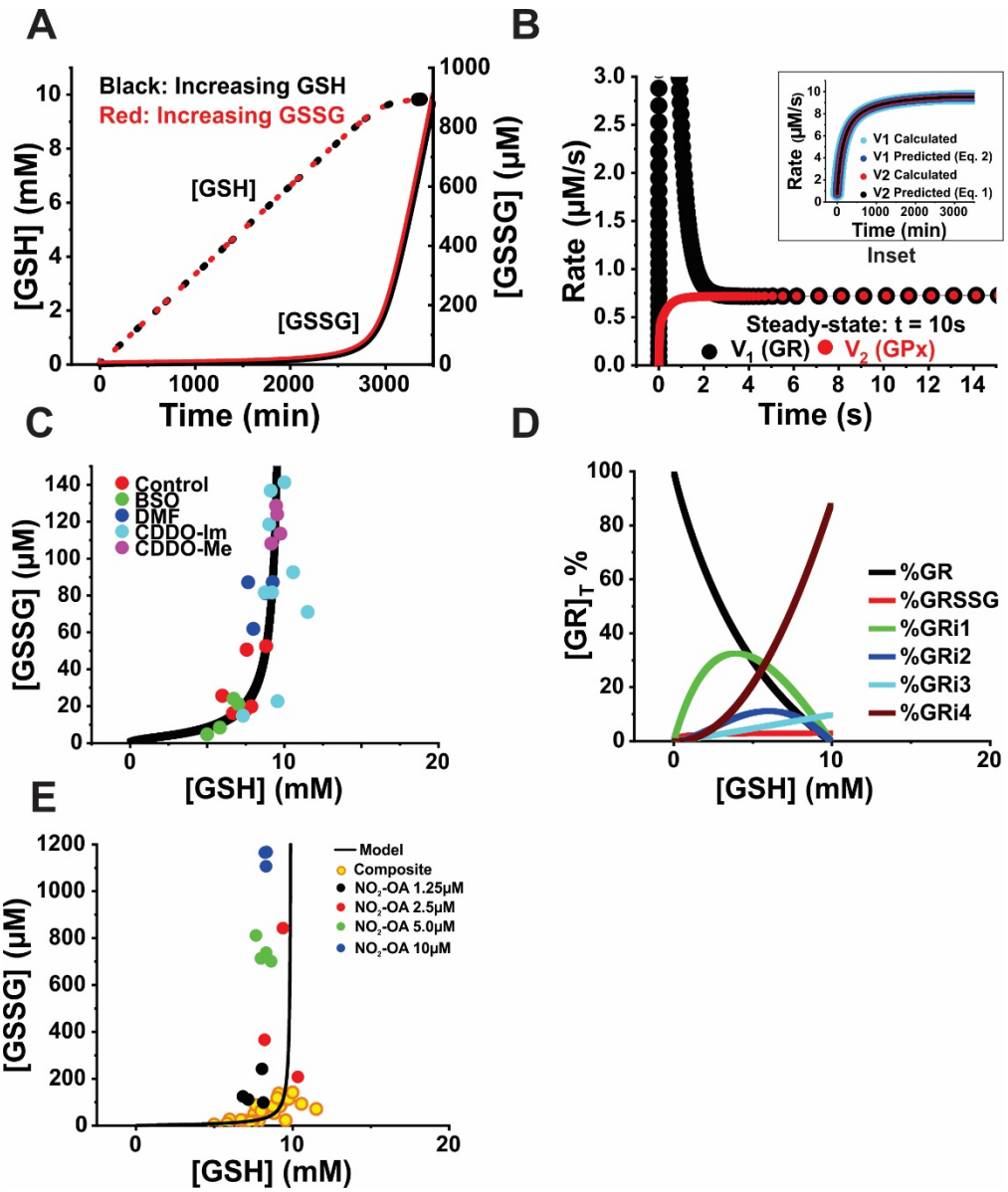

Figure 14: Theoretical predictions of GSH/GSSG couple support product inhibition of GR

(A) Computed increases in [GSH] (dashed line) and [GSSG] (solid line) with increasing $[GS]_T$ by generation of GSH (red) or GSSG (black), using the model described in Figure 13: Rate constants used for steady-state calculations.. (B)

Rapid establishment of steady-state equilibrium between GR (black) and GPx (red). Inset: Fidelity of predictions by calculation (integrated rate expressions) and steady-state (Michaelis-Menten) theory. (C) Unbiased assessment of GSH plotted as a function of GSSG in cells treated with vehicle (red), CDDO-Im (light blue), CDDO-ME (purple), DMF (dark blue), or BSO (green) for 6 hr. Each data point depicts one cell culture sample. Curves representing theoretically predicted distributions are superimposed with (black) and without (magenta) modeling uncompetitive inhibition of GR by GSH. (D) Simulation of relative abundances of active and inactive (inhibited) GR forms $GR_{i1\text{-}4}$. (E) [GSH] and [GSSG] in cells treated with pharmacologically relevant concentrations of NO_2-OA compared to simulation model (black line) and data shown in (C) (yellow).

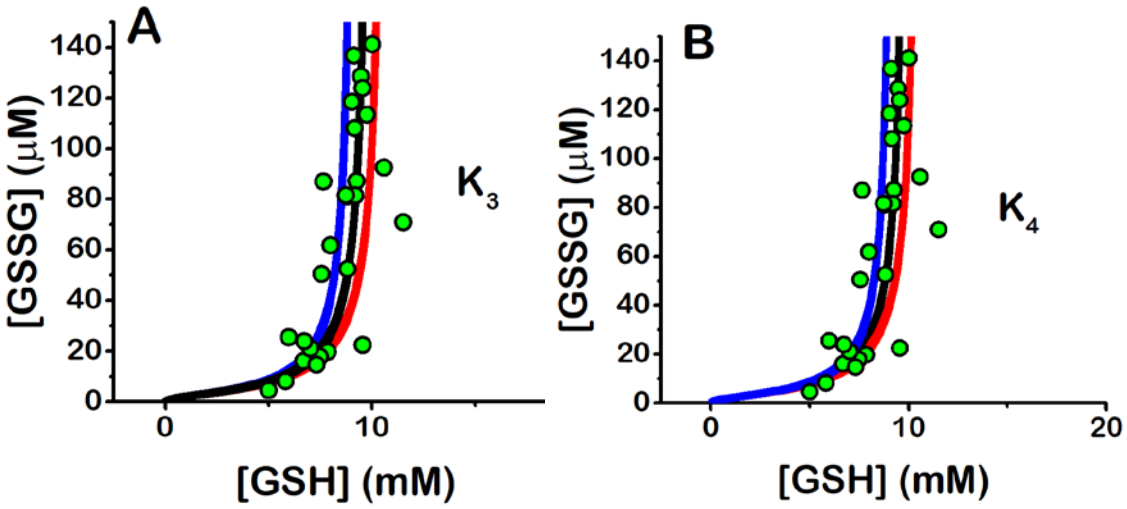

Figure 15: Model shows a reasonable fit of data when K_3 (A) and K_4 (B) are varied +/- 15%

3.2.8 Nrf2 activation increases protein S-glutathionylation

GSH and GSSG participate in the post-translation modification of cysteine thiols(196). Based on the contributions of GSH (GST catalyzed) and GSSG (thiol disulfide exchange) to S-glutathionylation, it was hypothesized that the elevation of both GSH and GSSG by NO_2-OA would promote cell protein glutathionylation. To quantitatively test this hypothesis, an analytical method was developed (**Figure 16A)**. Briefly, cell lysates were immediately alkylated with excess N-methylmaleimide (NMM) and proteins isolated by size-exclusion chromatography. The protein fraction was then treated with BME to release GSH from glutathionylated proteins, followed by free GSH alkylation with NEM and LC-MS/MS detection of the GS-NEM adduct. Applying this technique, total protein glutathionylation was found to increase 5-fold in RAW264.7 macrophages incubated with 5µM NO_2-OA for 6 hr, from a baseline of 0.10pmol/µg protein to 0.55pmol/µg protein (**Figure 16B-C)**.

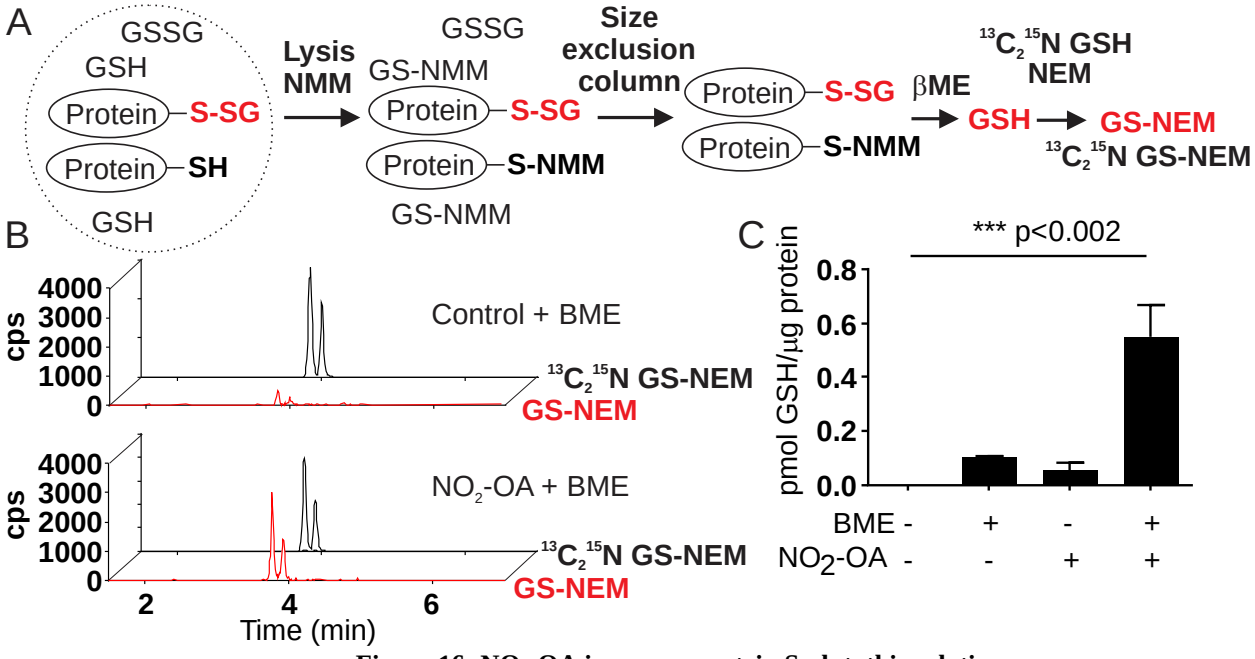

Figure 16: NO_2-OA increases protein S-glutathionylation

(A) Schematic of novel iterative alkylation-reduction-alkylation method for HPLC-MS/MS quantitative determination of protein S-glutathionylation. Representative traces of GS-NEM derived from protein S-glutathionylation (B) and quantification of protein S-glutathionylation (C) in RAW264.7 cells treated with control or 5μM NO2-OA for 6 hr. Results are shown as mean ± SD (n=3, *** $p < 0.002$, one-way ANOVA with Tukey's multiple comparison test)

3.2.9 GSH modulates the macrophage inflammatory response

NO_2-OA displays immunomodulatory effects in both *in vitro* and *in vivo* disease models(60, 75, 197, 198). In the context of NO_2-OA induced elevation in intracellular GSH, we sought to investigate if changes in intracellular GSH levels contributed to the modulation of inflammatory cell activation (**Figure 17**). RAW264.7 macrophages were incubated for 24 hr with BSO or vehicle, then activated with LPS and pro-inflammatory IL-6 expression was measured 6 hr later. Consistent with published reports(199), pharmacological GSH depletion led to a significant increase in transcript level of the pro-inflammatory cytokine IL-6 (**Figure 17A**). Subsequently, experiments were done to test if constitutive genetic Nrf2 activation recapitulated effects of NO_2-OA on inflammatory activation through modulation of GSH. Primary bone marrow-derived macrophages (BMDM) were generated from wild-type or $Keap1^{flox/flox}$ mice which exhibit constitutive Nrf2 activation due to hypomorphic expression of Keap1(41). At baseline, GCLM expression was elevated 3.4-fold in $Keap1^{flox/flox}$ BMDM compared to wild-type counterparts (**Figure 17B**). Importantly, this increase in GCLM expression is quantitatively comparable to that obtained upon pharmacological Nrf2 induction by NO_2-OA treatment. Intracellular GSH accumulated in concert with increased GCLM expression, with significantly more GSH in $Keap1^{flox/flox}$ BMDM as compared to WT BMDM (**Figure 17C**). Consistent with the observation in the immortalized RAW264.7 murine macrophage cell line, LPS-dependent IL-6 expression was

potentiated ~2-fold in GSH-depleted WT BMDM (**Figure 17D**) but was significantly lower in Keap1$^{flox/flox}$ cells. Notably, pharmacological GSH depletion of Keap1$^{flox/flox}$ BMDM led to a partial restoration of the inflammatory response to LPS.

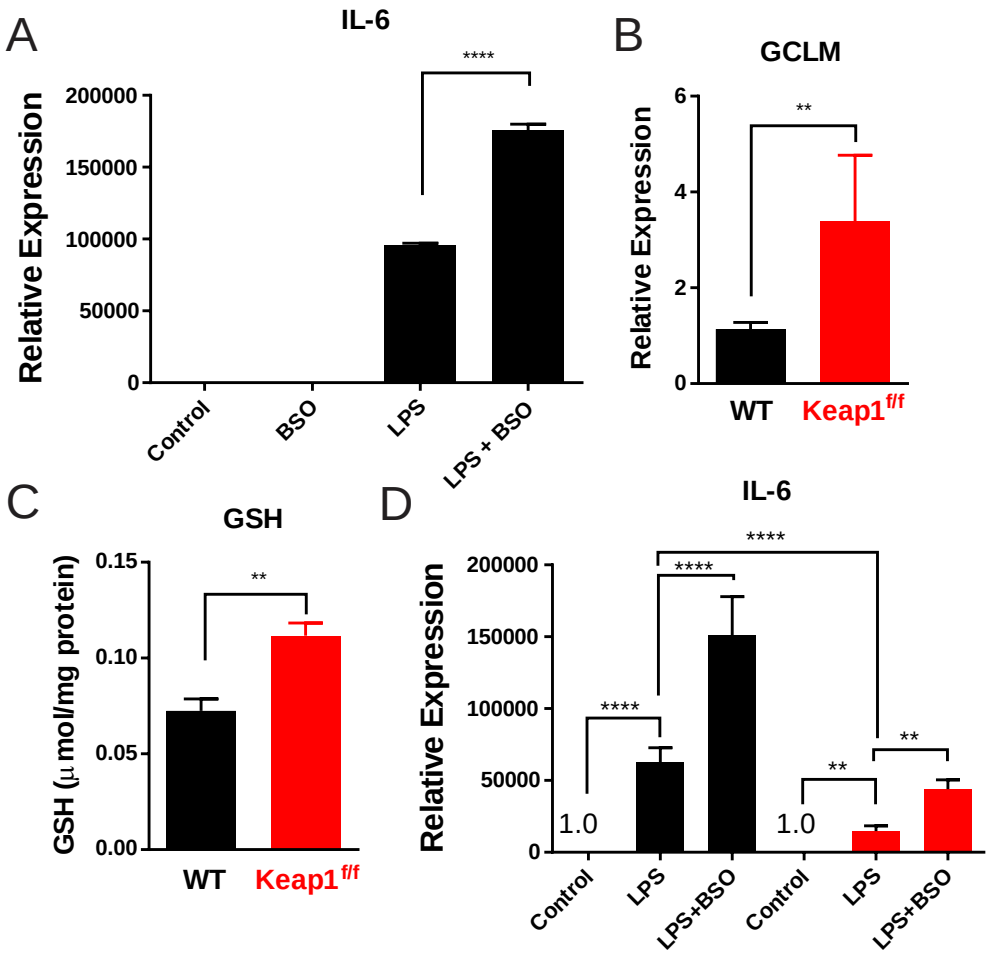

Figure 17: Glutathione reduces macrophage inflammatory responses.

(A) Increased IL-6 gene expression in RAW264.7 cells treated with 20 μM BSO for 24 hr followed by 6 hr activation with 200 ng/mL LPS. Increased GCLM gene expression (B) and GSH levels (C) in primary bone marrow-derived murine macrophages (BMDM) from Keap1$^{f/f}$ mice. *** Student's t-test, $p<0.005$. (D) Increased IL-6 expression in WT and Keap1$^{f/f}$ BMDM treated with BSO for 24 hr followed by stimulation with 200 ng/mL LPS for 6 hr. (A) Gene expression relative to actin. (B) and (D) Gene expression relative to GAPDH. ** $p<0.001$, **** $p<0.0001$ by one-way ANOVA.

3.3 DISCUSSION

The value of therapeutic electrophiles has gained recognition in the last decade, and considerable efforts are invested in both the addition of electrophilic groups to conventional inhibitors to decrease dissociation constants(200, 201), and the development of novel molecules to target signaling pathways that display a particular sensitivity to electrophiles (e.g. Nrf2, Nf-kB, heat shock responses)(202). In particular, DMF, an electrophile that targets Nrf2, has been shown to significantly reduce progression of relapsing-remitting multiple sclerosis and exert a protective effect in severe psoriasis. The DMF preparations Tecfidera® and Fumaderm® are approved for treatment of these diseases in the USA and Germany, respectively. In addition, other electrophilic molecules in the form of pharmacologic agents or dietary supplements (e.g. Bardoxolone, 10-NO_2-OA, sulforaphane) are in advanced stages of clinical trials. In this context, we initiated this work to characterize the effects of electrophiles, in particular NO_2-OA, on GSH levels and redox status regulation.

GSH, with intracellular concentrations in the millimolar range and numerous enzymatic and non-enzymatic modes of reactivity, is decisively positioned to act not only as a redox buffer but also as a main target of electrophiles. The molecular pleiotropy of the GSH system is further affirmed by its ubiquity, penetrance and complexity in modulating cell signaling activities, detoxification and downstream post-translational protein modifications. The genetic and pharmacological manipulation of the GSH/GSSG couple allowed us to study its impact on temporal responses to oxidative and electrophilic stress. Cell exposure to NO_2-OA for 1 hr leads

to a slight decrease in GSH levels, likely caused by adduct formation, which has been previously documented(176). This initial decrease was followed by a rebound in intracellular GSH levels that peaked at 6 hr. The increase in GSH was not temporally linked to GCLM protein expression, which was maximal at 24 hr and under Nrf2 control, suggesting GCLM levels are not the rate limiting factor on GSH synthesis at the early time points. It is known that activation of Nrf2 may also impact import of cysteine, a precursor in the synthesis of GSH(9).

Notably, the increase in GSH levels (1.5-2 fold) occurred concomitantly with an unexpected and paradoxical increase in intracellular GSSG. This result is in close agreement with prior observations which showed that both the thiol antioxidant/GSH-precursor N-acetylcysteine and GCLC/GCLM over-expression concomitantly increase GSH and GSSG levels (203). However, the authors in this prior study concluded that the mechanism underlying GSSG accumulation was related to cellular damage induced by reductive stress. In the setting of NO_2-OA-induced Nrf2 activation, analysis of Prdx 1 and 3 dimerization status did not indicate significant alterations in endogenous peroxide levels or impaired ability to respond to oxidative insults. Additionally, inhibition of MRP1 with known inhibitors MK571 and probenecid proved insufficient to elevate intracellular GSSG.

Rather, the present investigation revealed two discrete mechanisms underlying this phenomenon, both of which converge on the intuitive, yet underappreciated concept that the GSH:GSSG ratio is regulated primarily by the activity of GR. Specifically, our findings indicate that electrophiles modulate the GSH redox couple by direct pharmacological inhibition and indirect product inhibition of this enzyme (**Figure 18**).

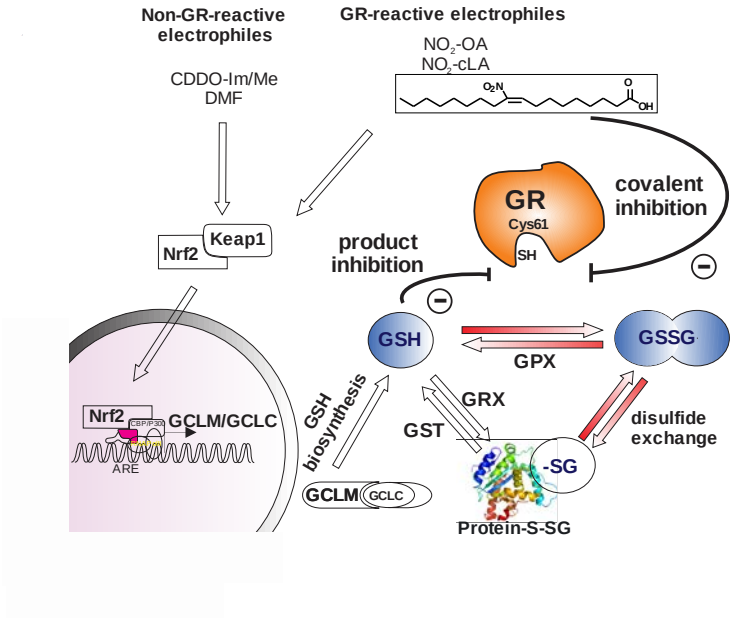

Figure 18: Schematic showing GR-dependent and GR-independent modulation of GSH homeostasis by electrophiles

Based on the fact that GR has two catalytic cysteines that form a disulfide during enzymatic redox cycling and that these cysteines are covalently modified by GR inhibitors(204), we explored the modulation of GR activity by NO_2-OA. NO_2-OA is known to modify several enzymes that contain catalytic thiol centers, such as glyceraldehyde-3-phosphate dehydrogenase, (83), 5-lipoxygenase(205) and soluble epoxide hydrolase(206). Herein, we showed that NO_2-OA directly inhibits GR in a NADPH dependent pathway that involved nitroalkylation of Cys61 as demonstrated by biotin-tagging and mass spectrometric analysis. Kinetic characterization shows that NO_2-OA reacts with GR ten times faster than with GAPDH. In cells, increases in GSSG induced by NO_2-OA displayed dose-dependence, suggesting that the *in vitro* inhibition of GR was recapitulated in a complex, intact cellular system. Nonetheless, NO_2-OA inhibition of GR was rapidly reversed by the low molecular weight thiol BME. Furthermore, when the reversibility assay was repeated using different concentrations of GSH as the competing thiol, the response was bell-

shaped, with increasing concentrations of GSH initially restoring GR activity while levels above 2.5 mM reducing GR activity. In this regard, macrophage incubation with other electrophiles (CDDO-Im, CDDO-Me, and DMF) that did not directly inhibit GR, resulted in GSH and GSSG accumulation. The increase in GSSG elicited by CDDO-Im was found to be proportional to the increase in [GSH] but independent of electrophile concentration. This led us to propose an additional mechanism for GSSG accumulation based on product inhibition of GR.

Evidence for product inhibition of GR by GSH was first published nearly three decades ago using isolated GR preparations but these observations were never further explored or extended to complex, dynamic cellular systems (183, 184). Of relevance, the range of concentration at which GSH allosterically inhibits GR activity in these studies was between 8-13 mM; in our experiments IC_{50} (~10 mM) directly relates to GSH concentrations found in cells (between 6-9 mM). Offering support to this regulatory process, depletion of GSH with BSO resulted in ~2-fold greater reduction in GSSG than in GSH (**Figure 3**).

Collective unbiased expression of [GSSG] as a function of [GSH] showed a positive non-linear correlation. BSO-treated cell populations clustered in the bottom-left quadrant of the distribution while electrophile-treated populations clustered in upper-right. Computational simulation of the steady-state GSH system using a numeric integration approach with published parameters showed that product inhibition of GR was necessary to accurately fit the model to these experimental data (**Figure 14C**) These results are incompatible with a "static" concept of glutathione cycling, in which the relative abundances of GSH and GSSG are solely dependent upon oxidant load and where GSH depletion via oxidation is prerequisite to GSSG accumulation. Instead, they suggest that in the absence of oxidative stress, [GSSG] is determined by flux through GR, which is subject to product inhibition by [GSH].

It is possible that the responsiveness of GR to intracellular [GSH] evolved as a mechanism to optimize allocation of reducing equivalents. In a reducing or unstressed state, this mechanism could redeploy energetically expensive reducing equivalents (NADPH) from generating unneeded GSH to other biosynthetic pathways, such as production of lipids and nucleic acids. At the same time, such a system would permit cells to immediately increase flux through the glutathione cycle when contending with oxidative insults by bypassing the need for *de novo* GR expression. In aggregate, the control of GSH:GSSG couple is shown to be independent of oxidative stress and supports the hypothesis that the kinetic couple reflects the antagonistic actions of enzymatic consumption and regeneration of GSH, as opposed to a thermodynamic state with discrete physiological correlates (139). In contrast, the covalent inhibition of GR by NO_2-OA resulted in dose-dependent increase in GSSG levels, demonstrating the importance of functional tuning of electrophile reactivity for specific targets and applications.

4.0 GENETIC ACTIVATION OF NRF2 PROTECTS AGAINST LITHIUM-INDUCED NEPHROGENIC DIABETES INSIPIDUS

4.1 INTRODUCTION

The Keap1/Nrf2 signaling pathway has been well-established as a druggable target which may be exploited to protect against oxidant- or electrophile-induced tissue damage in both acute and chronic disease processes. The last 30 years have seen a dramatic increase in interest in improving human health through pharmaceutical or nutraceutical supplementation of antioxidants. However, evidence showing protection by direct administration of antioxidants has remained elusive. In one recent study N-acetylcysteine, an antioxidant which has been used as prophylaxis for contrast-induced acute kidney injury, offered no more tissue protection than sodium bicarbonate(207). In contrast to chemical antioxidants, which are presumed to directly scavenge reactive species after administration, activation of Nrf2 pre-conditions cells to respond to these insults in a localized and efficient enzyme-mediated manner, and both preclinical and clinical trials utilizing natural or synthetic Nrf2 activators have shown promising results. One electrophilic Nrf2 activator, dimethylfumarate (DMF), is FDA approved and has been discussed in detail in section **1.3.4**. Oxidative stress contributes to the etiology of both acute and chronic kidney disease, and Nrf2 activation has been found to be protective in multiple models of these conditions. However, these studies investigated inflammation and deleterious fibrotic remodeling as the primary endpoints. Consequently, not much is known about the physiologic role of Keap1/Nrf2 signaling or the potential effects of long-term activation of this pathway on renal physiology.

Recent studies using genetic models of Nrf2 hyperactivation paradoxically showed development of severe nephrogenic diabetes insipidus(47, 48). In these studies, Nrf2 hyperactivation was induced by complete knock-out of the repressor Keap1. It is significant to note, however, that the complete ablation of Keap1 used in these models may not be a pharmacologically relevant, as mice with whole-body knockout of Keap1 display early mortality due to esophageal keratosis and malnutrition during post-natal development.

In the second half of this thesis, we first hypothesized that lithium may induce nephrogenic diabetes insipidus through hyperactivation of Nrf2. This was based on the published observations that (1) lithium is an inhibitor of GSK3β(208, 209), (2) GSK3β is an inhibitor of Nrf2 activity(162, 210, 211), and (3) lithium may activate Nrf2(159, 161). Since the kidneys are heterogeneous organs with diverse and highly specialized cell types along the nephron, we first characterized the spatial distribution of Nrf2 signaling. To determine if Nrf2 activation was involved in pathogenesis of Li-NDI, we used a murine model of dietary lithium. While the mice developed NDI rapidly, the expression of Nrf2 target genes was unchanged. To determine if Nrf2 was necessary for this disease process, the experiment was repeated using $Nrf2^{-/-}$ mice. Li-NDI developed in the absence of Nrf2. Finally, mice with constitutive activation of Nrf2 brought about by hypomorphic expression of Keap1 ($Keap1^{f/f}$) were protected against Li-NDI. The mechanisms underlying the protection were evaluated. Nrf2 hyperactivation impaired vasorelaxation in isolated mesenteric and thoracodorsal arteries in a nitric-oxide independent manner, an effect which extended to systemic cardiovascular autoregulation. It is well-known that Nrf2 activations tempers inflammatory responses. Accordingly, renal expression of cyclooxygenase-1 and cyclooxygenase-2 were downregulated in kidneys from $Keap1^{f/f}$ mice, accompanied by reduction in inflammation-derived vasodilatory factors prostacyclin and kynurenine. We theorize that these

changes in vascular function are also present in the afferent arteriole of the nephron, implicating altered tubuloglomerular feedback leading to protection against NDI.

4.2 RESULTS

4.2.1 Characterization of Keap1/Nrf2 signaling in kidney

Surprisingly, despite extensive research efforts both in academia and pharmaceutical industry evaluating Nrf2 as a pharmacologic target for renal diseases, the distribution and sensitivity of Nrf2 signaling activity in the kidney has not been characterized. Immunofluorescence microscopy was performed on kidney sections from WT mice probing for the Nrf2 target NQO1 and the marker Mucin 1 (MUC1) which is expressed in the distal convoluted tubule, connecting tubule, and collecting system (212–214). NQO1 was found to be highly expressed in the renal cortex with localization to the proximal tubules (PT), which stained negative for MUC1. By contrast, glomeruli (G), vessels (V), MUC1-positive distal/connecting tubules (DT/CT), and the renal medulla displayed low expression of NQO1 (**Figure 19**).

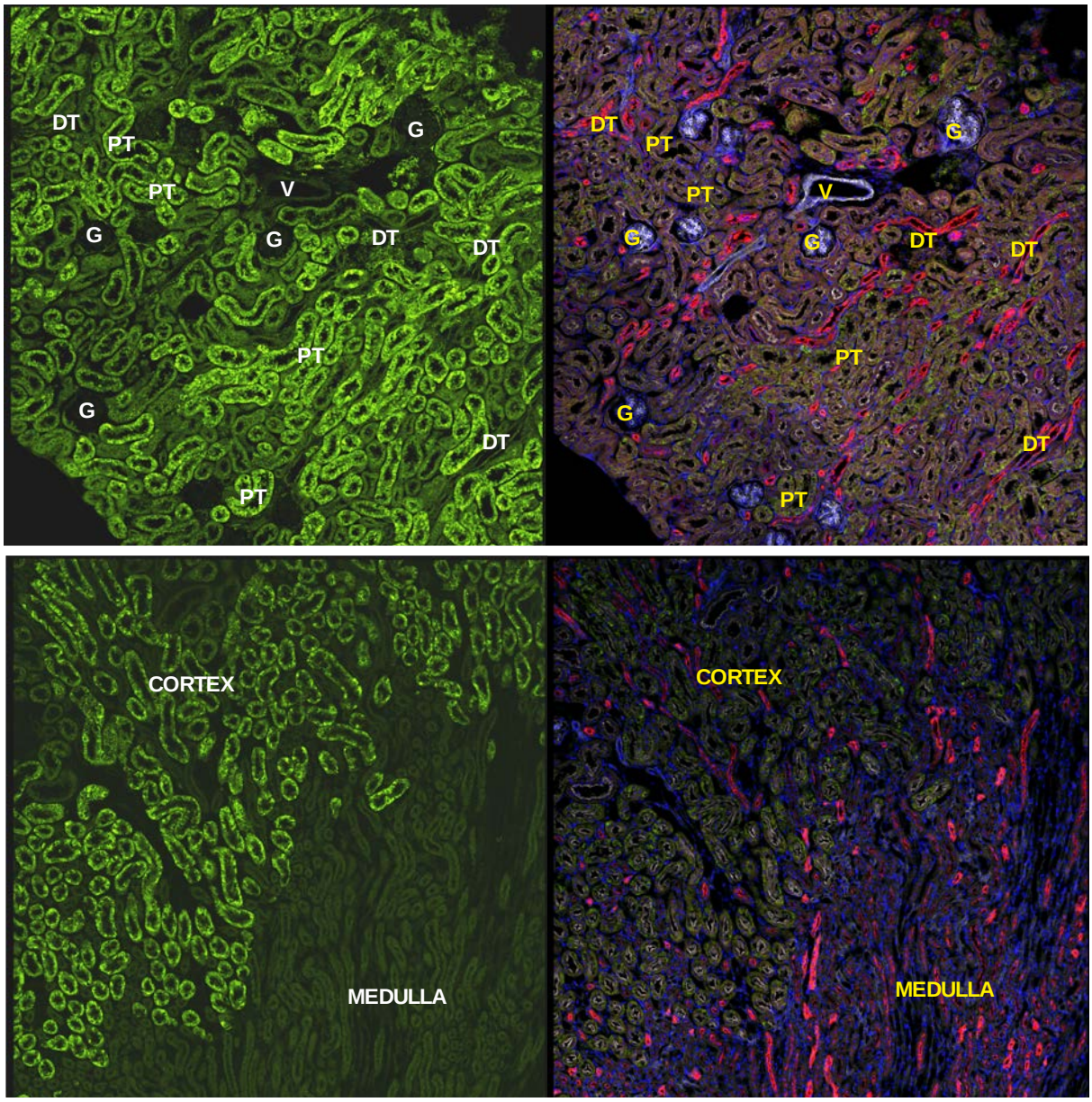

Figure 19: Localization of Nrf2 activity in murine kidney reveals proximal tubule enrichment.

Immunofluorescence microscopy evaluating NQO1 (green) and Muc1 (red) protein abundance with F-actin (phalloidin, white) and 4,6-diamidino-2-phenylindole (DAPI, blue) co-stains in wild-type mouse kidney. Left: NQO1 only. Right: Merge of NQO1, Muc1, actin, and nuclei. DT: Distal tubule; PT: Proximal tubule; V: vessel; G: glomerulus. Cortical section shown in upper panels, while junction of cortex and medulla shown in bottom panel illustrating significant cortical enrichment for NQO1.

Compared to kidneys from WT mice, Keap1$^{f/f}$ animals had hypertrophic kidneys and displayed evidence of tubular dilation (**Figure 20A, B**). NQO1 staining of kidneys from Keap1$^{f/f}$ mice showed upregulation of NQO1 in tubule segments with low Nrf2 activity in WT counterparts, but not glomeruli or vessels. Significantly, co-expression of MUC1 and NQO1 was observed in cortex suggesting increase of Nrf2 activity in DT/CT (**Figure 20C**). NQO1 abundance was found to be increased in both the outer and inner renal medulla of Keap1$^{f/f}$ animals (**Figure 20D**).

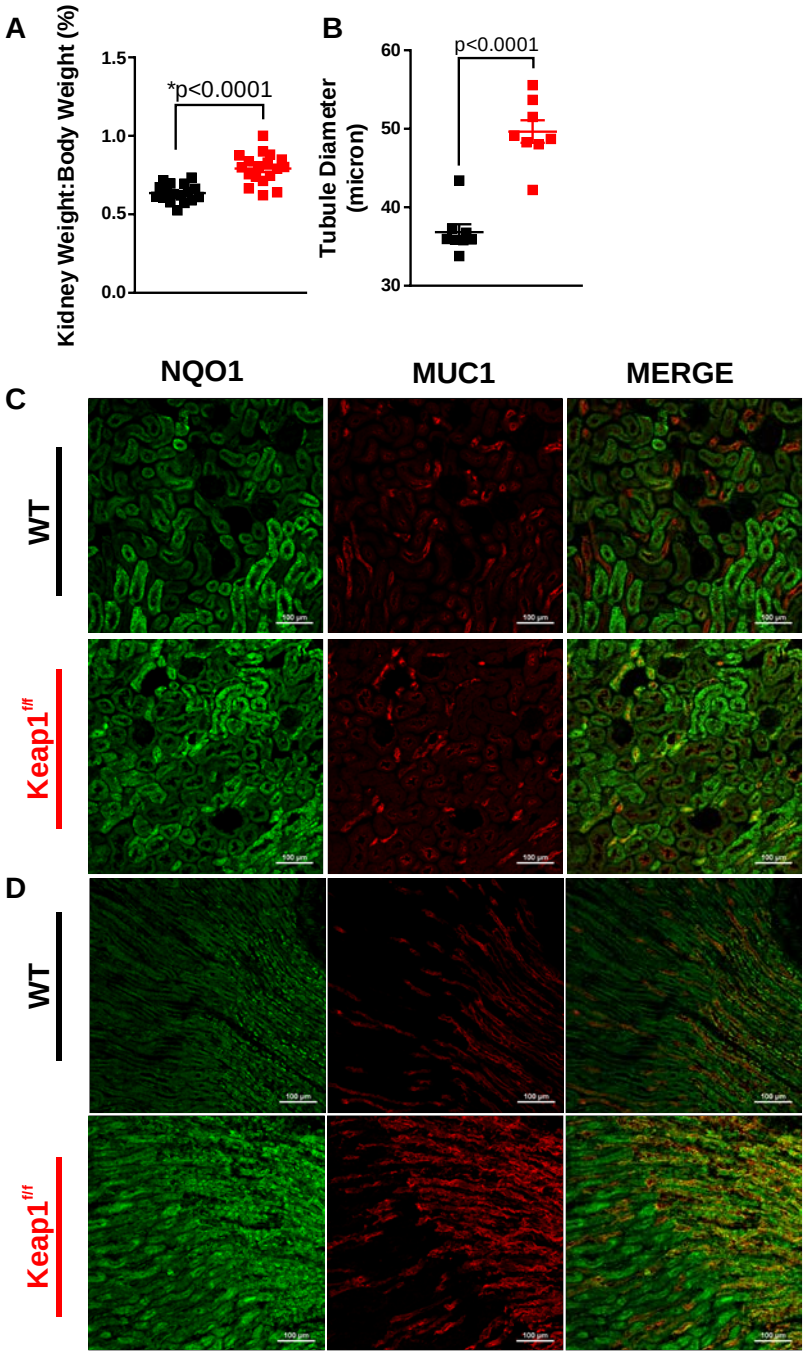

Figure 20: Nrf2 activation upregulates NQO1 in murine distal tubule and renal medulla.

Keap1$^{f/f}$ mice display renal hypertrophy (A) and tubular dilation (B). (C-D) Immunofluorescence staining for NQO1 (green) and Muc1 (red) in renal cortex (C) and medulla (D) reveals increased cortical co-localization and increased medullary expression in Keap1$^{f/f}$ mice.

Recently, a cell culture model systems of primary human renal cortical cells representing proximal and distal tubule cell populations was established(169). To test the distribution of Nrf2 and sensitivity to activation in a translational model, NQO1 expression was determined in cells immunoaffinity-isolated for CD-13 (PT) or MUC1 (DT). Cells were derived from 3 independent human donors designated HAK31, HAK10, HAK7 (2 male, 1 female) and cultured with or without the potent triterpenoid Nrf2 activator CDDO-Imidazolide (CDDO-Im) (**Figure 21**). Immunoblotting for CD-10 and MUC1 confirmed that the immunoaffinity isolation was successful and the cell populations represented the desired nephron segment. Supporting the observations made in mouse, NQO1 expression was significantly higher in proximal tubule than in distal tubule. Recapitulating the effects of genetic activation of Nrf2 in Keap1$^{f/f}$ mice, NQO1 expression was insensitive to CDDO-Im in CD-10/CD-13 positive HAK cells, whereas the MUC1 positive cells responded robustly with 3-fold elevation in NQO1.

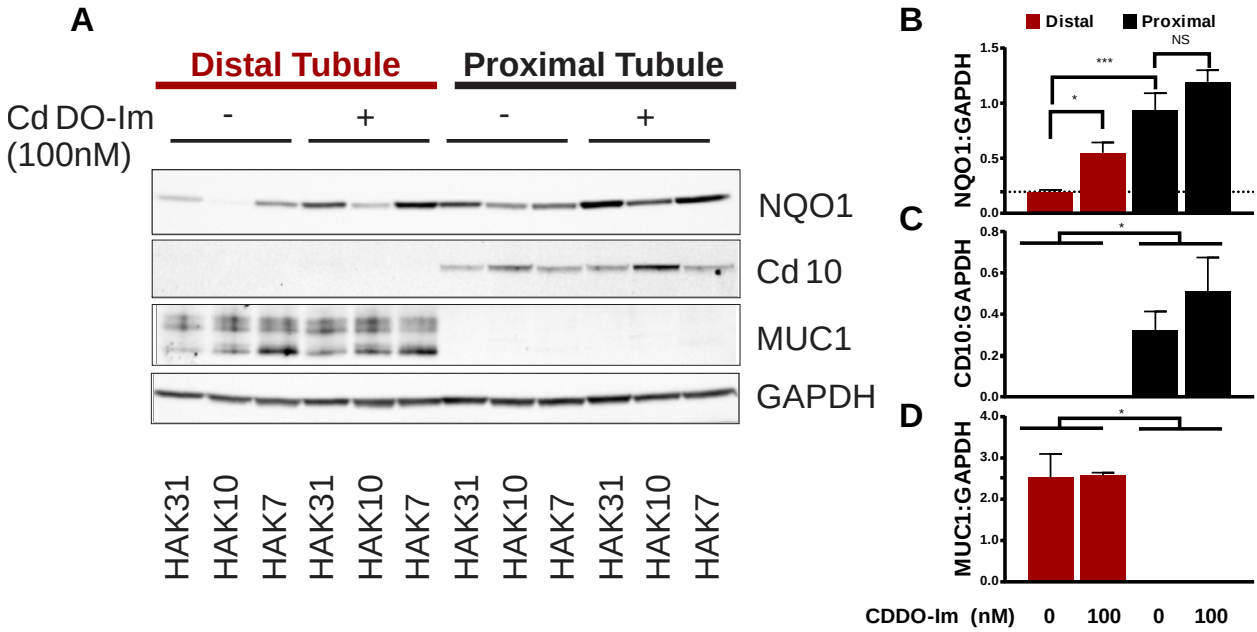

Figure 21: Distribution and electrophile responsivity of Nrf2 signaling in cultured primary human kidney epithelial cells

(A) Human kidney cortex epithelial cells from 3 separate cadaveric donor kidneys (HAK31, HAK10, and HAK7) were immunoaffinity isolated for CD13 yielding proximal tubule cell enriched population or MUC1 yielding distal tubule and cortical collecting duct cell enriched population. Cells were cultured with or without Nrf2 activator CDDO-Im (Bardoxolone analog). Immunoblotting for NQO1, CD10, MUC1, and loading control GAPD was performed. Densitometry for NQO1 (B), MUC1 (C), and CD10 (D). Results are mean +/- SEM of 3 replicates, each representing a unique human sample. Statistical testing by one-way ANOVA and significance denoted * $p<0.05$; *** $p<0.0005$.

Together with observations made in Keap1$^{f/f}$ mice, these results support a model in which Nrf2 activity is high in the proximal tubule and inducible in the distal convoluted tubule and collecting system (**Figure 22**).

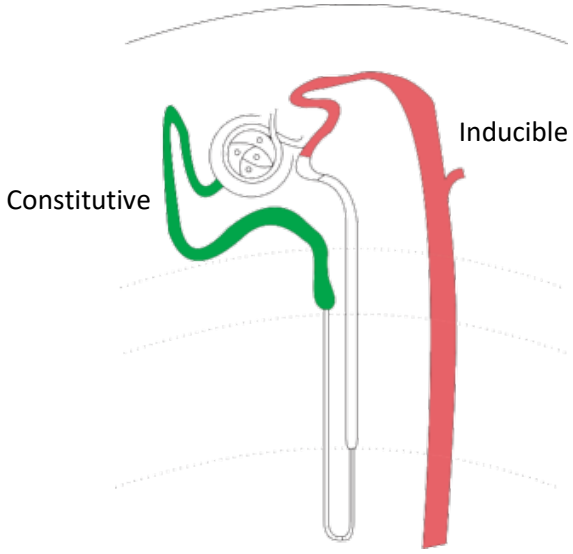

Figure 22: Schematic showing constitutive (green) and inducible (red) Nrf2 activity in nephron

4.2.2 Dietary administration of lithium leads to rapid development of nephrogenic diabetes insipidus in mice

To test whether Li caused NDI via hyperactivation of renal Nrf2 signaling, wild-type mice were administered LiCl (chow containing 0.17% LiCl, w/w) or control diet for 7 days. Mice fed the LiCl diet exhibited no change in body mass or food intake compared to animals on control diet (**Figure 23A-B**). Water intake increased as a function of duration of Li intake, with animals exhibiting overt polydipsia by 3 days and establishing a stable maximum of > 1mL H_2O per g body weight by 6 days of dosing (**Figure 23C**). At 7 days the Li cohort had significantly lower spot urine osmolality (505 +/- 335 mOsm/kg vs 1794 +/-598 mOsm/kg , $p<0.05$) indicating that polyuria was accompanied by hyposthenuria. Mice on control diet were water-deprived for 12h, and showed appropriate increase in urine osmolality to 3735 +/- 317 mOsm/kg (**Figure 23D**). In whole-kidney lysates, Li exposure down-regulated expression of both non-glycosylated and glycosylated Aqp2 by 90% (**Figure 23E**).

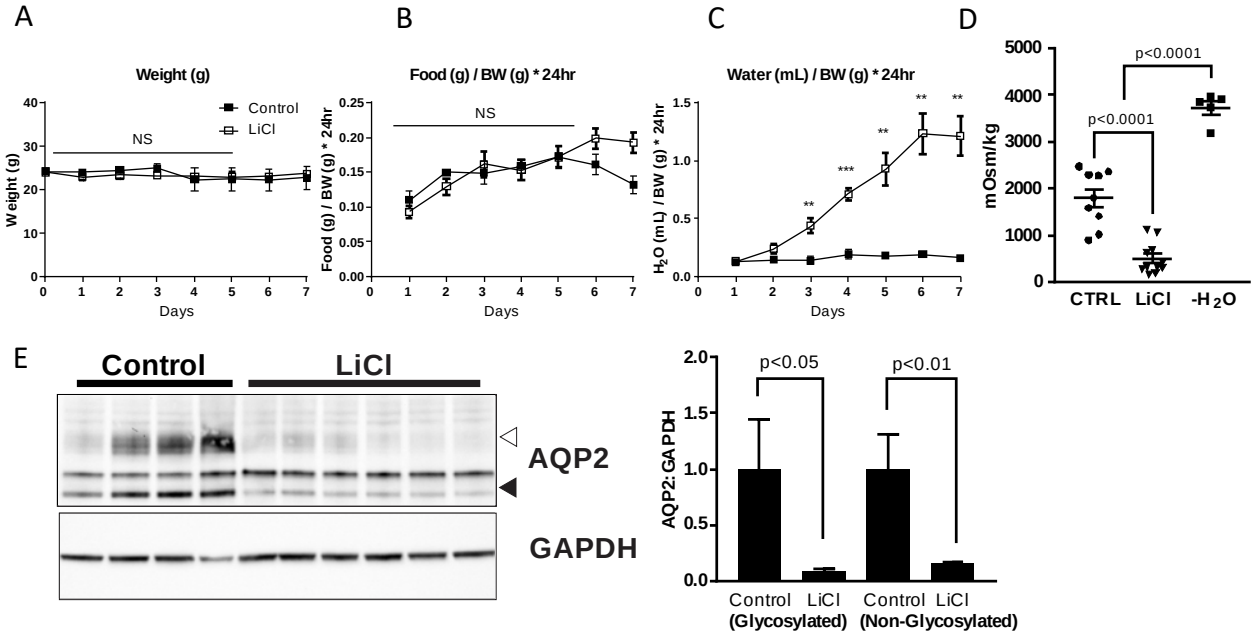

Figure 23: Mouse model of lithium-induced NDI

(A) Animal weight, (B) weight-corrected food intake, and (C) weight-corrected water intake of mice fed control diet or 0.17% LiCl diet for 7 days. Statistical analysis by two-way ANOVA comparing time and treatment, with Bonferroni multiple comparison test. (D) Spot-urine osmolality on day 7; urine from mice after 12h water deprivation (-H_2O) serves as positive control. Statistical analysis by one-way ANOVA comparing all groups by Bonferroni multiple comparison test. (E) AQP2 protein abundance in whole-kidney lysates with densitometry of glycosylated and non-glycosylated AQP2 bands (45 and 29kDa respectively). Statistical analysis of densitometry by Students t-test.

4.2.3 Renal Nrf2 signaling is not activated in Li-NDI

Immunoblotting for Nrf2 gene target NQO1 (NADPH Quinone Dehydrogenase 1) was performed in whole-kidney lysates from Li treated as compared to control mice (**Figure 24A-B**). As positive and negative controls, respectively, whole-kidney lysates from mice with constitutive genetic Nrf2 activation caused by partial loss of Nrf2 repressor Keap1 ($Keap1^{f/f}$) or knockout of Nrf2 were used. As expected, NQO1 expression was strongly upregulated in $Keap1^{f/f}$ genotype and accordingly down-regulated in the Nrf2 KO mouse. Lithium administration did not increase renal NQO1 expression. To test for potential dilution of cell-type specific induction of Nrf2 activity, immunofluorescence staining was performed for NQO1 and likewise revealed no differences in staining intensity within different functional segments of the nephron or within the kidney interstitium (**Figure 24C**). Using immunoaffinity isolated human cortical kidney cells enriched for distal tubule protein Mucin 1 or proximal tubule cells expressing CD10/CD13. Incubation with the triterpenoid Nrf2 agonist CDDO-imidazole showed significant 3-fold upregulation of NQO1, while two concentrations (10mM, 50mM) of LiCl had no effect (**Figure 24D**).

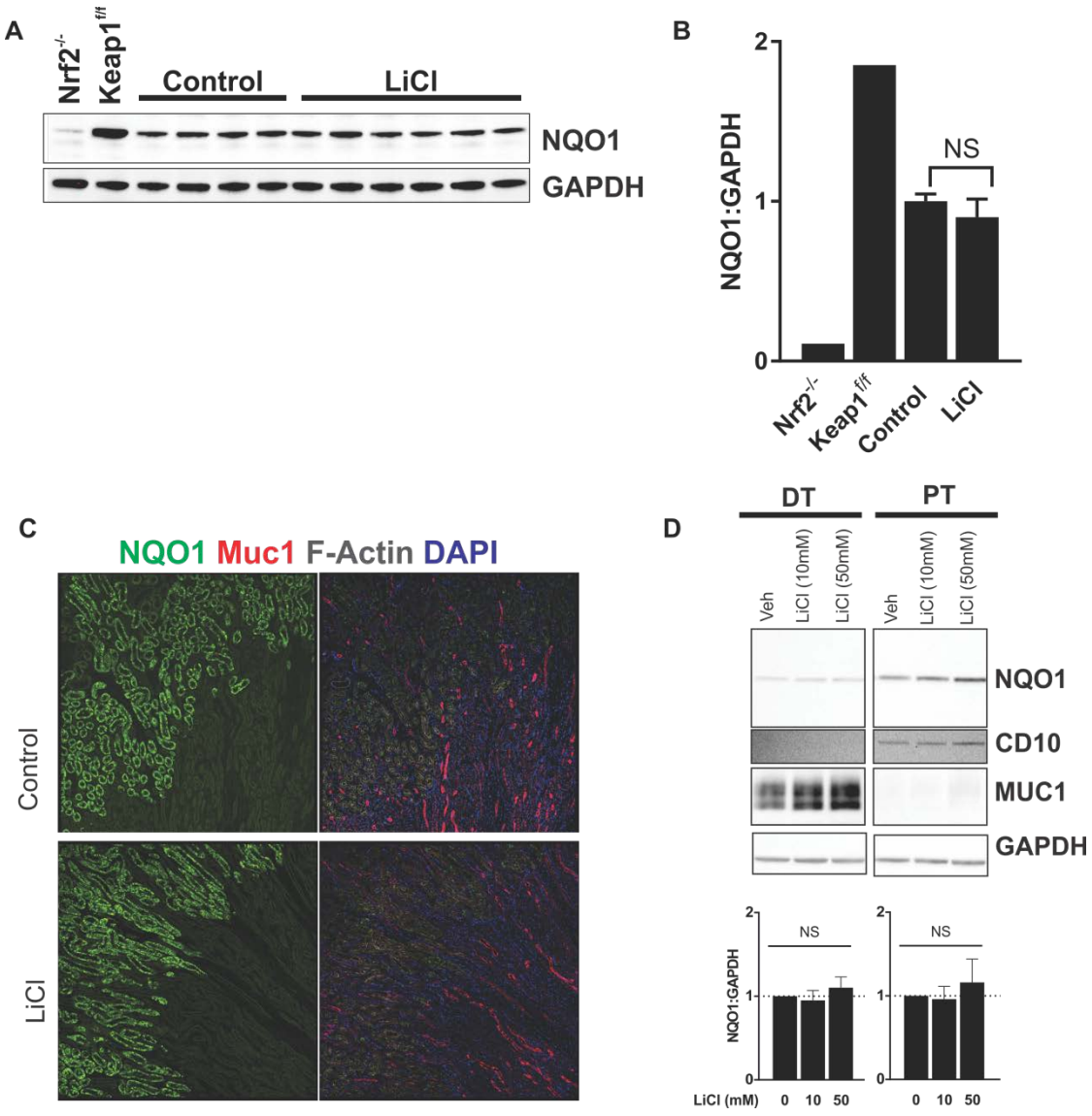

Figure 24: Lithium administration does not activate Nrf2 signaling in kidney.

(A) Immunoblots and (B) densitometry for Nrf2 target protein expression in kidneys from Nrf2$^{-/-}$, Keap1$^{f/f}$, Control, and LiCl-fed mice. Statistical analysis by Students t-test. (C) Immunofluorescence staining for NQO1 (green), MUC1 (red), F-actin (white), and DAPI (blue). (D) Immunoblotting and densitometry for NQO1 in primary human renal cortical cells immunoaffinity enriched for Muc1 or CD13 and cultured with LiCl or Nrf2 activator CDDO-Im. Statistical analysis of densitometry by one-way ANOVA with Dunnett test comparing treatment groups to control.

To test if Nrf2 activation is required for Li-induced NDI development, Li-administration was repeated in mice with global knock-out of Nrf2. 4 $Nrf2^{-/-}$ mice (2M, 2F) were maintained on control diet for 6 days followed by LiCl diet for 7 days. LiCl diet did not significantly impact body weight (**Figure 25A**). Food intake was suppressed in the first 3 days of LiCl diet administration, but rebounded to baseline by 4 days (**Figure 25B**). Despite Nrf2 ablation, dietary Li induced NDI with temporally similar onset of polydipsia (**Figure 25C**) as wild-type Li-treated mice. Urine osmolality was reduced compared to WT control (176 +/- 43 mOsm/kg vs 1230 +/- 163 mOsm/kg , $p<0.0001$) (**Figure 25D**), but was not significantly different between Li-treated $Nrf2^{-/-}$ and Li-treated WT mice.

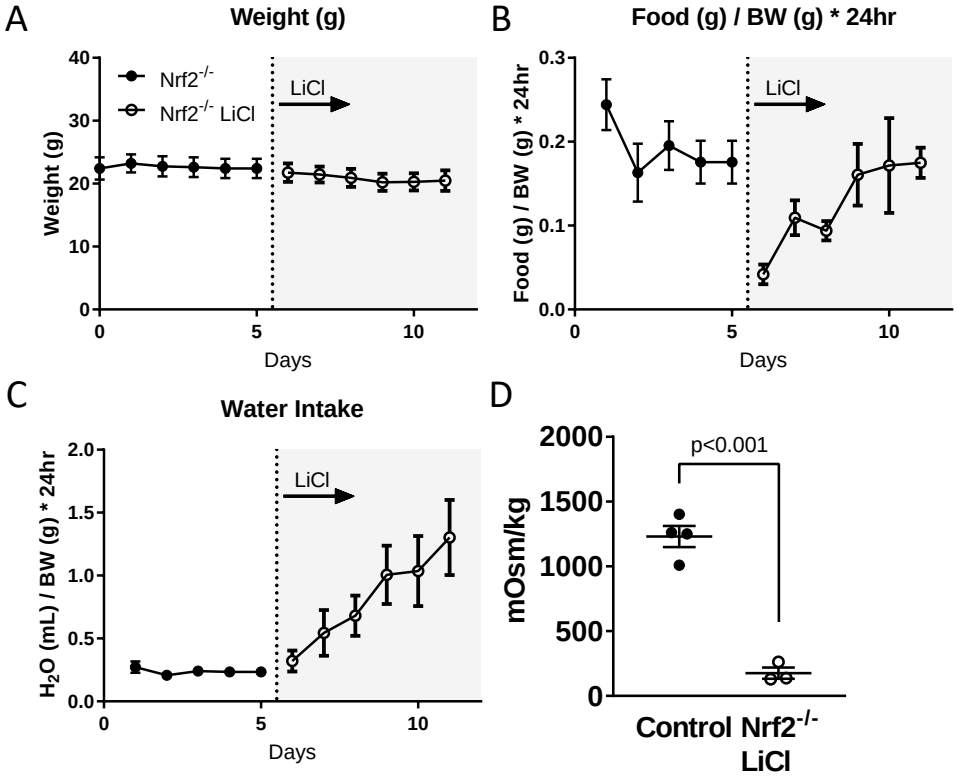

Figure 25: Nrf2 is not required for development of Li-NDI

(A) Animal weight, (B) weight-corrected food intake, and (C) weight-corrected water intake Nrf2$^{-/-}$ mice on control diet (0-5 days) followed by LiCl diet (6-11 days) , and (D) spot-urine osmolality of LiCl-treated Nrf2$^{-/-}$ or WT control mice. Statistical analysis by Student's t-test.

4.2.4 Mice with genetic hyperactivation of Nrf2 signaling are resistant to Li-NDI

To test whether activation of Nrf2 signaling exhibited protective effects on Li-NDI, wild-type (WT)and age-matched Keap1$^{f/f}$ mice were administered control diet for 5 days followed by LiCl (chow containing 0.17% LiCl, w/w) or control diet for 7 days (**Figure 26**A). Mice were housed individually and body weight, daily water intake, and daily food intake were monitored.

There were no statistically significant differences in baseline food or water intake between groups and no changes in body weight compared to Day 0. After 3 days on the LiCl diet, wild-type mice exhibited modest (~5%) reduction in body mass compared to no change in body mass for animals on control diet or Keap1$^{f/f}$ mice receiving LiCl (**Figure 26B**). Food intake was not affected by treatment or by genotype (**Figure 26C**). Water intake increased with Li intake in the WT cohort, with animals exhibiting overt polydipsia by 3 days and establishing a stable maximum of > 0.5mL H_2O per g body weight by 6 days of dosing (**Figure 26D**). Urine volumes were not quantified as metabolic cage housing is highly stressful for mice(215), but the bedding in cages housing these animals was saturated with urine daily. Strikingly, Keap1$^{f/f}$ mice receiving Li were normodipsic suggesting complete protection from onset of NDI.

Immunoblotting was performed on whole-kidney lysates to assess for expression of channel AQP2 and the canonical Nrf2 target NAD(P)H Quinone Oxidoreductase 1 (NQO1) (**Figure 26E**). Expression of NQO1 was not affected by Li treatment, but was significantly increased in Keap1$^{f/f}$ animals confirming constitutive activation of Nrf2 (**Figure 26E-F**). Glycosylated ~45kDa (open arrow, **Figure 26E, G**) and non-glycosylated 29kDa (closed arrow, **Figure 26E, H**) isoforms of the water channel aquaporin 2 (AQP2) were significantly reduced by Li exposure in both groups, consistent with NDI and with the hyposthenuria observed.

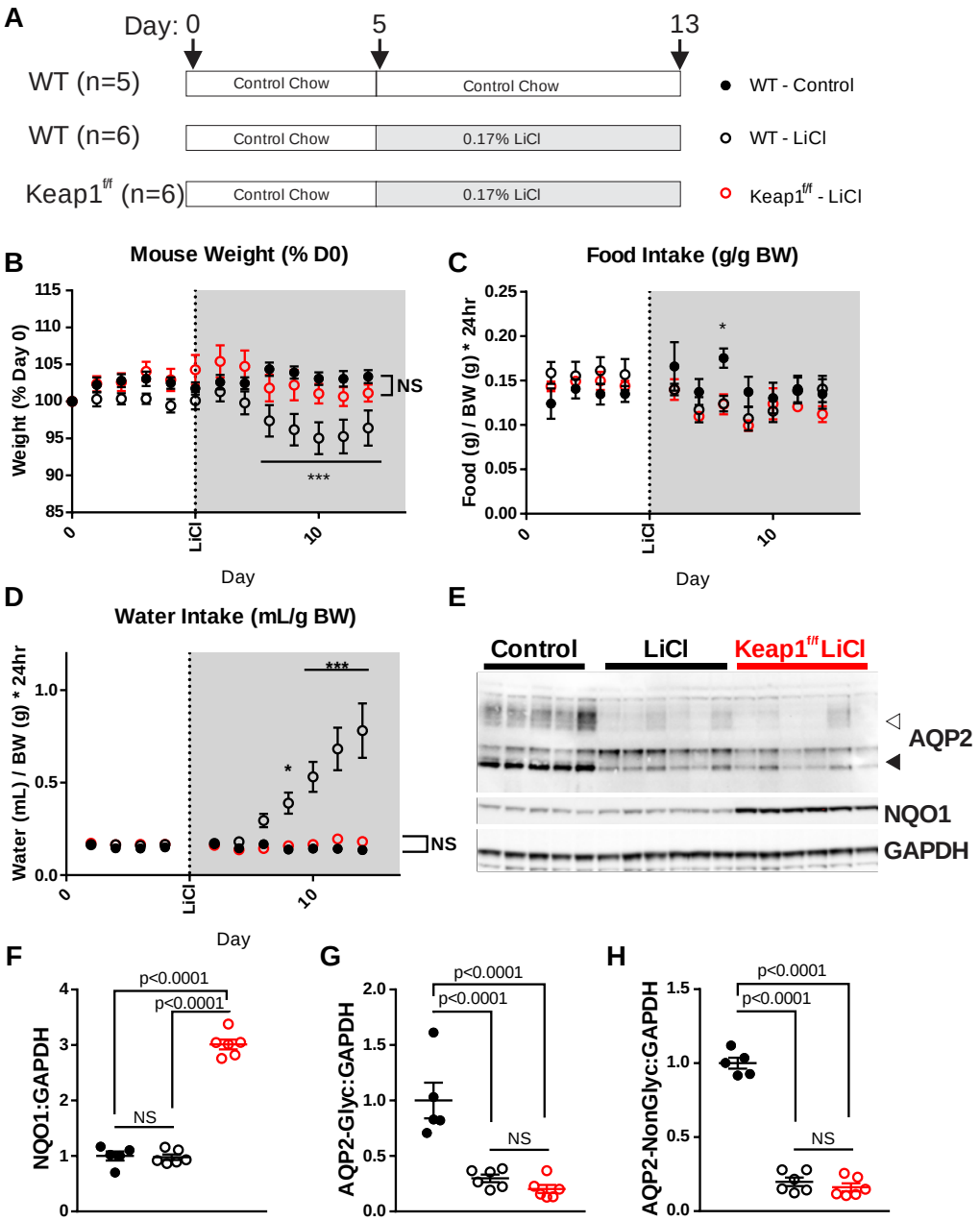

Figure 26: Nrf2 hyperactivation protects against development of Lithium-induced nephrogenic diabetes insipidus (Li-NDI)

(A) Schematic of model of Li-NDI. All mice received normal chow for 0-5d. At day 5, WT mice received either normal chow or 0.17% LiCl diet, and all Keap1$^{f/f}$ mice received LiCl diet. (B) Animal weights as a function of time, normalized to starting weight. (C) Food intake (g food/g body weight *24hr) and (D) Water intake (mL/g body weight*24hr). * ($p<0.05$) and *** ($p<0.001$) denote statistical significance by two-way ANOVA with Dunnet correction for multiple comparisons, means of each time point compared to control. Results plotted as mean ± standard error of 5 (WT-Chow) or 6 (WT-Li and Keap1-Li) animals per group. (E) Immunoblotting of whole-kidney lysates

for AQP2 and NQO1; each lane represents one animal from the study. Open arrowhead: glycosylated AQP2 (45kDa), shaded arrowhead: non-glycosylated AQP2 (29kDa). (F)-(H) Densitometry with statistical analysis by one-way ANOVA with Tukey's test comparing all group means.

After 8 days after Li administration, spot urine was collected and blood was sampled from the retroorbital plexus. Subsequently mice were sacrificed and tissues were collected. Blood chemistry analysis revealed no differences in plasma Na^+, K^+, or Cl^- between groups (**Figure 27A-C**), while plasma Li^+ was significantly elevated in both WT and $Keap1^{f/f}$ groups (**Figure 27D**) suggesting identical absorption, exposure, and clearance of Li. The WT-Li cohort had significantly lower spot urine osmolality than control diet cohort (359 +/- 192 mOsm/kg vs 1473 +/-332 mOsm/kg , $p<0.0001$) indicating that polyuria was accompanied by hyposthenuria consistent with NDI. Plasma osmolality and plasma renin concentration were measured and found to be identical across experimental groups suggesting that all mice were normovolemic and drinking to satiety (

Figure 27E-F). Despite complete normodipsia, urine osmolality was reduced in the $Keap1^{f/f}$-Li cohort and not significantly different from WT-Li (472 +/-209 mOsm/kg, $p<0.0001$ compared to control) (**Figure 27**

Figure 27G).

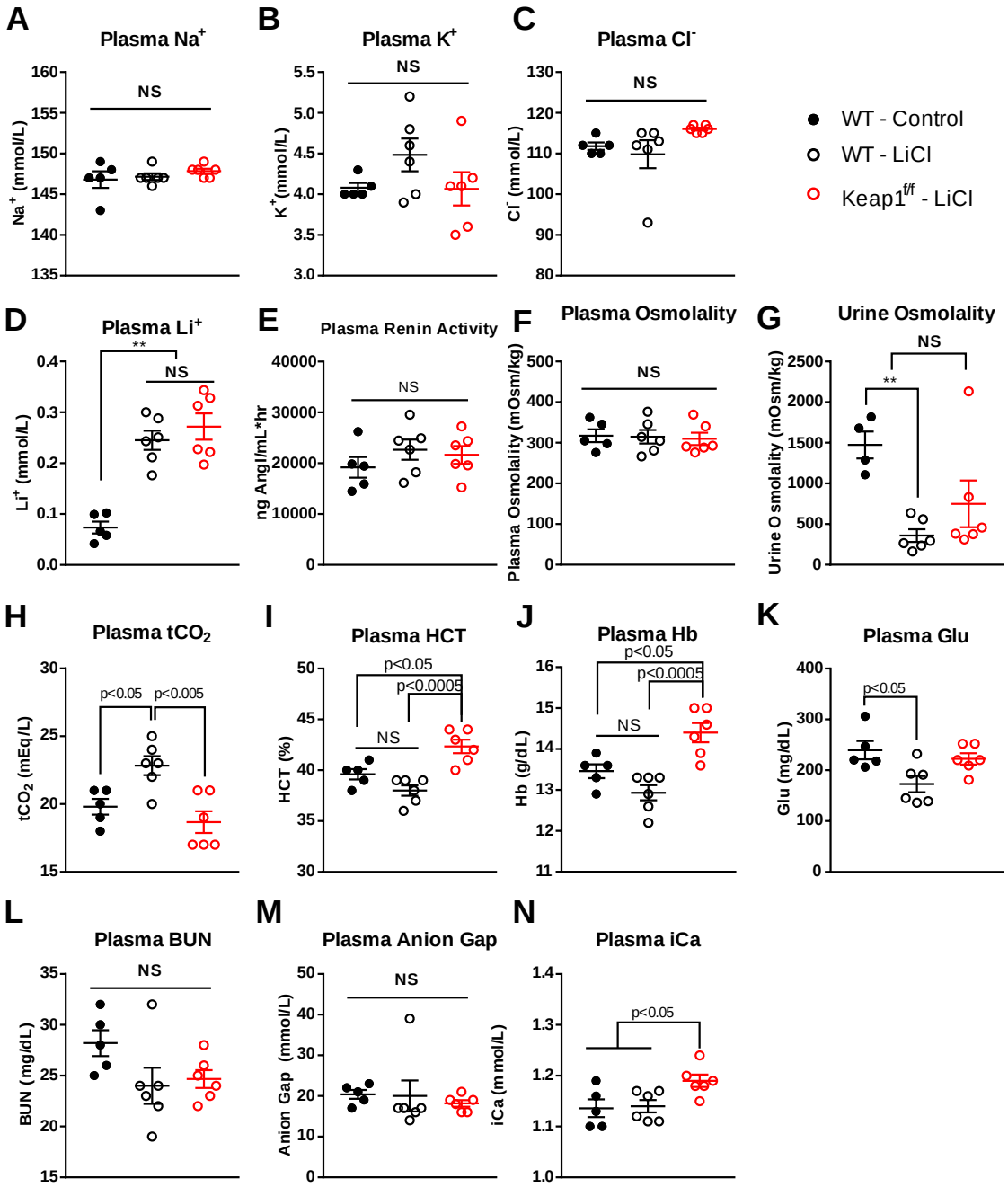

Figure 27: Plasma chemistry / Urine osmolality / PRA

(A) Plasma Na^+; (B) plasma K^+; (C) plasma Cl^-;(D) plasma Li^+; (E) plasma renin activity; (F) plasma osmolality; (G) urine osmolality; (H) plasma tCO_2; (I) hematocrit; (J) hemoglobin; (K) plasma glucose; (L) blood urea nitrogen (BUN); (M) plasma anion gap; (N) plasma ionized Ca^{2+}. Statistical analysis by one-way ANOVA with Tukey's test comparing all group means.

4.2.5 Alteration of renal ion transporter expression in Keap1$^{f/f}$ mice fed lithium

Clinically, Li-NDI is treated with inhibitors of sodium-chloride cotransporter (NCC, SLC12A3), epithelial sodium chloride channel (ENaC, SCNN1A/B/D/G), carbonic anhydrase (CA), or with non-steroidal anti-inflammatory compounds which inhibit prostaglandin biosynthesis. Effects of Nrf2 signaling on collecting duct expression of AQP2 have recently been published, but the effects of this signaling pathway on proximal and distal tubule transporters or prostaglandin biosynthesis have not been characterized. Immunoblotting was performed to determine if Nrf2 altered the expression of these pharmacologic targets (**Figure 28**).

Activating phosphorylation of NCC at threonine 53 (pNCC, T53) was reduced by lithium treatment in both genotypes, while total expression of NCC (tNCC) was unchanged in WT-Li cohort but significantly reduced in Keap1$^{f/f}$-Li cohort, while the ratio of pNCC:tNCC was significantly reduced in both Li-treated groups. Li likewise reduced expression of CAII in WT-Li animals, with additional reduction in Keap1$^{f/f}$-Li mice compared to WT and WT-Li.

Amiloride has been found to reduce polyuria in murine models of Li-NDI as well as in human patients, through reduction of ENaC mediated uptake of Li(216–218). No differences were observed between expression of ENaC subunits α, β, or γ suggesting that regulation of this transporter was not involved in Nrf2-mediated resistance to NDI.

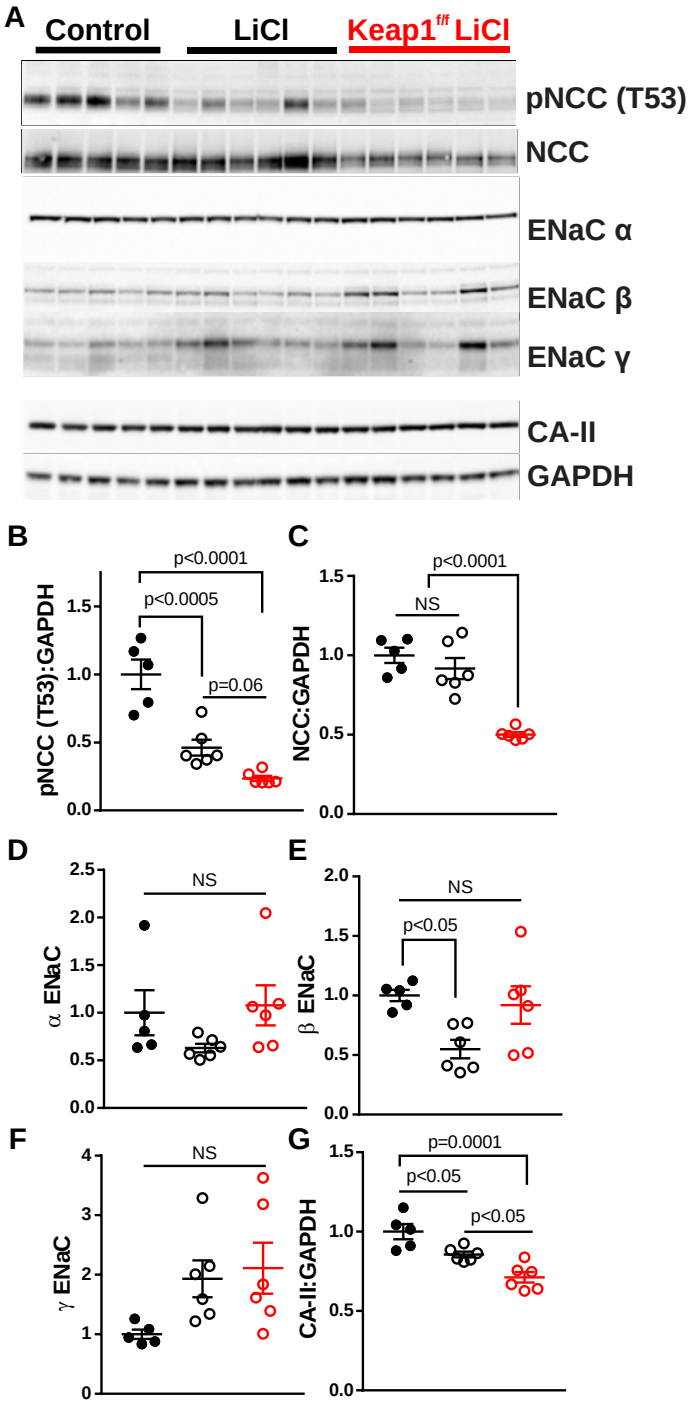

Figure 28: Nrf2 hyperactivation down-regulates NCC and CA-II expression.

(A) Immunoblotting of kidney lysates for solute transporters previously found to be protective in Li-NDI; each lane represents one animal from the study. (B)-(G) Densitometric analysis of immunoblots normalized to GAPDH. Statistical analysis by one-way ANOVA with Tukey's test comparing all means.

4.2.6 Evaluation of renal function in Keap1$^{f/f}$ mice at baseline and after water deprivation

Down-regulation of solute transporters such as NCC in Keap1$^{f/f}$ mice would suggest impaired Na^+ reabsorption and increased diuresis. While development of NDI in mice with total knock-out of Keap1(47, 48) or its ubiquitin ligase Cul3(49), the renal phenotype of mice with graded genetic activation of Nrf2 (Keap1$^{f/f}$) has not been studied. To characterize renal function Keap1$^{f/f}$ mice were studied under basal (water *ad libitum*) conditions as well as after 12-hour water deprivation. At baseline Keap1$^{f/f}$ mice were found to be mildly polyuric and hyposthenuric (**Figure 29A-B**) and had identical GFR (**Figure 29C**). Surprisingly, in contrast to mice with total ablation of Keap1, upregulation of plasma renin and urine concentration in response to 12-hour water deprivation were no different from WT (**Figure 29D-E**). These results suggest that in contrast to supra-pharmacologic activation caused by total ablation of Nrf2 repressors, graded pharmacomimetic activation of Nrf2 does not have deleterious renal effects. However, akin to preclinical and clinical protection observed via pharmacologic inhibition of these transporters in Li-NDI, Keap1$^{f/f}$ animals showed complete protection from development of polydipsia/polyuria.

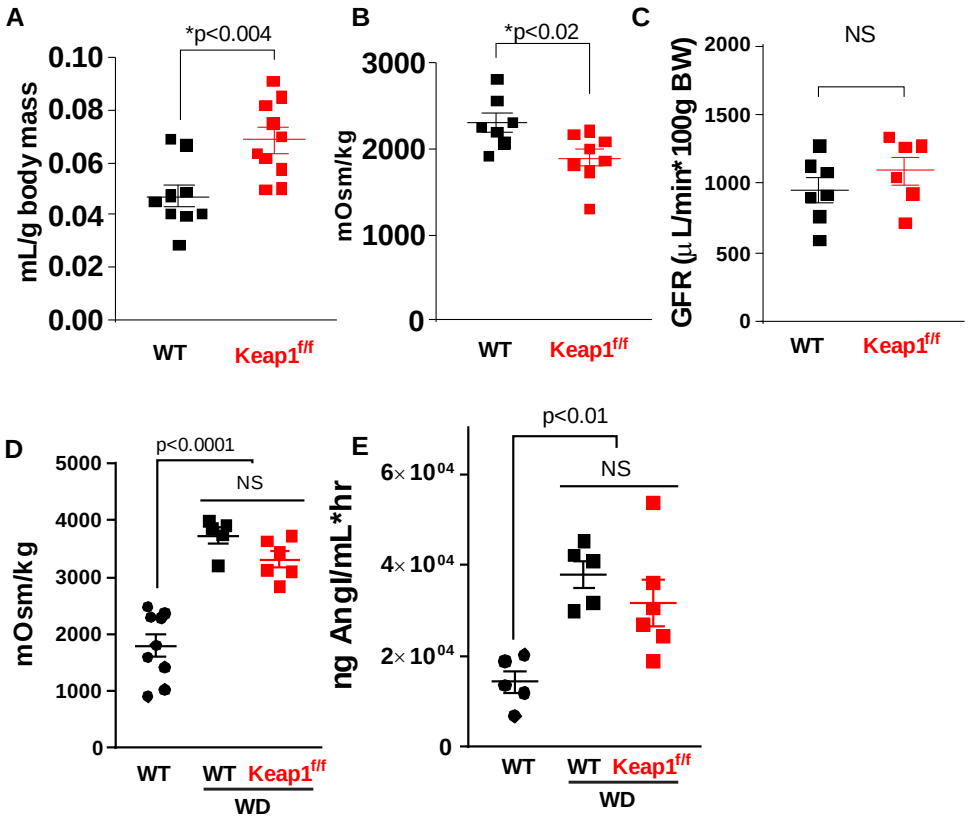

Figure 29: Graded genetic activation of Nrf2 causes polyuria and hyposthenuria but no defect in urine concentrating ability in response to water deprivation.

(A) 24-hour urine production determined by metabolic cage housing and (B) spot-urine osmolality of wild-type and Keap1$^{f/f}$ mice. (C) Glomerular filtration rate was determined by transdermal measurement of FITC-Sinistrin elimination. (D) Urine osmolality and (E) Plasma renin activity after 12-hr water deprivation (WD). Statistical analysis by Student's t-test (A-C) and one-way ANOVA with Tukey's multiple comparison test (D-E).

Of note, hematocrit was found to be significantly elevated in Keap1$^{f/f}$ mice after receiving Li for 7 days (**Figure 27**). Hematocrit (HCT) may be high due to volume contraction, as in relative polycythemia, or primary polycythemia. Despite normal plasma sodium level, the elevation of HCT in normodipsic, hyposthenuric Keap1$^{f/f}$ mice after lithium treatment aroused suspicion of volume contraction. To address this concern, hematocrit was measured in WT and Keap1$^{f/f}$ mice at baseline. Keap1$^{f/f}$ mice were polycythemic relative to control animals, suggesting that these

animals display primary polycythemia. To determine the etiology of the primary polycythemia, renal erythropoietin (EPO) production and red blood cell antioxidant contents were evaluated (**Figure 30**). Ferritin light chain (FTL1), ferritin heavy chain (FTH1), and EPO mRNA extracted from whole-kidney lysates was found to be identical between the two groups. As RBCs are exposed to high levels of oxygen, they encounter significant oxidative stress. Furthermore, as they are anucleate, RBC cannot synthesize new enzymes and proteins in response to ROS-induced stress. We hypothesized that increases in RBC antioxidant enzyme levels could lead to increased RBC lifespan and polycythemia, but found no change in RBC superoxide dismutase (SOD) and catalase (CAT) content and slight decrease in glutathione peroxidase (GPx) content.

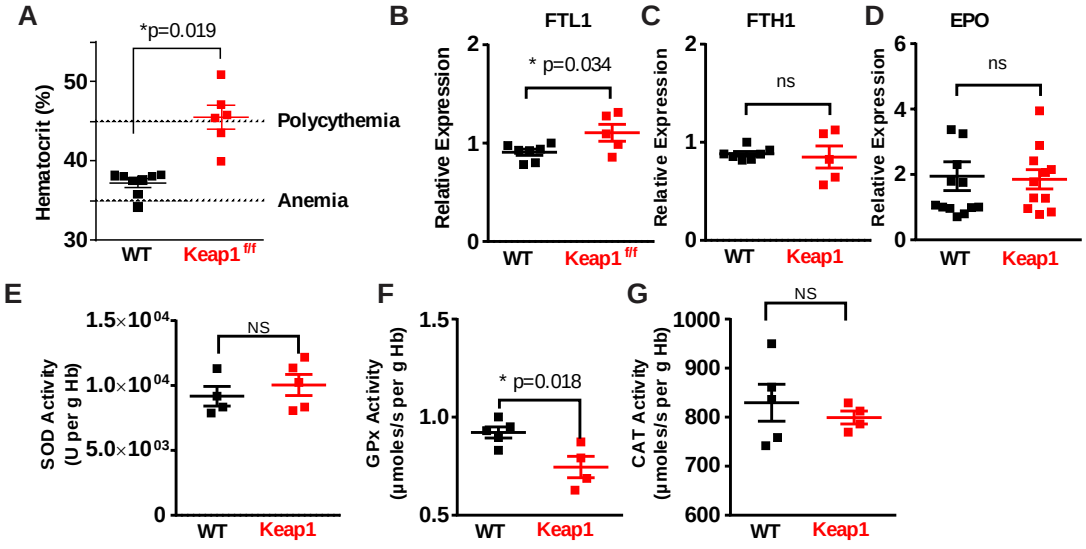

Figure 30: Hyperactivation of Nrf2 causes polycythemia.

(A) Keap1$^{f/f}$ mice are polycythemic but have no significant elevation in renal ferritin light or heavy chain (FTL1/FTH1) or erythropoietin (EPO) expression (B-D). Biochemical assays for superoxide dismutase (SOD), glutathione peroxidase (GPx), and catalase (CAT) activity revealed no differences (E-G).

4.2.7 Characterization of Nrf2 effects on vascular tone

Thiazides and acetazolamide dramatically diminish polyuria induced by Li but have only marginal effects on AQP2 abundance and urine osmolality(219–222). NSAIDs such as indomethacin, which are otherwise avoided in the context of chronic kidney disease, are also thought to reduce polyuria in Li-NDI through reduction of GFR(223, 224). While the precise mechanism remains unclear, paradoxical protection seen with both thiazides and acetazolamide in Li-NDI is thought to involve tubuloglomerular feedback (TGF) leading to reduction of glomerular filtration rate (GFR). TGF is a direct result of paracrine and endocrine signaling from the macula densa at the apex of the ascending limb of the loop of Henle to regulate afferent and efferent arteriolar tone. Both prostaglandin biosynthesis and the renin-angiotensin-aldosterone signaling (RAAS) have been implicated in this process.

Mechanistic studies of existing therapeutics in Li-NDI have relied on indirect evidence to conclude that protection is mediated by changes in TGF, as it is technically difficult to measure afferent and efferent arteriolar tone or glomerular capillary pressure. To determine if Nrf2 activation could affect renal vascular function, isolated medium-sized resistance vessels were studied as a surrogate. Wire myography was performed on isolated mesenteric and thoracodorsal arteries from WT and Keap1$^{f/f}$ mice. Vessels from Keap1$^{f/f}$ mice showed decreased sensitivity and blunted responses to the vasodilator acetylcholine, indicating endothelial dysfunction (**Figure 31A-B**). Phenylephrine-induced vasoconstriction was unaffected (**Figure 31C**).

To assess whether impaired vasodilation *in vitro* manifested as physiologic differences in intact animals, 6 WT and 5 Keap1$^{f/f}$ mice were instrumented with radiotelemeters and hemodynamic parameters were monitored. Readings were obtained at 5 minute intervals and pooled from nocturnal (10pm-4am) and diurnal (10am-4pm) time periods. At baseline, systolic or

diastolic blood pressure (BP) were identical between WT and Keap1$^{f/f}$ animals, but both nocturnal diurnal heart rates (HR) were significantly lower in Keap1$^{f/f}$ mice (**Figure 31E-H**). This reduction in HR was confirmed via direct left ventricular micro-catheterization under isoflurane sedation (**Figure 31I**). Consistent with vagus nerve baroreflex compensation for reduced vascular compliance, acute administration of atropine elicited larger increase in HR in Keap1$^{f/f}$ mice (**Figure 31J**).

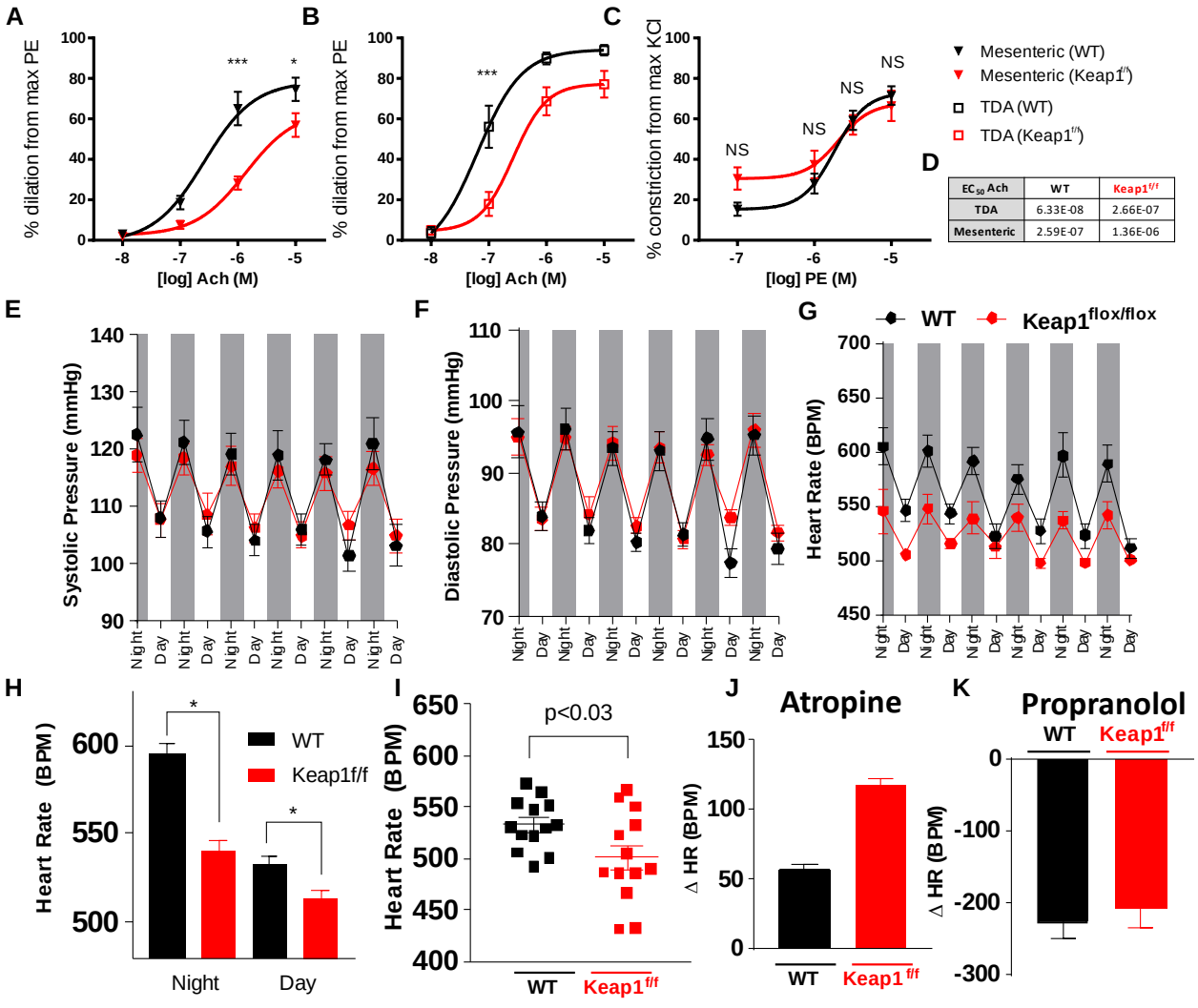

Figure 31: Keap1$^{f/f}$ mice have endothelial dysfunction resulting in impaired vasodilation

Acetylcholine-mediated vasodilation in (A) mesenteric and (B) thoracodorsal resistance vessels. (C) Vasoconstriction of mesenteric arteries in response to phenylephrine is identical in WT and Keap1$^{f/f}$ animals. (D) EC_{50} of ACh in mesenteric and thoracodorsal arteries. (E) Systolic and (F) diastolic blood pressures determined by radiotelemetry. (G) Heart rate determined by radiotelemetry. Average heart rates determined across 4 6-hour night or day periods, bars represent mean +/- 95% CI. (I) Heart rates measured by cardiac catheterization under isoflurane anesthesia, error bars represent mean +/- SEM. Changes in heart rate after (J) acute infusion of atropine (1mg/kg) and (K) propranolol (4mg/kg) IP n=3 (WT) and n=2 (Keap1$^{f/f}$). Error bars represent mean +/- standard error.

In addition to promoting retention of sodium and water, angiotensin II is a physiologic vasoconstrictor which acts directly on endothelial angiotensin receptors to afford vasoconstriction. Antagonists of the RAAS reduce blood pressure primarily through effects on vascular tone(225). To determine if vascular responses to RAAS inhibition were blunted in Keap1$^{f/f}$ mice, instrumented mice were maintained on a low-sodium diet for 1 week to minimize effect of sodium intake followed by addition of 6mg/kg*d enalapril for 4 days, after which time blood pressure responses were measured. Averaged BP traces over nocturnal and diurnal periods are shown in **Figure 32**. Significantly, sodium-depleted Keap1$^{f/f}$ displayed BP dipping refractory to the effects of low sodium and enalapril, indicating impaired vasodilation.

Significantly, in an independent experiment, plasma sodium determined in WT and Keap1$^{f'f}$ mice after 2 weeks of low-sodium diet was identical, while reduced NCC abundance was compensated by hyperphosphorylation of extant NCC (**Figure 33**). These results suggest that BP differences were not caused by differences in plasma Na^+ after sodium deprivation, and that the physiologic mechanisms regulating sodium retention are intact despite reduced abundance of NCC.

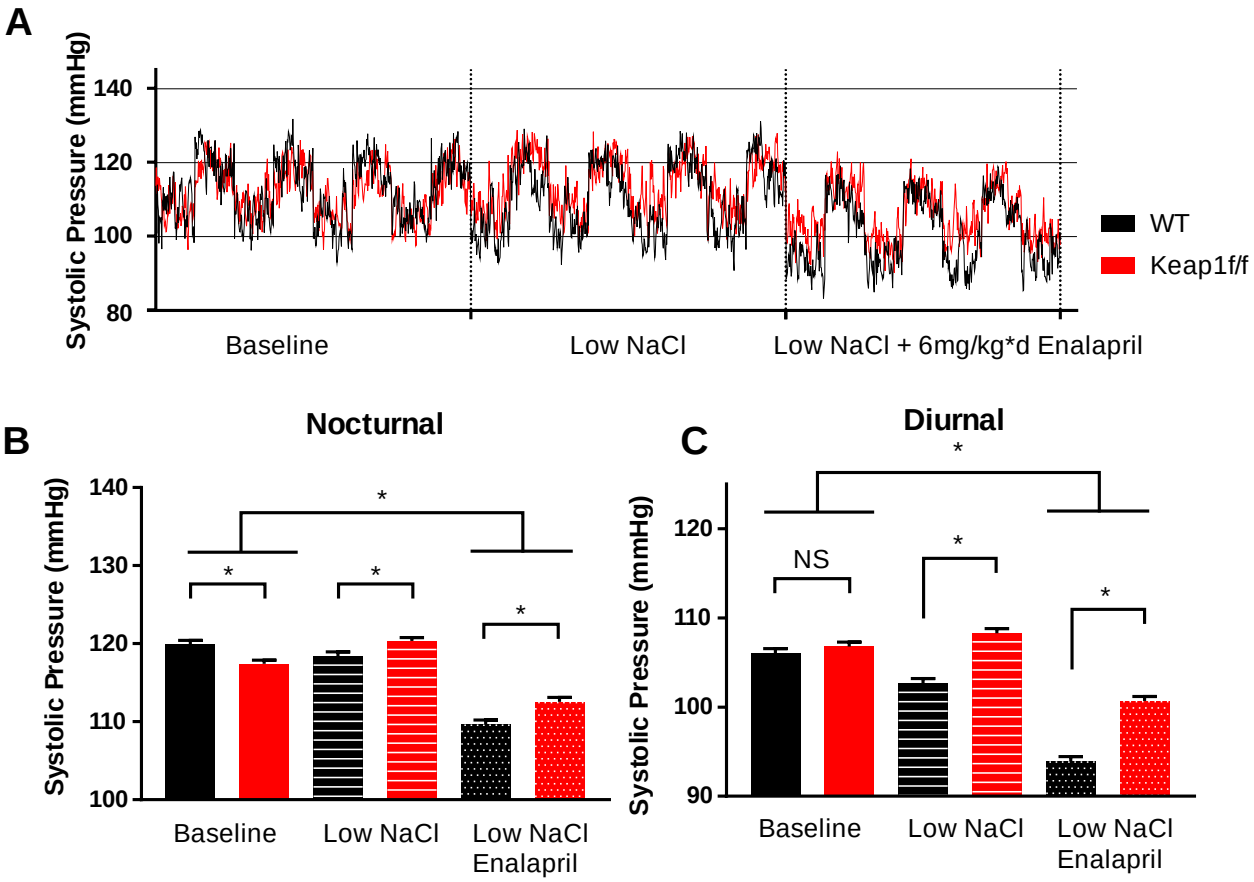

Figure 32: Keap1 hypomorphism impairs diurnal BP dipping after sodium depletion and ACE inhibition

(A) Averaged traces of systolic BP at baseline, after 4 days of NaCl deficient (0.01-0.02% NaCl) diet, and receiving 6mg/kg*d Enalapril. Average (B) Nocturnal and (C) diurnal systolic BP of experimental groups under different conditions; mean +/- 95% confidence interval. Statistical analysis by one-way ANOVA with Bonferroni multiple comparison correction, *p<0.0001.

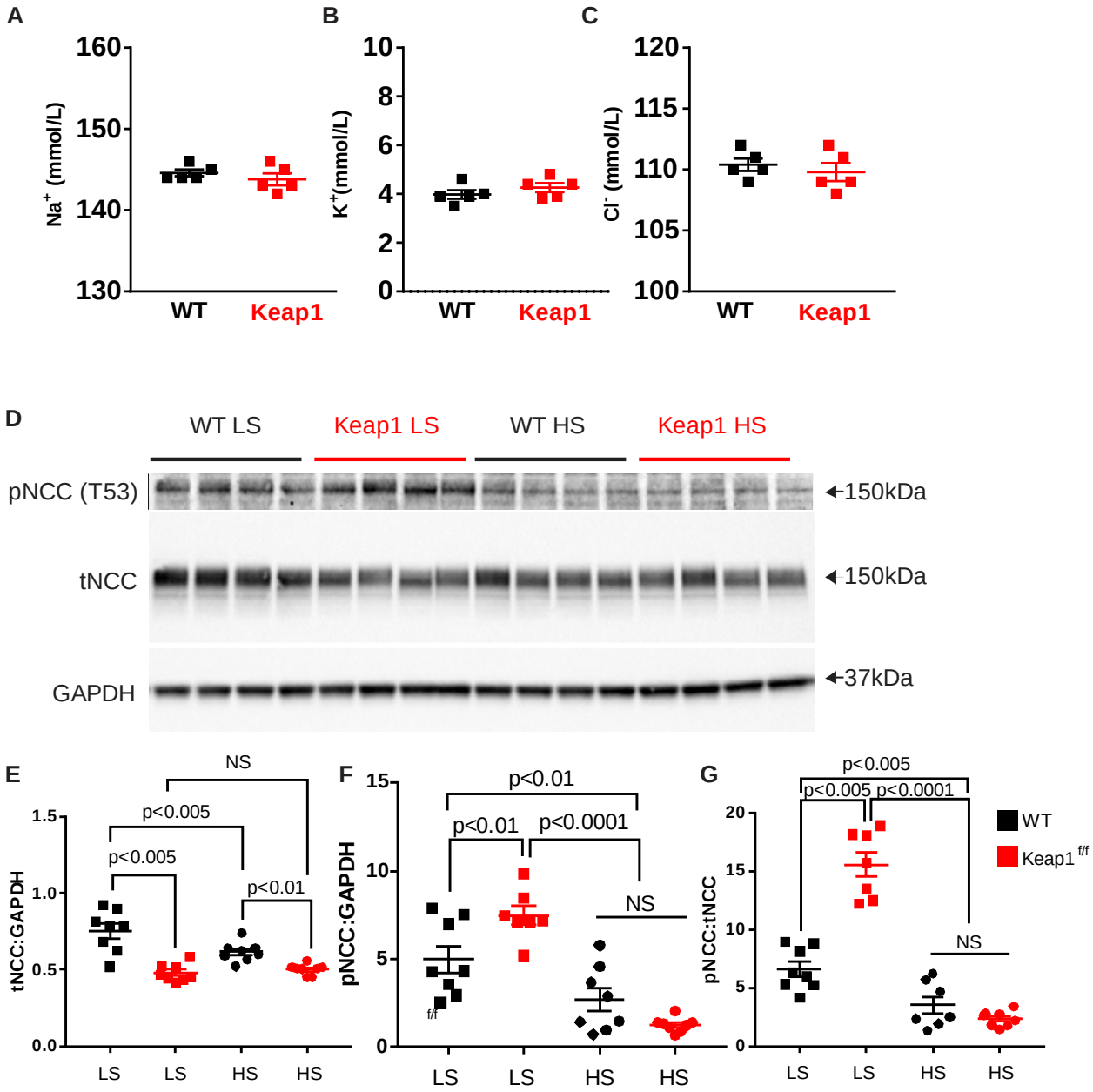

Figure 33: Plasma chemistry and renal NCC expression/phosphorylation after sodium deprivation

Plasma sodium (A), potassium (B), and chloride (C) of WT and Keap1$^{f/f}$ mice after 2 weeks on low-sodium (LS; 0.01% NaCl) diet. (D) Expression of total NCC and phospho-NCC (t53) in kidney lysates from mice after 2 weeks on low-sodium (LS) diet or 3 weeks on high-sodium (HS; 4% NaCl) diet. (E-G) densitometry quantifying tNCC, pNCC, and the ratio of pNCC:tNCC. Statistical analysis by one-way ANOVA with Tukey's test comparing all group means.

4.2.8 Endothelial nitric oxide (NO) signaling is not affected by hyperactivation of Nrf2

Dilation of resistance vessels is modulated by effects of paracrine relaxing factors produced by the vascular endothelium on vascular smooth muscle cells. To determine the mechanism underlying blunted vasodilation and increased vascular resistance, we evaluated the nitric oxide (NO) signaling pathway.

Nitrite is a marker of bioavailable NO, and can be formed by chemical or enzyme-catalyzed oxidation reactions(226). Plasma and urine were collected from WT and Keap1$^{f/f}$ mice and nitrite was measured by ozone chemiluminescence. Surprisingly, plasma and urine NO_2^- were significantly elevated in Keap1$^{f/f}$ animals (**Figure 34A-B)**. Plasma arginine, the precursor from which NO is produced, trended towards reduction in Keap1$^{f/f}$ mice but this difference was not statistically significant (**Figure 34C**). Plasma asymmetric dimethylarginine (ADMA), an inhibitor of eNOS(227), was likewise unchanged (data not shown). Expression and activating phosphorylation of endothelial nitric oxide synthase (eNOS) in kidney homogenates was normal in Keap1$^{f/f}$ mice. nNOS was detected in brain tissue (positive control) but not in kidney lysates. Renal expression of the NO signal transducer soluble guanylate cyclase β1 (sGC- β1) was marginally lower in Keap1$^{f/f}$ than in WT mice (**Figure 34D-E**). Although statistically significant, this was likely not physiologically significant as the sGC- β1 product cGMP was found to be higher in plasma from Keap1$^{f/f}$ mice (**Figure 34F**). Finally, vasodilation in response to the chemical NO-donor sodium nitroprusside (SNP) was identical between WT and Keap1$^{f/f}$ mice, indicating that impaired vasodilation was not caused by reduced sensitivity to NO (**Figure 34G**). Together, these results indicate that Nrf2 hyperactivation inhibits ACh-induced vasodilation independently of NO production or downstream signaling, and elevated plasma and urine nitrite together with plasma

cGMP suggest that this pathway may be hyperactivated to compensate for a defect in an alternate pathway.

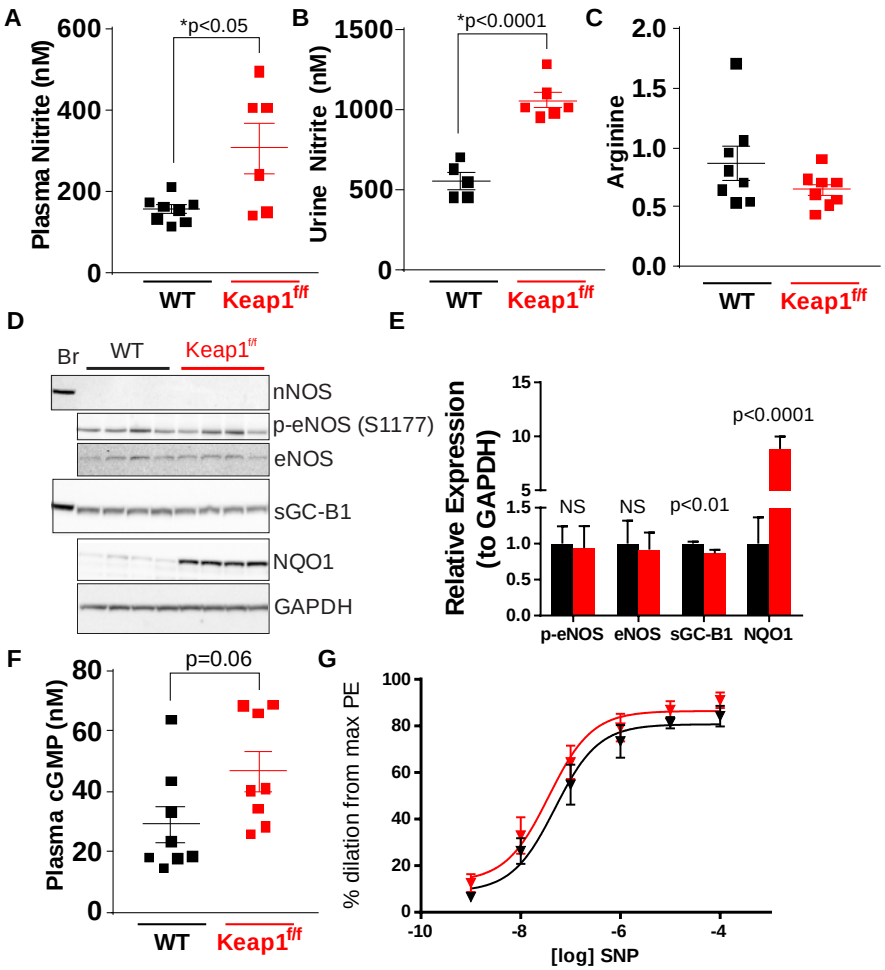

Figure 34: Endothelial dysfunction in Keap1$^{f/f}$ animals occurs independently of NO signaling

NO oxidation product nitrite measured in (A) plasma and (B) urine samples. (C) Plasma arginine measured by HPLC-MS/MS. (D) Expression of nNOS, eNOS, phospho-Ser1177 eNOS, sGC-B1, and NQO1 in kidney lysate. (E) Densitometry normalized to GAPDH loading. (F) cGMP measured in plasma. (G) Mesenteric artery dilation in response to the NO donor sodium nitroprusside (SNP). Statistical analysis by Student's t-test.

4.2.9 Nrf2 impairs endothelial function via down-regulation of inflammation-related autocoid vasodilators

Pharmacologic activators of Nrf2 have been evaluated in numerous disease models due to their independent anti-oxidant and anti-inflammatory effects, characterization of which is complicated by putative cross-talk between the Nrf2 and NF-kB pathways(110). The kidneys are unique among tissues in that both cyclooxygenase 1 and cyclooxygenase 2 are constitutively expressed, and play a critical physiologic role through production of prostaglandin precursors. COX-1 and COX-2 expression were found to be reduced in Keap1$^{f/f}$-Li mice (Supplemental Figure 2) suggesting that that Nrf2 activation has direct effects on renal expression of these proteins. Because Li was found to down-regulate COX-1 and COX-2 in WT mice, the experiment was repeated comparing tissues from WT and Keap1$^{f/f}$ mice on control diet, which confirmed these results (**Figure 36A-B**). Down-regulation of renal COX-2 was confirmed by immunohistochemical staining of kidney sections (**Figure 36E**). Additionally, kidneys from Nrf2$^{-/-}$ animals showed increased COX-1 and COX-2 expression compared to control (**Figure 36C-D**), further suggesting that Nrf2 signaling plays a regulatory role in COX-2 expression.

COX-1 and COX-2 catalyze the conversion of arachidonic acid (AA) to prostaglandin precursors. To determine if vasodilatory PGs were reduced in Keap1$^{f/f}$ mice, an isotope dilution HPLC-MS/MS method was developed **(Figure 35)**. Prostacyclin (PGI_2) is a potent vasodilator, but has a short half-life and is rapidly metabolized to 6-keto-$PGF_{1\alpha}$. 6-keto-$PGF_{1\alpha}$ was significantly reduced in kidney homogenate extracts from Keap1$^{f/f}$ mice, offering a putative mechanism by which Nrf2 hyperactivation affects vascular tone (**Figure 36F**).

Kynurenine is a recently discovered endothelium-derived relaxing factor derived from inflammation-related pathways that acts through activation of adenylate and soluble guanylate cyclase pathways(228, 229). Kynurenine was measured in plasma of Keap1$^{f/f}$ mice by HPLC-MS/MS and found to be significantly reduced compared to WT, paralleling the reduction in 6-keto-PGF$_{1\alpha}$ (**Figure 36G**). Together these results suggest that effects of constitutive Nrf2 activation on inflammation-related autocoid production impact vascular compliance and cardiovascular homeostasis, offering a putative mechanism for resistance to Li-NDI.

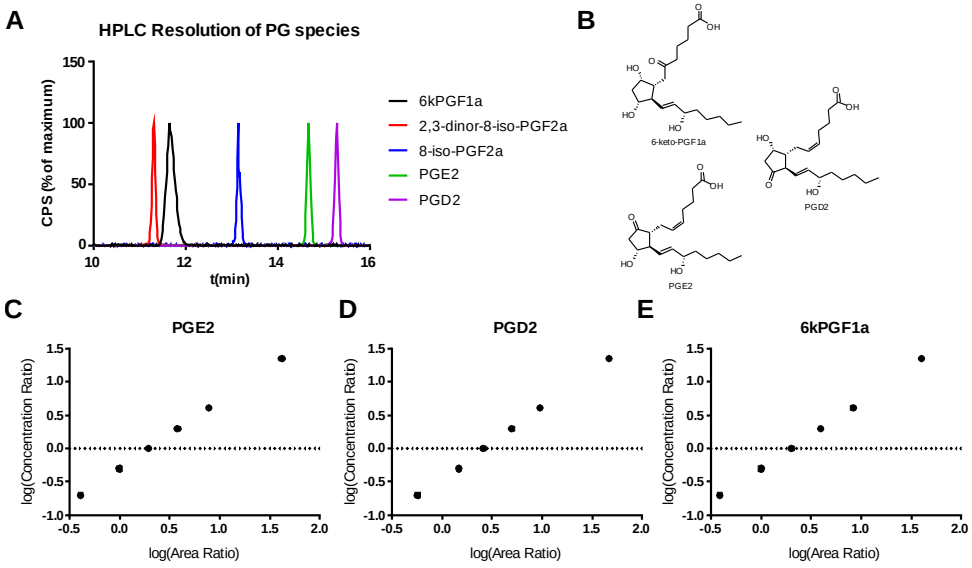

Figure 35: HPLC-MS/MS method to quantify prostaglandins

(A) Peaks showing chromatographic separation of 5 prostaglandin species. (B) chemical structures of 6-keto-PGF1α, 8-iso-PGF2α, 2,3-dinor-8-iso- PGF2α, PGE2, and PGD2. (C-E) 6-point calibration curves prepared for PGE2, PGD2, and 6-keto-PGF1α using isotope-labeled standards.

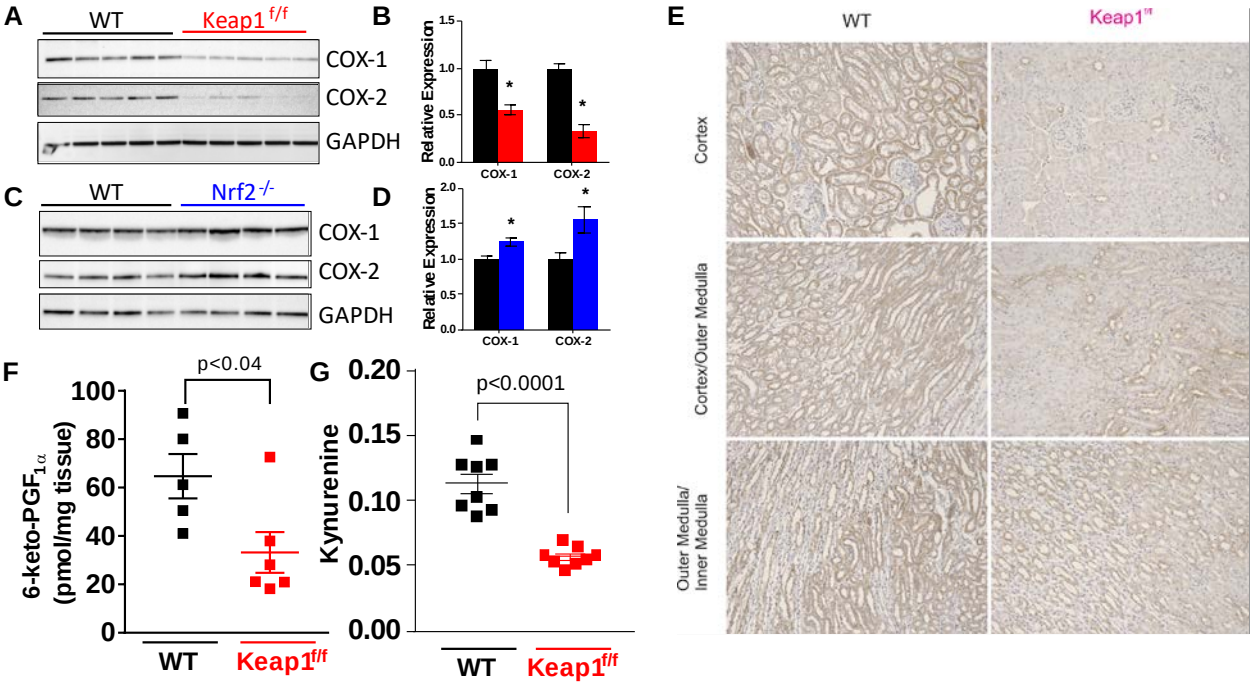

Figure 36: Constitutive Nrf2 activation suppresses COX-1 and COX-2 to down-regulate inflammation-related vasodilator production

Immunoblotting for cyclooxygenase 1 and 2 expression in kidneys of (A) Keap1$^{f/f}$ and (B) Nrf2$^{-/-}$ mice, densitometry shown in (C) and (D). (E) immunohistochemistry for COX-2 in kidney sections from WT and Keap1$^{f/f}$ mice. (F) Renal concentration of 6-keto-PGF$_{1\alpha}$, the stable metabolite of prostacyclin (PGI$_2$) measured in kidney homogenates by isotope-dilution HPLC-MS/MS. (G) Relative plasma levels of kynurenine, an endothelium-derived relaxing factor formed from tryptophan metabolism, measured by HPLC-MS/MS.

4.3 DISCUSSION

Lithium (Li) has remained a mainstay drug for mood stabilization in bipolar disorder for over a half-century, and is increasingly re-purposed for treatment of other central nervous system (CNS) diseases as new therapeutic effects are described and mechanisms documented. Disparagingly, the beneficial effects of Li are offset by adverse renal effects, most commonly impairment of urine concentrating function. In addition to the adverse effect of polyuria

(>3,000mL urine/day) on quality of life, Li causes deleterious functional and structural changes of the kidney. Quantitatively the major determinant of urine volume is the passive reuptake of water from pro-urine through aquaporin water channels in the collecting duct. Li-induced NDI is thought to cause AVP insensitivity with impaired insertion of mature AQP2 into the apical membrane of collecting duct epithelial cells.

Recent evidence implicates the Keap1/Nrf2 signaling pathway as playing a role in regulating Aqp2 via as-of-yet unknown mechanisms. Specifically, hyperactivation of Nrf2 signaling by ablation of its repressors Cul3, GSK3β, and Keap1 have independently been found to cause nephrogenic diabetes insipidus in mice(47–50). As Li is a known inhibitor of GSK3β, we hypothesized that Li induces NDI via hyperactivation of Nrf2. Our results demonstrate that NDI develops rapidly during dietary Li administration, with significant increase in water intake and production of dilute urine. Despite developing a robust NDI phenotype, Li-treated mice did not display engagement of Nrf2 signaling in the kidney. Both immunoblotting of whole-kidney lysate or by immunofluorescence staining for the downstream Nrf2 target NQO1 failed to show increased Nrf2 activation in the lithium treated group. Furthermore, $Nrf2^{-/-}$ mice developed NDI similarly to WT mice, suggesting that hyperactivation of this pathway was not involved.

On the contrary, Keap1 hypomorphism and resultant Nrf2 hyperactivity protected against development of Li-NDI, with significantly reduced water intake compared to WT mice receiving lithium, and water intake no different from WT mice receiving control diet. This is a surprising observation, as recent characterizations of transgenic mice with total ablation of Keap1 in the kidney epithelium(47) or whole animal (NEKO) (48) causes NDI. In comparison to Keap1 total-knock-out animals, which exhibit a range of developmental abnormalities(20, 47, 48, 230), hypomorphism via floxing of exons 4-6 with loxP sites leads to pharmaco-mimetic activation and

tissue protection against a variety of insults(41). In striking contrast to Keap1$^{-/-}$ animals, Keap1$^{f/f}$ mice exhibited only mild hyposthenuria and polyuria at baseline, and had normal urine concentrating ability and upregulation of plasma renin activity in response to 12hr water deprivation. While the Nrf2 activator CDDO-Me has been shown to increase GFR(91), genetic activation of Nrf2 in this model did not change GFR. It is possible that Nrf2 activation displays hormesis, with activity above a certain threshold causing adverse outcomes. It has also been documented that genetic and pharmacologic activation of this pathway result in overlapping yet distinct transcriptional profiles(54).

It is intriguing that the spatial distribution NQO1 expression in murine kidney, with high cortical and low medullary expression, appears to parallel postulated O_2 and glucose gradients. Moreover, it appears that in both mouse and human, Nrf2 activity is significantly higher in proximal than in distal tubule epithelium. The proximal tubules are responsible for the bulk of solute, water, and small-molecule reabsorption as well as for conjugation and excretion of toxins and wastes(231). Previously, human primary proximal tubule cells in culture have been found to express membrane transporters and conjugation enzymes required for these processes(232, 233), many of which are under Nrf2 transcriptional control(9). While NQO1 expression was significantly lower in distal tubule epithelial cells than proximal tubule epithelial cells at baseline, distal tubule cells were sensitive to both genetic activation (**Figure 20**) and the electrophilic Nrf2 inducer CDDO-Im (**Figure 21**).

Consistent with these observations, protein abundance of the DT marker NCC was reduced in kidneys from Keap1$^{f/f}$ mice. Recent evidence suggests that renal epithelial cells exhibit plasticity and can interconvert(234); it is possible that upregulation of Nrf2 steers these cell populations towards a different fate.

Existing therapeutic approaches for treating Li-NDI fall under four main categories: (1) inhibition of epithelial sodium channel (ENaC) mediated uptake of Li into the connecting tubule/collecting duct epithelium, (2) inhibition of sodium chloride cotransporter (NCC) and/or carbonic anhydrase II (CA-II) by thiazide diuretics, (3) specific inhibition of CA-II with acetazolamide, and (4) inhibition of renal COX-1 and/or COX-2 with non-steroidal anti-inflammatory drugs (NSAIDs). The preclinical and clinical literature on these four therapeutic approaches is summarized in **Table 2**.

While all of these interventions have been documented to reduce polyuria/polydipsia, the mechanisms by which this effect is achieved are unclear and remain the subject of speculation. The diuretics acetazolamide(221, 222, 235), amiloride (216–218, 236–239), furosemide(240), and hydrochlorothiazide(219, 220, 241–243) have been found to paradoxically reduce urine output in Li-NDI, while in patients without NDI, they promote diuresis. Furthermore, in a recent publication acetazolamide was shown to increase collecting duct abundance of AQP2(221), while a subsequent publication from the same research team concluded that the reduction of polyuria occurred independently of AQP2 abundance(222). Similarly, thiazides were long thought to paradoxically reduce polyuria through their inhibition of NCC, however, recent evidence shows that this class of drugs mitigates Li-NDI independently of NCC(219). With exception of amiloride, AQP2 protein abundance is not significantly increased by any of these treatments. Finally, while these diuretics rescue polyuria/polydipsia they improve maximal urine osmolality only minimally (generally <50% of control), suggesting that their site of action is not the collecting duct. Based on this evidence, the protection is thought to involve modulation of tubuloglomerular feedback. Reduction of distal sodium reabsorption is believed to deplete extracellular volume and lead to

reduction in GFR as well as increasing proximal sodium and water reabsorption through effects on medullary osmolality and proximal tubule function(244)

Drug		Mechanism	Model	Observation	Ref.
Amiloride	Amiloride(10μM)	Inhibition of ENaC-mediated Li uptake	mCCDc11 cells	↓ lithium-induced AQP2 downregulation	(217)
	Amiloride (10mg q.d.) 6 weeks		Human randomized placebo-controlled trial (n=11)	Partial ↑ urine osmolality following dDAVP	(236)
	Amiloride (0.2mmol/L in drinking water)		Rats administered 60mmol/kg Li in chow for 7 weeks	Partial ↑ urine osmolality, ↓ 24-hr water intake, increase in medullary osmolytes	(237)
	Amiloride (10mg q.d. increasing to 20mg q.d.)		Case study	Resolution of hypernatremia, ↓ plasma osmolality	(238)
	Amiloride (0.2mmol/L in drinking water) for duration of study		Rats administered 40mmol/kg Li in chow for 1 week then 60mmol/kg Li in chow for 5.75 months	Partial ↑ urine osmolality, partial ↓ 24-hr urine output, ↓ glomerular sclerosis, ↓ fibrotic markers	(239)
	Knockout of ENaCα subunit		CD-specific αENaC KO mice ($Scnn1a^{lox/lox}$/HoxB7:Cre) and control mice ($Scnn1a^{lox/lox}$) administered 40mmol/kg Li in chow for 24-25 days	↓lithium-induced AQP2 downregulation, complete ↑ urine osmolality, complete ↓ polyuria/polydipsia, ↓ H+ ATPase	(218)
	Amiloride (10-20mg q.d)		8 patients with Li-NDI previously treated with HCTZ	↓polyuria, ↑ urine osmolality, normalization of hypokalemia	(216)
Hydrochlorothiazide	Hydrochlorothiazide (HCTZ) 3.75mg q.d. s.c. last 7 days (osmotic minipump)	Inhibition of NCC and/or CA-II	Sprague-Dawley rats administered 40mmol/kg Li in chow for 3 weeks	Partial ↓ polyuria, partial ↑ urine osmolality, slight ↑ AQP2 expression, ↑ ENaCα, isoform shift ENaC γ	(220)
	HCTZ (100μM); HCTZ in diet (350mg/kg dry food) 10 days	Inhibition of CA-II	$mpkCCD_{c14}$ cells; C57BL6/J - $NCC^{-/-}$ mice administered 40mmol/kg Li in chow for 10 days	↑ AQP2 (mpkCCD cells); Partial ↓ polyuria, slight ↑ AQP2 expression and urine osmolality, ↓ urinary PGE_2 (mice)	(219)
	HCTZ in diet (350mg/kg dry food) 6-7 days	Not stated	Brattleboro rat (hereditary hypothalamic DI)	Complete ↑ urine osmolality, complete ↓ polyuria/polydipsia	(242)
	HCTZ in diet (350mg/kg dry food) 6-7 days	↑ in renal papillary fluid osmolality, ↑ proximal convoluted tubule fluid reabsorption		Complete ↑ urine osmolality, complete ↓ polyuria/polydipsia	(243)
	HCTZ ± amiloride/triamterene/acemetacin	↓ distal and ↑ proximal Na^+ reabsorption	Case study; 35y.o. Japanese male with congenital NDI due to deletion of AVPR2	HCTZ+Amiloride gave best response. ↓ polyuria and polydipsia from 8L/day to ~5L/day.	(241)

Acetazolamide	Acetazolamide 500mg b.i.d. 2 weeks	Inhibition of CA-II	Case study – patient with Li-NDI and 8-12L/day polyuria, unable to drink postoperatively leading to significant dehydration and hypernatremia	↓ polyuria from ~12L/day to 2-4L/d; normalization of plasma Na^+	(235)
	Acetazolamide 180 mg/kg dry food (mice) 10 days	Inhibition of CA-II	mpkCCDc14 cells; C57BL6/JOlaHsd mice administered 40mmol/kg Li in chow for 10 days	↑ AQP2 expression (mpkCCD cells); Partial ↓ polyuria/polydipsia, partial ↑ urine osmolality and partial ↑ AQP2 abundance, ↓ urinary PGE2 and GFR (mice)	(221)
	Acetazolamide 180 mg/kg dry food (mice) 2 weeks; Acetazolamide 250mg q.d. - 500mg b.i.d. 4 weeks (humans)	Inhibition of CA-II	C57BL6/JOlaHsd mice administered 40mmol/kg Li in chow 4 weeks; Human Li-NDI patients with urine osmolality <600 and >150 mosmol/kg with >15yr Li exposure.	Partial ↓ polyuria/polydipsia, partial ↑ urine osmolality and no change in AQP2 abundance (mice). No change in maximum urine concentration after dDAVP, ↓ GFR (humans)	(222)
NSAID	5,5-dimethyl-3-(3-fluorophenyl)-4-(4-methanesulfonylphenyl)-2(5H)-furanone 1 (DFU), 40mg/kg*day last 7 days	Specific inhibitor of COX-2(245)	40mmol/kg Li in chow 4 weeks	Partial ↓ polyuria, partial ↑ urine osmolality, ↑ AQP2 protein abundance, ↓ COX-2 expression and urinary PGE_2	(246)
	Indomethacin 50mg t.i.d.	Nonselective cyclooxygenase inhibitor	Case study; 44y.o. female receiving Li_2CO_3 300mg q.d.s. for 7 years	↓ polyuria, partial ↑ urine osmolality (effect on polyuria > osmolality)	(247)
	Indomethacin 75-150mg q.d.	Nonselective cyclooxygenase inhibitor	Case study; 47y.o. female receiving Li for 15 years, refractory to dDAVP, amiloride and hydrochlorothiazide	↓ polyuria (>90% decrease from maximum), ↑ creatinine	(248)
	Indomethacin ± aspirin/thiazide/dDAVP	Nonselective cyclooxygenase inhibitor	Literature review, 10 reports describing 22 patients in total	↓ polyuria (by ~2/3)	(248)

Table 2: Summary of preclinical and clinical studies evaluating treatment strategies for nephrogenic diabetes insipidus.

The phenotype displayed by $Keap1^{f/f}$ mice receiving Li mimicked aspects of the therapies reported in the studies outlined in **Table 2**. While Nrf2 hyperactivation completely prevented polyuria, the urine produced was dilute and expression of both glycosylated and non-glycosylated

AQP2 was significantly reduced compared to WT control, and no different from WT-Li. Expression of both NCC and CA-II was modestly down-regulated, suggesting that distal Na^+ reabsorption may be reduced. Reduction of distal tubular reabsorption with HCTZ has been shown to promote proximal tubular reabsorption to attenuate polyuria(241). Genetic Nrf2 activation and pharmacologic targeting of Nrf2 have been shown to be protective in murine models of vasculopathy(249–251). However, the effects of Nrf2 activation on vascular physiology have not been previously studied. This is especially significant since a recent clinical trial in which the potent Nrf2 activator CDDO-Me (Bardoxolone) was administered to an ESRD patient population was halted, citing increased adverse cardiovascular events and mortality(93).

In this context, the molecular mechanisms responsible for myogenic control of renal function were studied. Resistance arteries isolated from WT and $Keap1^{f/f}$ mice revealed that hyperactivation of Nrf2 caused endothelial dysfunction with impaired vasodilation in response to acetylcholine. Systemic systolic and diastolic blood pressures were found to be identical between WT and $Keap1^{f/f}$ mice, although mice with Nrf2 activation achieved the same BP with significantly reduced heart rate. Diurnal BP dipping in response to the angiotensin-converting enzyme inhibitor enalapril was found to be significantly blunted.

The vascular effects of Nrf2 activation occurred independently of NO signaling. Plasma and urine nitrite were elevated, consistent with the finding that siRNA knockdown of Nrf2 reduces nitrite production *in vitro*(252). Mesenteric artery dilation elicited by the NO donor sodium nitroprusside was normal in $Keap1^{f/f}$ mice. These results suggest that activation of Nrf2 may increase effectiveness of tubuloglomerular feedback via alteration of myogenic response mechanisms to reduce GFR and the volume delivered to the collecting system. Importantly, plasma

BUN was no different between these three groups indicating that the degree of afferent arteriolar constriction was likely within physiological tolerances and that renal function was not impaired.

The anti-inflammatory effects of Nrf2 activation have been the subject of extensive study and have motivated pharmacologic development of Nrf2 inducers for the treatment of a variety of disorders(253). The interplay between Nrf2 and inflammatory pathways is complex and remains incompletely understood. Nrf2 activation may help cells weather the storm of cytokines and reactive species released by immune cells by upregulating small-molecule cellular defenses such as glutathione as well as ROS-detoxifying enzymes such as NQO1. Nrf2 activation may directly promote a tolerogenic phenotype to reduce inflammatory cell activation and cytokine production(254). Direct interaction between Nrf2 accessory proteins such as Keap1 and the nuclear factor kappa B (NF-κB) pathway has also been documented(110, 255). It has been shown that COX-2 expression is elevated in colon of $Nrf2^{-/-}$ mice; however, COX expression in mice with hyperactivation of Nrf2 has not been investigated. In our present study we show that renal COX-1 and COX-2 expression are reduced in $Keap1^{f/f}$ mice and increased in $Nrf2^{-/-}$ mice. The reduction in COX expression was accompanied by diminished production of the vasodilator PGI_2.

Cyclooxygenase inhibitors have been used as a last-resort therapeutic for Li-NDI patients(224, 256), despite the well-documented risk of acute kidney injury associated with this class of drugs(257). Mice lacking the microsomal prostaglandin E synthase-1 (mPGES-1) were also found to be resistant to Li-NDI(258). However, these animals displayed normal AQP2 expression and maintained normal urine concentrating ability, in contrast to the $Keap1^{f/f}$ in this study which displayed reduced AQP2 abundance as well as hyposthenuria. These disparities suggest that the physiologic mechanism underlying the protection afforded by knockout of mPGES-1 and Nrf2-mediated reduction in cyclooxygenase products are not identical.

In summary, our results demonstrate that activation of the Keap1/Nrf2 signaling pathway completely protects mice from polydipsia/polyuria in Li-NDI. The reduction in polydipsia occurs without improvement in AQP2 expression or increase in urine osmolality. Activation of Nrf2 down-regulates expression of NCC and CA-II, mimicking the effects of two common diuretic therapies for Li-NDI. Nrf2 activation reduced COX-1 and -2 expression and down-regulated inflammation-derived vasodilator production, and caused impaired resistance vessel dilation in response to acetylcholine. We hypothesize that these vascular effects of Nrf2 activation are recapitulated in the afferent arteriole supplying the nephron, leading to tubuloglomerular feedback mediated protection against Li-NDI **(Figure 37)**. Future experiments will explore pharmacologic activation of Nrf2 as potential therapeutic intervention strategy for Li-NDI.

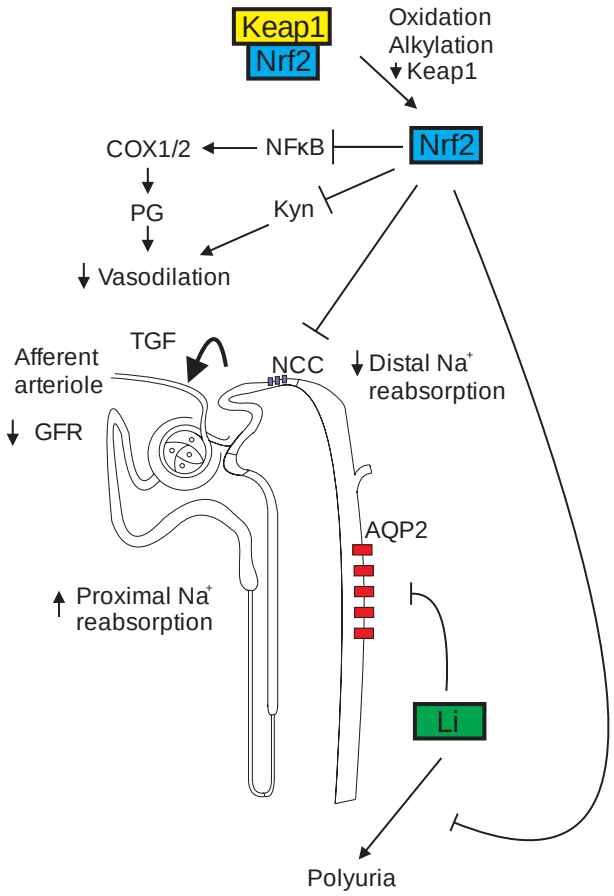

Figure 37: Schematic of putative mechanisms by which hyperactivation of Nrf2 protects against Li-NDI, showing direct and indirect effects along nephron

Lithium induces nephrogenic diabetes insipidus (Li-NDI) through down-regulation of collecting duct AQP2 water channel, rendering the collecting system insensitive to antidiuretic hormone. Hyperactivation of Nrf2 through partial genetic ablation of Keap1 completely protects against polyuria in Li-NDI, without rescuing AQP2 expression. Nrf2 impairs ACh-mediated vasodilation independently from NO signaling and coinciding with down-regulation of inflammation related vasodilatory autocoids such as prostacyclin and kynurenine. We postulate that the vascular effects of Nrf2 activation extend to renal hemodynamics and reduce polyuria through tubuloglomerular feedback effects.

5.0 GENERAL SUMMARY DISCUSSION AND FUTURE DIRECTIONS

Virtually every aspect of cellular life, from metabolism to signaling, relies on a foundation of controlled oxidation-reduction reactions. Enzymatically harnessing thermodynamic disequilibria within specific cellular compartments and within specific temporal contexts allows cells to capture, transduce, and use energy. Intrinsic errors as well as extrinsic insults inevitably disrupt this delicate system, leading to off-target oxidation of cellular macromolecules with resultant damage to membranes, proteins, and genetic material to the significant detriment of the organism. This occurrence, broadly termed “oxidative stress,” is the mechanistic underpinning for many diseases.

The last 30 years have seen a dramatic increase in interest in improving human health through pharmaceutical or nutraceutical supplementation of antioxidants. However, evidence showing protection by direct administration of antioxidants has remained elusive. Evaluating the clinical efficacy of antioxidants poses several unique challenges(259). Many anti-oxidants have been evaluated on their ability to change the course of chronic conditions such as chronic kidney disease. Clinical trials on an equivalent time-scale (years to decades) are logistically challenging and financially costly to carry out. Patient compliance, including adherence to medication or self-reporting in the case of dietary antioxidant intake, is also difficult to ensure over longer time periods. With long-duration trials it also becomes difficult to recruit and retain sufficient numbers of patients to achieve appropriate power. Additionally, many antioxidants are chosen for study based on availability or prevalence in certain diets rather than their chemical antioxidant properties. Finally, it is possible that while anti-oxidants may slow disease onset, they may be unable to reverse established tissue damage resulting from decades of oxidative stress.

It is also possible that antioxidant supplementation displays no beneficial effects. In the PRESERVE study, the antioxidant GSH precursor N-acetylcysteine (oral N-acetylcysteine and IV physiologic saline) was compared to control (IV sodium bicarbonate and oral placebo) in 5,177 patients at high risk for renal complications who were scheduled for angiography. Despite numerous smaller trials showing kidney protection by N-acetylcysteine(260), in this study N-acetylcysteine was no more effective than sodium bicarbonate for preventing contrast-induced acute kidney injury (207).

Thiol redox chemistry likely predates oxygen-based redox chemistry: early anaerobic, chemoautotrophic life forms relied on sulfur instead of oxygen for energy. In this context, it is not surprising that thiol-based redox-sensing and redox-buffering systems are ubiquitous and highly conserved among eukaryotes.

Recently, electrophilic chemical agents, which activate the thiol-based redox-sensor Keap1/Nrf2 to elicit protective cellular antioxidant responses, have been identified as promising drug candidates. This thesis, and my research as a graduate student, has focused on improving basic understanding of how pharmacologic activators of Nrf2 signaling affect thiol homeostasis, and exploring a preclinical animal model of Nrf2 activation to uncover potentially beneficial effects on renal physiology.

5.1 ELECTROPHILE MODULATION OF THIOL HOMEOSTASIS

The question posed in Chapter 3 of this dissertation was whether therapeutic electrophiles NO_2-OA, CDDO-derivatives, or DMF reduces intracellular GSH through conjugation reactions, or whether electrophile-mediated activation of Nrf2 signaling bolsters intracellular antioxidant

defenses through increasing GSH. Electrophiles were found to predominantly increase intracellular GSH in RAW264.7 macrophage cells through upregulation of Nrf2-dependent biosynthetic machinery including GCL, although a reduction in GSH was observed at early time-points (~1hr) after electrophiles exposure. The effects on GSH depletion and GSH biosynthesis were temporally distinct. Unexpectedly, the studies also demonstrated a paradoxical increase in intracellular GSSG which exceeded the increase in GSH. This phenomenon was studied in detail to test whether electrophile-mediated GSSG accumulation was the result of increased oxidative stress. Peroxiredoxin oxidation state was evaluated *via* immunoblotting for monomeric (reduced) and dimeric (oxidized) Prdx1 and Prdx3; LPS and H_2O_2 but not electrophiles induced Prdx oxidation.

Finally, the ratio of GSH to GSSG was found to be regulated by the activity of GR, which was shown to act as a GSH- and electrophile-sensitive rheostat. GR was found to be product-inhibited by GSH, with increases in GSH reducing GR activity *in vitro* and in cells. Electrophilic NO_2-OA was found to covalently inhibit GR through reactivity with Cys61 at the GR catalytic site.

5.2 FUTURE DIRECTIONS: ELECTROPHILE EFFECTS ON GLUTATHIONE HOMEOSTASIS

This line of inquiry leaves several questions unanswered. First, while this dissertation shows that electrophiles increase protein S-glutathionylation, the mechanisms, specificity, and biological sequelae of this post-translational modification are not known. Non-reducing gel electrophoresis followed by immunoblotting with anti-GSH antibody (Virogen, Watertown, MA) showed

numerous bands (data not shown) and an increase in band intensity following NO_2-OA treatment. This suggests that multiple proteins may be S-glutathionylation and confirms the quantitative increase in S-glutathionylation induced by NO_2-OA shown in **Figure 16**. However, the small size of the GSH epitope raises concerns about the specificity of this antibody-based approach, and S-glutathionylation of specific proteins identified by this approach should be confirmed using mass spectrometry techniques. Follow-up experiments will also be needed to determine the extent and mechanism by which GSH and/or S-glutathionylation impact macrophage inflammatory function.

Second, it remains to be shown how the concomitant increases in intracellular GSH and GSSG induced by electrophile exposure translate from a simplified cell-culture system to animal models or human patients. These studies will be complicated by the lability of GSH and the need for rapid and consistent blocking of samples with reactive alkyl compounds such as NEM, both for enhancing detection of GSH and for prevention of GSH auto-oxidation.

5.3 NRF2 PROTECTS AGAINST LI-NDI

In Chapter 4 of this thesis, the relationship between hyperactivation of Nrf2 and development of nephrogenic diabetes insipidus was investigated. Despite beneficial effects of genetic or pharmacologic Nrf2 activation in diverse disease models, recent publications(47, 48) have shown that hyperactivation of this pathway due to complete absence of renal Keap1 results in severe renal insufficiency. These animals develop nephrogenic diabetes insipidus with polyuria/polydipsia as well as structural kidney damage in the form of hydronephrosis. Clinically, nephrogenic diabetes insipidus occurs most commonly in patients chronically receiving Li for management of

psychiatric disorders. Moreover, Li is thought to be an inhibitor of the Nrf2 repressor GSK3β(159, 209, 261). *It was therefore hypothesized that Li induces NDI via hyperactivation of Nrf2.* A mouse model of iatrogenic Li-NDI was studied to determine if Li caused NDI through activation of Nrf2 *in vivo*. An *in vitro* model system using primary human renal cortical cells was also evaluated. In these models Li failed to activate Nrf2 signaling, as tested by immunoblotting and immunofluorescence for the canonical Nrf2 target protein NQO1. Unexpectedly, graded genetic activation of Nrf2 achieved through hypomorphism of floxed Keap1 completely protected mice from Li-NDI. Existing therapeutic strategies are limited to diuretics targeting NCC and ENaC, carbonic anhydrase inhibitors, and NSAIDs, as reviewed in **Table 2**. The mechanism by which Nrf2 activation in the $Keap1^{f/f}$ mouse model protected against Li-NDI appeared to involve downregulation of distal tubule expression of NCC mimicking thiazides, downregulation of CA-II, and alteration of endothelial function which could affect renal hemodynamics and tubuloglomerular feedback.

5.4 FUTURE DIRECTIONS: PRECLINICAL EVALUATION OF ELECTROPHILIC NRF2 ACTIVATORS FOR LI-NDI

The discovery that graded genetic activation of Nrf2 protects against Li-NDI development suggests significant clinical implications for the treatment of this disease. Fortuitously, targeted electrophilic activators of Nrf2 are already in clinical development for treatment of both acute kidney injury (AKI) and CKD. In addition to the significant risk of Li-NDI, the incidence of CKD is significantly increased by Li administration(262–264). It is possible that as an electrophilic Nrf2 activator could ameliorate or treat both of these side effects of Li. To evaluate the clinical potential

of Nrf2 activators in this context, testing will be continued in preclinical models. Future experiments in our laboratory will evaluate Nrf2 activators including Bardoxolone (CDDO-Me) and CDDO-Im, as well as electrophilic NO_2-FA including NO_2-OA and NO_2-cLA, in our murine model of Li-NDI. In addition to evaluating whether Li-NDI develops in mice pre-treated with electrophiles, it will be important to independently test whether these compounds are efficacious in mitigating symptoms in established disease. Furthermore, electrophile effects on progression to CKD in a chronic lithium exposure model will be assessed by evaluating fibrotic markers including fibronectin and α-smooth muscle actin (α-SMA).

If Nrf2 activation is an effective strategy for treating Li-NDI, it may also hold clinical relevance in hereditary nephrogenic diabetes insipidus. Hereditary NDI is the result of defects in the gene encoding the vasopressin V2 receptor, or less commonly, a mutation in AQP2(265). Mouse models of AQP2 mutation have been developed in the last 10 years which would facilitate this line of inquiry(266). Importantly, the beneficial effect of Nrf2 hyperactivation appears to be independent of AQP2 expression.

A preclinical research program to develop Nrf2 activators for treatment of NDI will necessitate additional mechanistic studies. Based on the present study, as well as previously published reports, it is thought that sensitivity or resistance to polyuria is determined at the level of renal microvasculature, as protection is not necessarily correlated with AQP2 expression. While we were able to demonstrate Nrf2-mediated reduction in two vasodilatory autocoid signaling molecules, kynurenine (in plasma) and prostacyclin (in kidney homogenate), it remains to be shown whether protection is conferred by down-regulation one or both of these molecules.

While efficacious as a last-resort therapy for Li-NDI, COX inhibition poses non-trivial risks for renal patients(267–269). It remains to be seen if the adverse renal effects of selective or

non-selective COX-inhibition, or facets thereof, are recapitulated by Nrf2-mediated down-regulation of COX. Renal injury caused by COX inhibition is attributable to hypoperfusion. Nrf2 hyperactivation has been previously shown to protect against renal ischemia-reperfusion injury(46), suggesting that Nrf2 activators may exert beneficial renal vascular effects protecting against Li-NDI while simultaneously preventing ischemic tubular damage.

Finally, while gene expression profiles of transgenic and pharmacologic activation of Nrf2 overlap, they are also distinct. To our knowledge RNA-seq experiments comparing renal gene expression in these models has not been published . Moreover, studies of NO_2-FA have shown that even structurally-related electrophiles differentially engage the Nrf2 and NFkB pathways(109). Thus, it may be necessary to further elucidate structure-function relationships to identify electrophiles with greatest clinical promise for treating Li-NDI.

BIBLIOGRAPHY

1. Lyons, T. W., Reinhard, C. T., and Planavsky, N. J. (2014) The rise of oxygen in Earth's early ocean and atmosphere. *Nature*. **506**, 307–315
2. Go, Y.-M., and Jones, D. P. (2013) The redox proteome. *J. Biol. Chem.* **288**, 26512–20
3. Itoh, K., Wakabayashi, N., Katoh, Y., Ishii, T., Igarashi, K., Engel, J. D., and Yamamoto, M. (1999) Keap1 represses nuclear activation of antioxidant responsive elements by Nrf2 through binding to the amino-terminal Neh2 domain. *Genes Dev.* **13**, 76–86
4. Lau, A., Tian, W., Whitman, S. A., and Zhang, D. D. (2013) The Predicted Molecular Weight of Nrf2: It Is What It Is Not. *Antioxid. Redox Signal.* **18**, 91–93
5. MacLeod, A. K., McMahon, M., Plummer, S. M., Higgins, L. G., Penning, T. M., Igarashi, K., and Hayes, J. D. (2009) Characterization of the cancer chemopreventive NRF2-dependent gene battery in human keratinocytes: demonstration that the KEAP1-NRF2 pathway, and not the BACH1-NRF2 pathway, controls cytoprotection against electrophiles as well as redox-cycling compounds. *Carcinogenesis*. **30**, 1571–1580
6. Hayes, J. D., and McMahon, M. (2009) NRF2 and KEAP1 mutations: permanent activation of an adaptive response in cancer. *Trends Biochem. Sci.* **34**, 176–188
7. Hayes, J. D., McMahon, M., Chowdhry, S., and Dinkova-Kostova, A. T. (2010) Cancer Chemoprevention Mechanisms Mediated Through the Keap1–Nrf2 Pathway. *Antioxid. Redox Signal.* **13**, 1713–1748
8. Kansanen, E., Kuosmanen, S. M., Leinonen, H., and Levonen, A.-L. (2013) The Keap1-Nrf2 pathway: Mechanisms of activation and dysregulation in cancer. *Redox Biol.* **1**, 45–49
9. Hayes, J. D., and Dinkova-Kostova, A. T. (2014) The Nrf2 regulatory network provides an

interface between redox and intermediary metabolism. *Trends Biochem. Sci.* **39**, 199–218

10. Ogura, T., Tong, K. I., Mio, K., Maruyama, Y., Kurokawa, H., Sato, C., and Yamamoto, M. (2010) Keap1 is a forked-stem dimer structure with two large spheres enclosing the intervening, double glycine repeat, and C-terminal domains. *Proc. Natl. Acad. Sci.* **107**, 2842–2847
11. Baird, L., and Dinkova-Kostova, A. T. (2011) The cytoprotective role of the Keap1-Nrf2 pathway. *Arch. Toxicol.* **85**, 241–272
12. Alam, J., Stewart, D., Touchard, C., Boinapally, S., Choi, A. M. K., and Cook, J. L. (1999) Nrf2, a Cap'n'Collar transcription factor, regulates induction of the heme oxygenase-1 gene. *J. Biol. Chem.* **274**, 26071–26078
13. Ishii, T., Itoh, K., Takahashi, S., Sato, H., Yanagawa, T., Katoh, Y., Bannai, S., and Yamamoto, M. (2000) Transcription factor Nrf2 coordinately regulates a group of oxidative stress-inducible genes in macrophages. *J. Biol. Chem.* **275**, 16023–16029
14. Hayashi, A., Suzuki, H., Itoh, K., Yamamoto, M., and Sugiyama, Y. (2003) Transcription factor Nrf2 is required for the constitutive and inducible expression of multidrug resistance-associated protein 1 in mouse embryo fibroblasts. *Biochem. Biophys. Res. Commun.* **310**, 824–829
15. Maher, J. M., Dieter, M. Z., Aleksunes, L. M., Slitt, A. L., Guo, G., Tanaka, Y., Scheffer, G. L., Chan, J. Y., Manautou, J. E., Chen, Y., Dalton, T. P., Yamamoto, M., and Klaassen, C. D. (2007) Oxidative and electrophilic stress induces multidrug resistance-associated protein transporters via the nuclear factor-E2-related factor-2 transcriptional pathway. *Hepatology*. **46**, 1597–1610
16. Jeyapaul, J., and Jaiswal, A. K. (2000) Nrf2 and c-Jun regulation of antioxidant response

element (ARE)-mediated expression and induction of γ-glutamylcysteine synthetase heavy subunit gene. *Biochem. Pharmacol.* **59**, 1433–1439

17. Favreau, L. V., and Pickett, C. B. (1991) Transcriptional regulation of the rat NAD(P)H:quinone reductase gene. Identification of regulatory elements controlling basal level expression and inducible expression by planar aromatic compounds and phenolic antioxidants. *J. Biol. Chem.* **266**, 4556–4561

18. Lewerenz, J., Hewett, S. J., Huang, Y., Lambros, M., Gout, P. W., Kalivas, P. W., Massie, A., Smolders, I., Methner, A., Pergande, M., Smith, S. B., Ganapathy, V., and Maher, P. (2013) The Cystine/Glutamate Antiporter System x c − in Health and Disease: From Molecular Mechanisms to Novel Therapeutic Opportunities. *Antioxid. Redox Signal.* **18**, 522–555

19. Itoh, K., Wakabayashi, N., Katoh, Y., Ishii, T., O'Connor, T., and Yamamoto, M. (2003) Keap1 regulates both cytoplasmic-nuclear shuttling and degradation of Nrf2 in response to electrophiles. *Genes to Cells*. **8**, 379–391

20. Wakabayashi, N., Itoh, K., Wakabayashi, J., Motohashi, H., Noda, S., Takahashi, S., Imakado, S., Kotsuji, T., Otsuka, F., Roop, D. R., Harada, T., Engel, J. D., and Yamamoto, M. (2003) Keap1-null mutation leads to postnatal lethality due to constitutive Nrf2 activation. *Nat. Genet.* **35**, 238–245

21. Devling, T. W. P., Lindsay, C. D., McLellan, L. I., McMahon, M., and Hayes, J. D. (2005) Utility of siRNA against Keap1 as a strategy to stimulate a cancer chemopreventive phenotype. *Proc. Natl. Acad. Sci. U. S. A.* **102**, 7280–7285A

22. Li, X., Zhang, D., Hannink, M., and Beamer, L. J. (2004) Crystal structure of the Kelch domain of human Keap1. *J. Biol. Chem.* **279**, 54750–54758

23. Kensler, T. W., Wakabayashi, N., and Biswal, S. (2007) Cell Survival Responses to Environmental Stresses Via the Keap1-Nrf2-ARE Pathway. *Annu. Rev. Pharmacol. Toxicol.* **47**, 89–116

24. Taguchi, K., Motohashi, H., and Yamamoto, M. (2011) Molecular mechanisms of the Keap1–Nrf2 pathway in stress response and cancer evolution. *Genes Cells*. **16**, 123–40

25. Chorley, B. N., Campbell, M. R., Wang, X., Karaca, M., Sambandan, D., Bangura, F., Xue, P., Pi, J., Kleeberger, S. R., and Bell, D. A. (2012) Identification of novel NRF2-regulated genes by ChiP-Seq: Influence on retinoid X receptor alpha. *Nucleic Acids Res.* **40**, 7416–7429

26. Nguyen, T., Sherratt, P. J., Nioi, P., Yang, C. S., and Pickett, C. B. (2005) Nrf2 controls constitutive and inducible expression of ARE-driven genes through a dynamic pathway involving nucleocytoplasmic shuttling by Keap1. *J. Biol. Chem.* **280**, 32485–32492

27. Chan, K., Lu, R., Chang, J. C., and Kan, Y. W. (1996) NRF2, a member of the NFE2 family of transcription factors, is not essential for murine erythropoiesis, growth, and development. *Proc. Natl. Acad. Sci. U. S. A.* **93**, 13943–8

28. Itoh, K., Chiba, T., Takahashi, S., Ishii, T., Igarashi, K., Katoh, Y., Oyake, T., Hayashi, N., Satoh, K., Hatayama, I., Yamamoto, M., and Nabeshima, Y. (1997) An Nrf2/Small Maf Heterodimer Mediates the Induction of Phase II Detoxifying Enzyme Genes through Antioxidant Response Elements. *Biochem. Biophys. Res. Commun.* **236**, 313–322

29. McMahon, M., Itoh, K., Yamamoto, M., Chanas, S. A., Henderson, C. J., McLellan, L. I., Wolf, C. R., Cavin, C., and Hayes, J. D. (2001) The cap “n” collar basic leucine zipper transcription factor Nrf2 (NF-E2 p45-related factor 2) controls both constitutive and inducible expression of intestinal detoxification and glutathione biosynthetic enzymes.

Cancer Res. **61**, 3299–3307

30. Leung, L., Kwong, M., Hou, S., Lee, C., and Chan, J. Y. (2003) Deficiency of the Nrf1 and Nrf2 Transcription Factors Results in Early Embryonic Lethality and Severe Oxidative Stress. *J. Biol. Chem.* **278**, 48021–48029
31. Lee, J.-M., Chan, K., Kan, Y. W., and Johnson, J. A. (2004) Targeted disruption of Nrf2 causes regenerative immune-mediated hemolytic anemia. *Proc. Natl. Acad. Sci. U. S. A.* **101**, 9751–6
32. Yoh, K., Itoh, K., Enomoto, A., Hirayama, A., Yamaguchi, N., Kobayashi, M., Morito, N., Koyama, A., Yamamoto, M., and Takahashi, S. (2001) Nrf2-deficient female mice develop lupus-like autoimmune nephritis. *Kidney Int.* **60**, 1343–1353
33. Córdova, E. J., Velázquez-Cruz, R., Centeno, F., Baca, V., and Orozco, L. (2010) The NRF2 gene variant, -653G/A, is associated with nephritis in childhood-onset systemic lupus erythematosus. *Lupus*. **19**, 1237–1242
34. Yoh, K., Hirayama, A., Ishizaki, K., Yamada, A., Takeuchi, M., Yamagishi, S. I., Morito, N., Nakano, T., Ojima, M., Shimohata, H., Itoh, K., Takahashi, S., and Yamamoto, M. (2008) Hyperglycemia induces oxidative and nitrosative stress and increases renal functional impairment in Nrf2-deficient mice. *Genes Cells*. **13**, 1159–1170
35. Jiang, T., Huang, Z., Lin, Y., Zhang, Z., Fang, D., and Zhang, D. D. (2010) The Protective Role of Nrf2 in Streptozotocin-Induced Diabetic Nephropathy. *Diabetes*. **59**, 850–860
36. Kudoh, K., Uchinami, H., Yoshioka, M., Seki, E., and Yamamoto, Y. (2014) Nrf2 activation protects the liver from ischemia/reperfusion injury in Mice. *Ann. Surg.* **260**, 118–127
37. Thimmulappa, R. K., Lee, H., Rangasamy, T., Reddy, S. P., Yamamoto, M., Kensler, T. W., and Biswal, S. (2006) Nrf2 is a critical regulator of the innate immune response and

survival during experimental sepsis. *J. Clin. Invest.* **116**, 984–995

38. Aoki, Y., Sato, H., Nishimura, N., Takahashi, S., Itoh, K., and Yamamoto, M. (2001) Accelerated DNA adduct formation in the lung of the Nrf2 knockout mouse exposed to diesel exhaust. *Toxicol. Appl. Pharmacol.* **173**, 154–160

39. Iida, K., Itoh, K., Kumagai, Y., Oyasu, R., Hattori, K., Kawai, K., Shimazui, T., Akaza, H., and Yamamoto, M. (2004) Nrf2 is essential for the chemopreventive efficacy of oltipraz against urinary bladder carcinogenesis. *Cancer Res.* **64**, 6424–6431

40. Yu, X., and Kensler, T. (2005) Nrf2 as a target for cancer chemoprevention. *Mutat. Res. - Fundam. Mol. Mech. Mutagen.* **591**, 93–102

41. Taguchi, K., Maher, J. M., Suzuki, T., Kawatani, Y., Motohashi, H., and Yamamoto, M. (2010) Genetic Analysis of Cytoprotective Functions Supported by Graded Expression of Keap1. *Mol. Cell. Biol.* **30**, 3016–3026

42. Osburn, W. O., Yates, M. S., Dolan, P. D., Chen, S., Liby, K. T., Sporn, M. B., Taguchi, K., Yamamoto, M., and Kensler, T. W. (2008) Genetic or pharmacologic amplification of Nrf2 signaling inhibits acute inflammatory liver injury in mice. *Toxicol. Sci.* **104**, 218–227

43. Ke, B., Shen, X. Da, Zhang, Y., Ji, H., Gao, F., Yue, S., Kamo, N., Zhai, Y., Yamamoto, M., Busuttil, R. W., and Kupiec-Weglinski, J. W. (2013) KEAP1-NRF2 complex in ischemia-induced hepatocellular damage of mouse liver transplants. *J. Hepatol.* **59**, 1200–1207

44. Miyazaki, Y., Shimizu, A., Pastan, I., Taguchi, K., Naganuma, E., Suzuki, T., Hosoya, T., Yokoo, T., Saito, A., Miyata, T., Yamamoto, M., and Matsusaka, T. (2014) Keap1 inhibition attenuates glomerulosclerosis. *Nephrol. Dial. Transplant.* **29**, 783–791

45. Nezu, M., Souma, T., Yu, L., Suzuki, T., Saigusa, D., Ito, S., Suzuki, N., and Yamamoto,

M. (2017) Transcription factor Nrf2 hyperactivation in early-phase renal ischemia-reperfusion injury prevents tubular damage progression. *Kidney Int.* **91**, 387–401

46. Tan, R. J., Chartoumpekis, D. V., Rush, B. M., Zhou, D., Fu, H., Kensler, T. W., and Liu, Y. (2016) Keap1 hypomorphism protects against ischemic and obstructive kidney disease. *Sci. Rep.* **6**, 36185

47. Noel, S., Arend, L. J., Bandapalle, S., Reddy, S. P., and Rabb, H. (2016) Kidney epithelium specific deletion of kelch-like ECH-associated protein 1 (Keap1) causes hydronephrosis in mice. *BMC Nephrol.* 10.1186/s12882-016-0310-y

48. Suzuki, T., Seki, S., Hiramoto, K., Naganuma, E., Kobayashi, E. H., Yamaoka, A., Baird, L., Takahashi, N., Sato, H., and Yamamoto, M. (2017) Hyperactivation of Nrf2 in early tubular development induces nephrogenic diabetes insipidus. *Nat. Commun.* **8**, 14577

49. McCormick, J. A., Yang, C. L., Zhang, C., Davidge, B., Blankenstein, K. I., Terker, A. S., Yarbrough, B., Meermeier, N. P., Park, H. J., McCully, B., West, M., Borschewski, A., Himmerkus, N., Bleich, M., Bachmann, S., Mutig, K., Argaiz, E. R., Gamba, G., Singer, J. D., and Ellison, D. H. (2014) Hyperkalemic hypertension-associated cullin 3 promotes WNK signaling by degrading KLHL3. *J. Clin. Invest.* **124**, 4723–4736

50. Rao, R., Patel, S., Hao, C., Woodgett, J., and Harris, R. (2010) GSK3beta mediates renal response to vasopressin by modulating adenylate cyclase activity. *J. Am. Soc. Nephrol.* **21**, 428–37

51. Pearson, G. (1963) Hard and Soft Acids and Bases. *J. Am. Chem. Soc.* **85**, 3533–3539

52. Lopachin, R. M., Gavin, T., Decaprio, A., and Barber, D. S. (2012) Application of the Hard and Soft, Acids and Bases (HSAB) theory to toxicant--target interactions. *Chem. Res. Toxicol.* **25**, 239–51

53. Netto, L. E. S., de Oliveira, M. A., Monteiro, G., Demasi, A. P. D., Cussiol, J. R. R., Discola, K. F., Demasi, M., Silva, G. M., Alves, S. V., Faria, V. G., and Horta, B. B. (2007) Reactive cysteine in proteins: Protein folding, antioxidant defense, redox signaling and more. *Comp. Biochem. Physiol. - C Toxicol. Pharmacol.* **146**, 180–193

54. Yates, M. S., Tran, Q. T., Dolan, P. M., Osburn, W. O., Shin, S., McCulloch, C. C., Silkworth, J. B., Taguchi, K., Yamamoto, M., Williams, C. R., Liby, K. T., Sporn, M. B., Sutter, T. R., and Kensler, T. W. (2009) Genetic versus chemoprotective activation of Nrf2 signaling: Overlapping yet distinct gene expression profiles between Keap1 knockout and triterpenoid-treated mice. *Carcinogenesis*. **30**, 1024–1031

55. Rudolph, V., Rudolph, T. K., Schopfer, F. J., Bonacci, G., Woodcock, S. R., Cole, M. P., Baker, P. R. S., Ramani, R., and Freeman, B. A. (2010) Endogenous generation and protective effects of nitro-fatty acids in a murine model of focal cardiac ischaemia and reperfusion. *Cardiovasc. Res.* **85**, 155–166

56. Bonacci, G., Baker, P. R. S., Salvatore, S. R., Shores, D., Khoo, N. K. H., Koenitzer, J. R., Vitturi, D. A., Woodcock, S. R., Golin-Bisello, F., Cole, M. P., Watkins, S., St. Croix, C., Batthyany, C. I., Freeman, B. A., and Schopfer, F. J. (2012) Conjugated linoleic acid is a preferential substrate for fatty acid nitration. *J. Biol. Chem.* **287**, 44071–44082

57. Pryor, W. A., Lightsey, J. W., and Church, D. F. (1982) Reaction of nitrogen dioxide with alkenes and polyunsaturated fatty acids: Addition and hydrogen abstraction mechanisms. *J. Am. Chem. Soc.* **104**, 6685–6692

58. Liu, X., Miller, M. J., Joshi, M. S., Thomas, D. D., and Lancaster, J. R. (1998) Accelerated reaction of nitric oxide with O2 within the hydrophobic interior of biological membranes. *Proc. Natl. Acad. Sci. U. S. A.* **95**, 2175–9

59. Fazzari, M., Trostchansky, A., Schopfer, F. J., Salvatore, S. R., Sánchez-Calvo, B., Vitturi, D., Valderrama, R., Barroso, J. B., Radi, R., Freeman, B. A., and Rubbo, H. (2014) Olives and olive oil are sources of electrophilic fatty acid nitroalkenes. *PLoS One*. **9**, e84884

60. Cui, T., Schopfer, F. J., Zhang, J., Chen, K., Ichikawa, T., Baker, P. R. S. S., Batthyany, C., Chacko, B. K., Feng, X., Patel, R. P., Agarwal, A., Freeman, B. A., and Chen, Y. E. (2006) Nitrated fatty acids: Endogenous anti-inflammatory signaling mediators. *J. Biol. Chem.* **281**, 35686–98

61. Ferreira, A. M., Ferrari, M. I., Trostchansky, A., Batthyany, C., Souza, J. M., Alvarez, M. N., López, G. V., Baker, P. R. S., Schopfer, F. J., O'Donnell, V., Freeman, B. A., and Rubbo, H. (2009) Macrophage activation induces formation of the anti-inflammatory lipid cholesteryl-nitrolinoleate. *Biochem. J.* **417**, 223–238

62. Nadtochiy, S. M., Baker, P. R. S., Freeman, B. A., and Brookes, P. S. (2009) Mitochondrial nitroalkene formation and mild uncoupling in ischaemic preconditioning: Implications for cardioprotection. *Cardiovasc. Res.* **82**, 333–340

63. Delmastro-Greenwood, M., Hughan, K. S., Vitturi, D. A., Salvatore, S. R., Grimes, G., Potti, G., Shiva, S., Schopfer, F. J., Gladwin, M. T., Freeman, B. A., and Gelhaus Wendell, S. (2015) Nitrite and nitrate-dependent generation of anti-inflammatory fatty acid nitroalkenes. *Free Radic. Biol. Med.* **89**, 333–41

64. Lima, E. S., Di Mascio, P., and Abdalla, D. S. P. (2003) Cholesteryl nitrolinoleate, a nitrated lipid present in human blood plasma and lipoproteins. *J. Lipid Res.* **44**, 1660–1666

65. Baker, P. R. S., Schopfer, F. J., Sweeney, S., and Freeman, B. A. (2004) Red cell membrane and plasma linoleic acid nitration products: synthesis, clinical identification, and quantitation. *Proc. Natl. Acad. Sci. U. S. A.* **101**, 11577–82

66. Schopfer, F. J., Lin, Y., Baker, P. R. S., Cui, T., Garcia-Barrio, M., Zhang, J., Chen, K., Chen, Y. E., and Freeman, B. A. (2005) Nitrolinoleic acid: an endogenous peroxisome proliferator-activated receptor gamma ligand. *Proc. Natl. Acad. Sci. U. S. A.* **102**, 2340–2345

67. Baker, P. R. S., Lin, Y., Schopfer, F. J., Woodcock, S. R., Groeger, A. L., Batthyany, C., Sweeney, S., Long, M. H., Iles, K. E., Baker, L. M. S., Branchaud, B. P., Chen, Y. E., and Freeman, B. A. (2005) Fatty acid transduction of nitric oxide signaling: multiple nitrated unsaturated fatty acid derivatives exist in human blood and urine and serve as endogenous peroxisome proliferator-activated receptor ligands. *J. Biol. Chem.* **280**, 42464–42475

68. Tsikas, D., Zoerner, A. A., Mitschke, A., and Gutzki, F.-M. (2009) Nitro-fatty Acids Occur in Human Plasma in the Picomolar Range: a Targeted Nitro-lipidomics GC–MS/MS Study. *Lipids*. **44**, 855–865

69. Salvatore, S. R., Vitturi, D. A., Baker, P. R. S., Bonacci, G., Koenitzer, J. R., Woodcock, S. R., Freeman, B. A., and Schopfer, F. J. (2013) Characterization and quantification of endogenous fatty acid nitroalkene metabolites in human urine. *J. Lipid Res.* **54**, 1998–2009

70. Salvatore, S. R., Vitturi, D. A., Fazzari, M., Jorkasky, D. K., and Schopfer, F. J. (2017) Evaluation of 10-Nitro Oleic Acid Bio-Elimination in Rats and Humans. *Sci. Rep.* **7**, 39900

71. Hinchman, C. A., and Ballatori, N. (1994) Glutathione conjugation and conversion to mercapturic acids can occur as an intrahepatic process. *J. Toxicol. Environ. Health*. **41**, 387–409

72. Fu, J., Schoeman, J. C., Harms, A. C., van Wietmarschen, H. A., Vreeken, R. J., Berger, R., Cuppen, B. V. J., Lafeber, F. P. J. G., van der Greef, J., and Hankemeier, T. (2016) Metabolomics profiling of the free and total oxidised lipids in urine by LC-MS/MS:

application in patients with rheumatoid arthritis. *Anal. Bioanal. Chem.* **408**, 6307–19

73. Liu, H., Jia, Z. Z., Soodvilai, S., Guan, G., Wang, M.-H. M.-H., Dong, Z., Symons, J. D., Yang, T., Yang, T., Jia, Z. Z., Soodvilai, S., Guan, G., Wang, M.-H. M.-H., Dong, Z., Symons, J. D., and Yang, T. (2008) Nitro-oleic acid protects the mouse kidney from ischemia and reperfusion injury. *Am. J. Physiol. - Ren. Physiol.* **295**, F942-9

74. Zhang, J., Villacorta, L., Chang, L., Fan, Z., Hamblin, M., Zhu, T., Chen, C. S., Cole, M. P., Schopfer, F. J., Deng, C. X., Garcia-Barrio, M. T., Feng, Y.-H. H., Freeman, B. A., and Chen, Y. E. (2010) Nitro-oleic acid inhibits angiotensin II-induced hypertension. *Circ. Res.* **107**, 540–8

75. Villacorta, L., Chang, L., Salvatore, S. R., Ichikawa, T., Zhang, J., Petrovic-Djergovic, D., Jia, L., Carlsen, H., Schopfer, F. J., Freeman, B. A., and Chen, Y. E. (2013) Electrophilic nitro-fatty acids inhibit vascular inflammation by disrupting LPS-dependent TLR4 signalling in lipid rafts. *Cardiovasc. Res.* **98**, 116–24

76. Reddy, A. T., Lakshmi, S. P., Dornadula, S., Pinni, S., Rampa, D. R., and Reddy, R. C. (2013) The nitrated fatty acid 10-nitro-oleate attenuates allergic airway disease. *J. Immunol.* **191**, 2053–63

77. Wang, W., Li, C., and Yang, T. (2015) Protection of Nitro-Fatty Acid against Kidney Diseases. *Am. J. Physiol. - Ren. Physiol.* **310**, ajprenal.00321.2015

78. Hwang, J., Lee, K. E., Lim, J.-Y., and Park, S. I. (2009) Nitrated fatty acids prevent TNFalpha-stimulated inflammatory and atherogenic responses in endothelial cells. *Biochem. Biophys. Res. Commun.* **387**, 633–40

79. Reddy, A. T., Lakshmi, S. P., Kleinhenz, J. M., Sutliff, R. L., Hart, C. M., and Reddy, R. C. (2012) Endothelial cell peroxisome proliferator-activated receptor γ reduces

endotoxemic pulmonary inflammation and injury. *J. Immunol.* **189**, 5411–20

80. Kansanen, E., Jyrkkänen, H.-K., Volger, O. L., Leinonen, H., Kivelä, A. M., Häkkinen, S.-K., Woodcock, S. R., Schopfer, F. J., Horrevoets, A. J., Ylä-Herttuala, S., Freeman, B. A., and Levonen, A.-L. (2009) Nrf2-dependent and -independent responses to nitro-fatty acids in human endothelial cells: identification of heat shock response as the major pathway activated by nitro-oleic acid. *J. Biol. Chem.* **284**, 33233–41

81. Levonen, A. L., Hill, B. G., Kansanen, E., Zhang, J., and Darley-Usmar, V. M. (2014) Redox regulation of antioxidants, autophagy, and the response to stress: Implications for electrophile therapeutics. *Free Radic. Biol. Med.* **71**, 196–207

82. Uruno, A., and Motohashi, H. (2011) The Keap1-Nrf2 system as an in vivo sensor for electrophiles. *Nitric Oxide - Biol. Chem.* **25**, 153–160

83. Batthyany, C., Schopfer, F. J., Baker, P. R. S., Durán, R., Baker, L. M. S., Huang, Y., Cerveñansky, C., Branchaud, B. P., Freeman, B. A., Duran, R., Baker, L. M. S., Huang, Y., Cervenansky, C., Branchaud, B. P., and Freeman, B. A. (2006) Reversible post-translational modification of proteins by nitrated fatty acids in vivo. *J. Biol. Chem.* **281**, 20450–63

84. Liu, J., Liu, Y., Madhu, C., and Klaassen, C. D. (1993) Protective effects of oleanolic acid on acetaminophen-induced hepatotoxicity in mice. *J. Pharmacol. Exp. Ther.* **266**, 1607–13

85. Honda, T., Rounds, B. V, Gribble, G. W., Suh, N., Wang, Y., and Sporn, M. B. (1998) Design and synthesis of 2-cyano-3,12-dioxoolean-1,9-dien-28-oic acid, a novel and highly active inhibitor of nitric oxide production in mouse macrophages. *Bioorg. Med. Chem. Lett.* **8**, 2711–2714

86. Suh, N., Wang, Y., Honda, T., Gribble, G. W., Dmitrovsky, E., Hickey, W. F., Maue, R. A., Place, A. E., Porter, D. M., Spinella, M. J., Williams, C. R., Wu, G., Dannenberg, A. J.,

Flanders, K. C., Letterio, J. J., Mangelsdorf, D. J., Nathan, C. F., Nguyen, L., Porter, W. W., Ren, R. F., Roberts, A. B., Roche, N. S., Subbaramaiah, K., and Sporn, M. B. (1999) A novel synthetic oleanane triterpenoid, 2-cyano-3,12-dioxoolean-1,9- dien-28-oic acid, with potent differentiating, antiproliferative, and anti- inflammatory activity. *Cancer Res.* **59**, 336–341

87. Samudio, I., Konopleva, M., Hail, N., Shi, Y. X., McQueen, T., Hsu, T., Evans, R., Honda, T., Gribble, G. W., Sporn, M., Gilbert, H. F., Safe, S., and Andreeff, M. (2005) 2-Cyano-3,12-dioxooleana-1,9-dien-28-imidazolide (CDDO-Im) directly targets mitochondrial glutathione to induce apoptosis in pancreatic cancer. *J. Biol. Chem.* **280**, 36273–36282

88. Liby, K., Hock, T., Yore, M. M., Suh, N., Place, A. E., Risingsong, R., Williams, C. R., Royce, D. B., Honda, T., Honda, Y., Gribble, G. W., Hill-Kapturczak, N., Agarwal, A., and Sporn, M. B. (2005) The synthetic triterpenoids, CDDO and CDDO-imidazolide, are potent inducers of heme oxygenase-1 and Nrf2/ARE signaling. *Cancer Res.* **65**, 4789–4798

89. Cleasby, A., Yon, J., Day, P. J., Richardson, C., Tickle, I. J., Williams, P. A., Callahan, J. F., Carr, R., Concha, N., Kerns, J. K., Qi, H., Sweitzer, T., Ward, P., and Davies, T. G. (2014) Structure of the BTB Domain of Keap1 and Its Interaction with the Triterpenoid Antagonist CDDO. *PLoS One*. **9**, e98896

90. Mathis, B. J., and Cui, T. (2016) CDDO and its role in chronic diseases. in *Advances in Experimental Medicine and Biology*, pp. 291–314, Springer, Cham, **929**, 291–314

91. Ding, Y., Stidham, R. D., Bumeister, R., Trevino, I., Winters, A., Sprouse, M., Ding, M., Ferguson, D. A., Meyer, C. J., Christian Wigley, W., and Ma, R. (2013) The synthetic triterpenoid, RTA 405, increases the glomerular filtration rate and reduces angiotensin II-induced contraction of glomerular mesangial cells. *Kidney Int.* **83**, 845–854

92. de Zeeuw, D., Akizawa, T., Audhya, P., Bakris, G. L., Chin, M., Christ-Schmidt, H., Goldsberry, A., Houser, M., Krauth, M., Lambers Heerspink, H. J., McMurray, J. J., Meyer, C. J., Parving, H.-H., Remuzzi, G., Toto, R. D., Vaziri, N. D., Wanner, C., Wittes, J., Wrolstad, D., Chertow, G. M., and BEACON Trial Investigators (2013) Bardoxolone Methyl in Type 2 Diabetes and Stage 4 Chronic Kidney Disease. *N. Engl. J. Med.* **369**, 2492–2503

93. Chin, M. P., Reisman, S. A., Bakris, G. L., O'Grady, M., Linde, P. G., McCullough, P. A., Packham, D., Vaziri, N. D., Ward, K. W., Warnock, D. G., and Meyer, C. J. (2014) Mechanisms Contributing to Adverse Cardiovascular Events in Patients with Type 2 Diabetes Mellitus and Stage 4 Chronic Kidney Disease Treated with Bardoxolone Methyl. *Am. J. Nephrol.* **39**, 499–508

94. Pergola, P. E., Raskin, P., Toto, R. D., Meyer, C. J., Huff, J. W., Grossman, E. B., Krauth, M., Ruiz, S., Audhya, P., Christ-Schmidt, H., Wittes, J., Warnock, D. G., and BEAM Study Investigators (2011) Bardoxolone Methyl and Kidney Function in CKD with Type 2 Diabetes. *N. Engl. J. Med.* **365**, 327–336

95. Zoja, C., Benigni, A., and Remuzzi, G. (2014) The Nrf2 pathway in the progression of renal disease. *Nephrol. Dial. Transplant.* **29 Suppl 1**, i19–i24

96. SCHWECKENDIEK, W. (1959) Heilung von Psoriasis vulgaris. *Med. Monatsschr.* **13**, 103–104

97. Werdenberg, D., Joshi, R., Wolffram, S., Merkle, H. P., and Langguth, P. (2003) Presystemic metabolism and intestinal absorption of antipsoriatic fumaric acid esters. *Biopharm. Drug Dispos.* **24**, 259–73

98. Venci, J. V., and Gandhi, M. A. (2013) Dimethyl Fumarate (Tecfidera): A New Oral Agent

for Multiple Sclerosis. *Ann. Pharmacother.* **47**, 1697–1702

99. Kappos, L., Gold, R., Miller, D. H., Macmanus, D. G., Havrdova, E., Limmroth, V., Polman, C. H., Schmierer, K., Yousry, T. A., Yang, M., Eraksoy, M., Meluzinova, E., Rektor, I., Dawson, K. T., Sandrock, A. W., and O'Neill, G. N. (2008) Efficacy and safety of oral fumarate in patients with relapsing-remitting multiple sclerosis: a multicentre, randomised, double-blind, placebo-controlled phase IIb study. *Lancet.* **372**, 1463–72

100. Linker, R. A., Lee, D.-H., Ryan, S., van Dam, A. M., Conrad, R., Bista, P., Zeng, W., Hronowsky, X., Buko, A., Chollate, S., Ellrichmann, G., Brück, W., Dawson, K., Goelz, S., Wiese, S., Scannevin, R. H., Lukashev, M., and Gold, R. (2011) Fumaric acid esters exert neuroprotective effects in neuroinflammation via activation of the Nrf2 antioxidant pathway. *Brain.* **134**, 678–92

101. Linker, R. A., and Gold, R. (2013) Dimethyl fumarate for treatment of multiple sclerosis: mechanism of action, effectiveness, and side effects. *Curr. Neurol. Neurosci. Rep.* **13**, 394

102. Brennan, M. S., Matos, M. F., Li, B., Hronowski, X., Gao, B., Juhasz, P., Rhodes, K. J., and Scannevin, R. H. (2015) Dimethyl fumarate and monoethyl fumarate exhibit differential effects on KEAP1, NRF2 activation, and glutathione depletion in vitro. *PLoS One.* 10.1371/journal.pone.0120254

103. Long, M. J. C., and Aye, Y. (2017) Privileged Electrophile Sensors: A Resource for Covalent Drug Development. *Cell Chem. Biol.* **24**, 787–800

104. Tak, P. P., Firestein, G. S., Tak, P. P., and Firestein, G. S. (2001) NF-kappaB: a key role in inflammatory diseases. *J. Clin. Invest.* **107**, 7–11

105. Hayden, M. S., and Ghosh, S. (2011) NF-κB in immunobiology. *Cell Res.* **21**, 223–244

106. Moynagh, P. N. (2005) The NF-kappaB pathway. *J. Cell Sci.* **118**, 4589–4592

107. Delmastro-Greenwood, M., Freeman, B. A., and Wendell, S. G. (2014) Redox-Dependent Anti-Inflammatory Signaling Actions of Unsaturated Fatty Acids. *Annu. Rev. Physiol.* **76**, 79–105

108. Kastrati, I., Siklos, M. I., Calderon-Gierszal, E. L., El-Shennawy, L., Georgieva, G., Thayer, E. N., Thatcher, G. R. J., and Frasor, J. (2016) Dimethyl Fumarate Inhibits the Nuclear Factor κB Pathway in Breast Cancer Cells by Covalent Modification of p65 Protein. *J. Biol. Chem.* **291**, 3639–47

109. Khoo, N. K. H., Li, L., Salvatore, S. R., Schopfer, F. J., and Freeman, B. A. (2018) Electrophilic fatty acid nitroalkenes regulate Nrf2 and NF-κB signaling:A medicinal chemistry investigation of structure-function relationships. *Sci. Rep.* 10.1038/s41598-018-20460-8

110. Wardyn, J. D., Ponsford, A. H., and Sanderson, C. M. (2015) Dissecting molecular cross-talk between Nrf2 and NF-κB response pathways. *Biochem. Soc. Trans.* **43**, 621–6

111. Beeby, M., O'Connor, B. D., Ryttersgaard, C., Boutz, D. R., Perry, L. J., and Yeates, T. O. (2005) The genomics of disulfide bonding and protein stabilization in thermophiles. *PLoS Biol.* **3**, 1549–1558

112. Haugaard, N. (2006) Reflections on the Role of the Thiol Group in Biology. *Ann. N. Y. Acad. Sci.* **899**, 148–158

113. Go, Y. M., Chandler, J. D., and Jones, D. P. (2015) The cysteine proteome. *Free Radic. Biol. Med.* **84**, 227–245

114. Kortemme, T., and Creighton, T. E. (1995) Ionisation of Cysteine Residues at the Termini of Model α-Helical Peptides. Relevance to Unusual Thiol pKaValues in Proteins of the Thioredoxin Family. *J. Mol. Biol.* **253**, 799–812

115. Ferrer-Sueta, G., Manta, B., Botti, H., Radi, R., Trujillo, M., and Denicola, A. (2011) Factors affecting protein thiol reactivity and specificity in peroxide reduction. *Chem. Res. Toxicol.* **24**, 434–450

116. Poole, L. B. (2015) The basics of thiols and cysteines in redox biology and chemistry. *Free Radic. Biol. Med.* **80**, 148–157

117. Marino, S. M., and Gladyshev, V. N. (2010) Cysteine Function Governs Its Conservation and Degeneration and Restricts Its Utilization on Protein Surfaces. *J. Mol. Biol.* **404**, 902–916

118. Meister, A. (1988) Glutathione metabolism and its selective modification. *J. Biol. Chem.* **263**, 17205–17208

119. Portillo-Ledesma, S., Sardi, F., Manta, B., Tourn, M. V., Clippe, A., Knoops, B., Alvarez, B., Coitiño, E. L., and Ferrer-Sueta, G. (2014) Deconstructing the catalytic efficiency of peroxiredoxin-5 peroxidatic cysteine. *Biochemistry*. **53**, 6113–6125

120. Tajc, S. G., Tolbert, B. S., Basavappa, R., and Miller, B. L. (2004) Direct determination of thiol pKa by isothermal titration microcalorimetry. *J. Am. Chem. Soc.* **126**, 10508–9

121. Hwang, C., Sinskey, A. J., and Lodish, H. F. (1992) Oxidized redox state of glutathione in the endoplasmic reticulum. *Science*. **257**, 1496–502

122. Maher, P. (2005) The effects of stress and aging on glutathione metabolism. *Ageing Res. Rev.* **4**, 288–314

123. Griffith, O. W. (1999) Biologic and pharmacologic regulation of mammalian glutathione synthesis. *Free Radic. Biol. Med.* **27**, 922–935

124. Dalton, T. P., Dieter, M. Z., Yang, Y., Shertzer, H. G., and Nebert, D. W. (2000) Knockout of the mouse glutamate cysteine ligase catalytic subunit (Gclc) gene: Embryonic lethal

when homozygous, and proposed model for moderate glutathione deficiency when heterozygous. *Biochem. Biophys. Res. Commun.* **279**, 324–329

125. Schmidt, T. J., Ak, M., and Mrowietz, U. (2007) Reactivity of dimethyl fumarate and methylhydrogen fumarate towards glutathione and N-acetyl-l-cysteine-Preparation of S-substituted thiosuccinic acid esters. *Bioorganic Med. Chem.* **15**, 333–342

126. Dibbert, S., Clement, B., Skak-Nielsen, T., Mrowietz, U., and Rostami-Yazdi, M. (2013) Detection of fumarate-glutathione adducts in the portal vein blood of rats: Evidence for rapid dimethylfumarate metabolism. *Arch. Dermatol. Res.* **305**, 447–451

127. Baker, L. M. S., Baker, P. R. S., Golin-Bisello, F., Schopfer, F. J., Fink, M., Woodcock, S. R., Branchaud, B. P., Radi, R., and Freeman, B. A. (2007) Nitro-fatty acid reaction with glutathione and cysteine. Kinetic analysis of thiol alkylation by a Michael addition reaction. *J. Biol. Chem.* **282**, 31085–31093

128. Woodcock, C.-S. C., Huang, Y., Woodcock, S. R., Salvatore, S. R., Singh, B., Golin-Bisello, F., Davidson, N. E., Neumann, C., Freeman, B. A., and Wendell, S. G. (2017) Nitro-fatty acid inhibition of triple negative breast cancer cell viability, migration, invasion and tumor growth. *J. Biol. Chem.* **293**, 1120–1137

129. Miller, C. G., Holmgren, A., Arnér, E. S. J., and Schmidt, E. E. (2018) NADPH-dependent and -independent disulfide reductase systems. *Free Radic. Biol. Med.* 10.1016/j.freeradbiomed.2018.03.051

130. Conn, E. E., and Vennesland, B. (1951) Glutathione reductase of wheat germ. *J. Biol. Chem.* **192**, 17–28

131. Rall, T. W., and Lehninger, A. L. (1952) Glutathione reductase of animal tissues. *J Biol Chem*. **194**, 119–130

132. Kanzok, S. M., Fechner, A., Bauer, H., Ulschmid, J. K., Müller, H. M., Botella-Munoz, J., Schneuwly, S., Schirmer, R. H., and Becker, K. (2001) Substitution of the thioredoxin system for glutathione reductase in Drosophila melanogaster. *Science (80-.).* **291**, 643–646

133. Montero, S., de Arriaga, D., Busto, F., and Soler, J. (1990) A study of the kinetic mechanism followed by glutathione reductase from mycelium of Phycomyces blakesleeanus. *Arch. Biochem. Biophys.* **278**, 52–59

134. Ballatori, N., Krance, S. M., Notenboom, S., Shi, S., Tieu, K., and Hammond, C. L. (2009) Glutathione dysregulation and the etiology and progression of human diseases. *Biol. Chem.* **390**, 191–214

135. Johnson, W. M., Wilson-Delfosse, A. L., and Mieyal, J. J. (2012) Dysregulation of glutathione homeostasis in neurodegenerative diseases. *Nutrients*. **4**, 1399–1440

136. Traverso, N., Ricciarelli, R., Nitti, M., Marengo, B., Furfaro, A. L., Pronzato, M. A., Marinari, U. M., and Domenicotti, C. (2013) Role of glutathione in cancer progression and chemoresistance. *Oxid. Med. Cell. Longev.* 10.1155/2013/972913

137. Giustarini, D., Dalle-Donne, I., Tsikas, D., and Rossi, R. (2009) Oxidative stress and human diseases: Origin, link, measurement, mechanisms, and biomarkers. *Crit. Rev. Clin. Lab. Sci.* **46**, 241–281

138. Schafer, F. Q., and Buettner, G. R. (2001) Redox environment of the cell as viewed through the redox state of the glutathione disulfide/glutathione couple. *Free Radic. Biol. Med.* **30**, 1191–1212

139. Flohé, L. (2013) The fairytale of the GSSG/GSH redox potential. *Biochim. Biophys. Acta*. **1830**, 3139–42

140. Rhee, S. G. (2016) Overview on Peroxiredoxin. *Mol. Cells*. **39**, 1–5

141. Neumann, C. a, Cao, J., and Manevich, Y. (2009) Peroxiredoxin 1 and its role in cell signaling. *Cell Cycle*. **8**, 4072–4078

142. Dubuisson, M., Vander Stricht, D., Clippe, A., Etienne, F., Nauser, T., Kissner, R., Koppenol, W. H., Rees, J.-F., and Knoops, B. (2004) Human peroxiredoxin 5 is a peroxynitrite reductase. *FEBS Lett.* **571**, 161–165

143. Ogusucu, R., Rettori, D., Munhoz, D. C., Soares Netto, L. E., and Augusto, O. (2007) Reactions of yeast thioredoxin peroxidases I and II with hydrogen peroxide and peroxynitrite: Rate constants by competitive kinetics. *Free Radic. Biol. Med.* **42**, 326–334

144. Cox, A. G., Peskin, A. V., Paton, L. N., Winterbourn, C. C., and Hampton, M. B. (2009) Redox potential and peroxide reactivity of human peroxiredoxin 3. *Biochemistry*. **48**, 6495–6501

145. Peskin, A. V, Dickerhof, N., Poynton, R. A., Paton, L. N., Pace, P. E., Hampton, M. B., and Winterbourn, C. C. (2013) Hyperoxidation of peroxiredoxins 2 and 3: Rate constants for the reactions of the sulfenic acid of the peroxidatic cysteine. *J. Biol. Chem.* **288**, 14170–14177

146. Chen, Y., Fry, B. C., and Layton, A. T. (2016) Modeling Glucose Metabolism in the Kidney. *Bull. Math. Biol.* **78**, 1318–1336

147. Murphy, M. P. (2009) How mitochondria produce reactive oxygen species. *Biochem. J.* **417**, 1–13

148. Kim, H. J., and Vaziri, N. D. (2010) Contribution of impaired Nrf2-Keap1 pathway to oxidative stress and inflammation in chronic renal failure. *Am. J. Physiol. Renal Physiol.* **298**, F662-71

149. Kim, H. J., Sato, T., Rodriguez-Iturbe, B., and Vaziri, N. D. (2011) Role of Intrarenal

Angiotensin System Activation, Oxidative Stress, Inflammation, and Impaired Nuclear Factor-Erythroid-2-Related Factor 2 Activity in the Progression of Focal Glomerulosclerosis. *J. Pharmacol. Exp. Ther.* **337**, 583–590

150. Aminzadeh, M. A., Nicholas, S. B., Norris, K. C., and Vaziri, N. D. (2013) Role of impaired Nrf2 activation in the pathogenesis of oxidative stress and inflammation in chronic tubulo-interstitial nephropathy. *Nephrol. Dial. Transplant.* **28**, 2038–2045

151. Nezu, M., Suzuki, N., and Yamamoto, M. (2017) Targeting the KEAP1-NRF2 System to Prevent Kidney Disease Progression. *Am. J. Nephrol.* **45**, 473–483

152. Jobbagy, S., and Tan, R. J. (2018) Nitrolipids in kidney physiology and disease. *Nitric Oxide - Biol. Chem.* 10.1016/j.niox.2018.03.021

153. Gitlin, M. (2016) Lithium side effects and toxicity: prevalence and management strategies. *Int. J. bipolar Disord.* **4**, 27

154. Boton, R., Gaviria, M., Batlle, D. C., and al., et (1987) Prevalence, Pathogenesis, and Treatment of Renal Dysfunction Associated With Chronic Lithium Therapy. *Am. J. Kidney Dis.* **10**, 329–345

155. Kessing, L. V., Gerds, T. A., Feldt-Rasmussen, B., Andersen, P. K., and Licht, R. W. (2015) Use of Lithium and Anticonvulsants and the Rate of Chronic Kidney Disease. *JAMA Psychiatry*. **72**, 1182

156. Thomsen, K., and Shirley, D. G. (2005) A hypothesis linking sodium and lithium reabsorption in the distal nephron. *Nephrol. Dial. Transplant.* **21**, 869–880

157. Kwon, T. H., Laursen, U. H., Marples, D., Maunsbach, A. B., Knepper, M. A., Frokiaer, J., and Nielsen, S. (2000) Altered expression of renal AQPs and Na(+) transporters in rats with lithium-induced NDI. *Am. J. Physiol. Renal Physiol.* **279**, F552-64

158. Yang, B., Zhao, D., Qian, L., and Verkman, A. S. (2006) Mouse model of inducible nephrogenic diabetes insipidus produced by floxed aquaporin-2 gene deletion. *Am. J. Physiol. Physiol.* **291**, F465–F472

159. Castillo-Quan, J. I., Li, L., Kinghorn, K. J., Ivanov, D. K., Tain, L. S., Slack, C., Kerr, F., Nespital, T., Thornton, J., Hardy, J., Bjedov, I., and Partridge, L. (2016) Lithium Promotes Longevity through GSK3/NRF2-Dependent Hormesis. *Cell Rep.* **15**, 638–650

160. Jain, A. K., and Jaiswal, A. K. (2006) Phosphorylation of tyrosine 568 controls nuclear export of Nrf2. *J. Biol. Chem.* **281**, 12132–42

161. Alural, B., Ozerdem, A., Allmer, J., Genc, K., and Genc, S. (2015) Lithium protects against paraquat neurotoxicity by NRF2 activation and miR-34a inhibition in SH-SY5Y cells. *Front. Cell. Neurosci.* **9**, 209

162. Chen, X., Liu, Y., Zhu, J., Lei, S., Dong, Y., Li, L., Jiang, B., Tan, L., Wu, J., Yu, S., and Zhao, Y. (2016) GSK-3β downregulates Nrf2 in cultured cortical neurons and in a rat model of cerebral ischemia-reperfusion. *Sci. Rep.* **6**, 20196

163. Wakabayashi, N., Shin, S., Slocum, S. L., Agoston, E. S., Wakabayashi, J., Kwak, M. K., Misra, V., Biswal, S., Yamamoto, M., and Kensler, T. W. (2010) Regulation of Notch1 signaling by Nrf2: Implications for tissue regeneration. *Sci. Signal.* 10.1126/scisignal.2000762

164. Li, Y.-J., Shimizu, T., Shinkai, Y., Hirata, Y., Inagaki, H., Takeda, K., Azuma, A., Yamamoto, M., and Kawada, T. (2017) Nrf2 Regulates the Risk of a Diesel Exhaust Inhalation-Induced Immune Response during Bleomycin Lung Injury and Fibrosis in Mice. *Int. J. Mol. Sci.* 10.3390/ijms18030649

165. Manzanero, S. (2012) Generation of Mouse Bone Marrow-Derived Macrophages. in

Leucocytes: Methods and Protocols (Ashman, R. B. ed), pp. 177–181, Humana Press, Totowa, NJ, 10.1007/978-1-61779-527-5_12

166. Okawa, H., Motohashi, H., Kobayashi, A., Aburatani, H., Kensler, T. W., and Yamamoto, M. (2006) Hepatocyte-specific deletion of the keap1 gene activates Nrf2 and confers potent resistance against acute drug toxicity. *Biochem. Biophys. Res. Commun.* **339**, 79–88

167. Rahman, I., Kode, A., and Biswas, S. K. (2007) Assay for quantitative determination of glutathione and glutathione disulfide levels using enzymatic recycling method. *Nat. Protoc.* **1**, 3159–3165

168. Harwood, D. T., Kettle, A. J., Brennan, S., and Winterbourn, C. C. (2009) Simultaneous determination of reduced glutathione, glutathione disulphide and glutathione sulphonamide in cells and physiological fluids by isotope dilution liquid chromatography-tandem mass spectrometry. *J. Chromatogr. B.* **877**, 3393–9

169. Emlet, D. R., Pastor-Soler, N., Marciszyn, A., Wen, X., Gomez, H., Humphries, W. H., Morrisroe, S., Volpe, J. K., and Kellum, J. A. (2017) Insulin-like growth factor binding protein 7 and tissue inhibitor of metalloproteinases-2: differential expression and secretion in human kidney tubule cells. *Am. J. Physiol. - Ren. Physiol.* [online] http://ajprenal.physiology.org/content/312/2/F284.long (Accessed July 6, 2017)

170. Schock-Kusch, D., Sadick, M., Henninger, N., Kraenzlin, B., Claus, G., Kloetzer, H. M., Weiß, C., Pill, J., and Gretz, N. (2009) Transcutaneous measurement of glomerular filtration rate using FITC-sinistrin in rats. *Nephrol. Dial. Transplant.* **24**, 2997–3001

171. Jackson, L. E., Kulkarni, S., Wang, H., Lu, J., Dolezal, J. M., Bharathi, S. S., Ranganathan, S., Patel, M. S., Deshpande, R., Alencastro, F., Wendell, S. G., Goetzman, E. S., Duncan, A. W., and Prochownik, E. V. (2017) Genetic dissociation of glycolysis and the TCA cycle

affects neither normal nor neoplastic proliferation. *Cancer Res.* **77**, 5795–5807

172. Attia, S. M. (2010) Deleterious effects of reactive metabolites: *Oxid. Med. Cell. Longev.* **3**, 238–253

173. Rishton, G. M. (1997) Reactive compounds and in vitro false positives in HTS. *Drug Discov. Today*. **2**, 382–384

174. Rishton, G. M. (2003) Nonleadlikeness and leadlikeness in biochemical screening. *Drug Discov. Today*. **8**, 86–96

175. Stark, K. L., Harris, C., and Juchau, M. R. (1989) Influence of electrophilic character and glutathione depletion on chemical dysmorphogenesis in cultured rat embryos. *Biochem Pharmacol*. **38**, 2685–92

176. Turell, L., Vitturi, D. A., Coitiño, E. L., Lebrato, L., Möller, M. N., Sagasti, C., Salvatore, S. R., Woodcock, S. R., Alvarez, B., and Schopfer, F. J. (2017) The chemical basis of thiol addition to nitro-conjugated linoleic acid, a protective cell-signaling lipid. *J. Biol. Chem.* **292**, 1145–1159

177. Zou, W., Yue, P., Khuri, F. R., and Sun, S.-Y. (2008) Coupling of endoplasmic reticulum stress to CDDO-Me-induced up-regulation of death receptor 5 via a CHOP-dependent mechanism involving JNK activation. *Cancer Res.* **68**, 7484–92

178. Couch, R. D., Browning, R. G., Honda, T., Gribble, G. W., Wright, D. L., Sporn, M. B., and Anderson, A. C. (2005) *Studies on the reactivity of CDDO, a promising new chemopreventive and chemotherapeutic agent: implications for a molecular mechanism of action*, 10.1016/j.bmcl.2005.03.031

179. Iskusnykh, I. Y., Popova, T. N., Agarkov, A. A., Pinheiro De Carvalho, M. A. A., and Rjevskiy, S. G. (2013) Expression of glutathione peroxidase and glutathione reductase and

level of free radical processes under toxic hepatitis in rats. *J. Toxicol.* **2013**, 8706–8728

180. Cole, S. P. C. (2014) Multidrug Resistance Protein 1 (MRP1, ABCC1), a "Multitasking" ATP-binding Cassette (ABC) Transporter. *J. Biol. Chem.* **289**, 30880–30888

181. Wu, K. C., Cui, J. Y., and Klaassen, C. D. (2011) Beneficial role of Nrf2 in regulating NADPH generation and consumption. *Toxicol. Sci.* **123**, 590–600

182. Berndt, C., Lillig, C. H., and Flohé, L. (2014) Redox regulation by glutathione needs enzymes. *Front. Pharmacol.* 10.3389/fphar.2014.00168

183. Chung, P. M., Cappel, R. E., and Gilbert, H. F. (1991) Inhibition of glutathione disulfide reductase by glutathione. *Arch. Biochem. Biophys.* **288**, 48–53

184. Sexton, D. J., and Mutus, B. (1992) Glutathione reductases from a variety of sources are inhibited by physiological levels of glutathione. *Comp. Biochem. Physiol. -- Part B Biochem.* **103**, 897–901

185. Antunes, F., Han, D., and Cadenas, E. (2002) Relative contributions of heart mitochondria glutathione peroxidase and catalase to H2O2 detoxification in in vivo conditions. *Free Radic. Biol. Med.* **33**, 1260–1267

186. Cortassa, S., Aon, M. A., Winslow, R. L., and O'Rourke, B. (2004) A Mitochondrial Oscillator Dependent on Reactive Oxygen Species. *Biophys. J.* **87**, 2060–2073

187. Deponte, M. (2017) The Incomplete Glutathione Puzzle: Just Guessing at Numbers and Figures? *Antioxid. Redox Signal.* **27**, 1130–1161

188. Kranner, I., Birtić, S., Anderson, K. M., and Pritchard, H. W. (2006) Glutathione half-cell reduction potential: A universal stress marker and modulator of programmed cell death? *Free Radic. Biol. Med.* **40**, 2155–2165

189. Kemp, M., Go, Y.-M. Y., and Jones, D. D. P. (2008) Nonequilibrium thermodynamics of

thiol/disulfide redox systems: a perspective on redox systems biology. *Free Radic. Biol. Med.* **44**, 921–937

190. Toppo, S., Flohé, L., Ursini, F., Vanin, S., and Maiorino, M. (2009) Catalytic mechanisms and specificities of glutathione peroxidases: Variations of a basic scheme. *Biochim. Biophys. Acta - Gen. Subj.* **1790**, 1486–1500

191. Adimora, N. J., Jones, D. P., and Kemp, M. L. (2010) A Model of Redox Kinetics Implicates the Thiol Proteome in Cellular Hydrogen Peroxide Responses. *Antioxid. Redox Signal.* **13**, 731–743

192. Aon, M. A., Stanley, B. A., Sivakumaran, V., Kembro, J. M., O'Rourke, B., Paolocci, N., and Cortassa, S. (2012) Glutathione/thioredoxin systems modulate mitochondrial H2O2 emission: An experimental-computational study. *J. Gen. Physiol.* **139**, 479–491

193. Brito, P. M., and Antunes, F. (2014) Estimation of kinetic parameters related to biochemical interactions between hydrogen peroxide and signal transduction proteins. *Front. Chem.* **2**, 82

194. Altıntaş, A., Davidsen, K., Garde, C., Mortensen, U. H., Brasen, J. C., Sams, T., and Workman, C. T. (2016) High-resolution kinetics and modeling of hydrogen peroxide degradation in live cells. *Free Radic. Biol. Med.* **101**, 143–153

195. Antunes, F., and Brito, P. M. (2017) Quantitative biology of hydrogen peroxide signaling. *Redox Biol.* **13**, 1–7

196. Grek, C. L., Zhang, J., Manevich, Y., Townsend, D. M., and Tew, K. D. (2013) Causes and consequences of cysteine s-glutathionylation. *J. Biol. Chem.* **288**, 26497–26504

197. Ambrozova, G., Fidlerova, T., Verescakova, H., Koudelka, A., Rudolph, T. K., Woodcock, S. R., Freeman, B. A., Kubala, L., and Pekarova, M. (2016) Nitro-oleic acid inhibits

vascular endothelial inflammatory responses and the endothelial-mesenchymal transition. *Biochim. Biophys. Acta*. **1860**, 2428–2437

198. Wang, H., Liu, H., Jia, Z., Olsen, C., Litwin, S., Guan, G., Yang, T., and Yang, T. (2010) Nitro-oleic acid protects against endotoxin-induced endotoxemia and multiorgan injury in mice. *AJP Ren. Physiol.* **298**, F754–F762

199. Salim, S., Asghar, M., Taneja, M., Hovatta, I., Chugh, G., Vollert, C., and Vu, A. (2011) Potential contribution of oxidative stress and inflammation to anxiety and hypertension. *Brain Res.* **1404**, 63–71

200. Jones, E., Michael, S., and Sittampalam, G. S. (2012) Basics of Assay Equipment and Instrumentation for High Throughput Screening. *Assay Guid. Man.* [online] http://www.ncbi.nlm.nih.gov/pubmed/22553861 (Accessed October 18, 2017)

201. Bauer, R. A. (2015) *Covalent inhibitors in drug discovery: From accidental discoveries to avoided liabilities and designed therapies*, Elsevier Current Trends, **20**, 1061–1073

202. Singh, J., Petter, R. C., Baillie, T. A., and Whitty, A. (2011) The resurgence of covalent drugs. *Nat. Rev. Drug Discov.* **10**, 307–17

203. Zhang, H., Limphong, P., Pieper, J., Liu, Q., Rodesch, C. K., Christians, E., and Benjamin, I. J. (2012) Glutathione-dependent reductive stress triggers mitochondrial oxidation and cytotoxicity. *FASEB J.* **26**, 1442–1451

204. Seefeldt, T., Zhao, Y., Chen, W., Raza, A. S., Carlson, L., Herman, J., Stoebner, A., Hanson, S., Foll, R., and Guan, X. (2009) Characterization of a novel dithiocarbamate glutathione reductase inhibitor and its use as a tool to modulate intracellular glutathione. *J. Biol. Chem.* **284**, 2729–2737

205. Awwad, K., Steinbrink, S. D., Frömel, T., Lill, N., Isaak, J., Häfner, A.-K., Roos, J.,

Hofmann, B., Heide, H., Geisslinger, G., Steinhilber, D., Freeman, B. A., Maier, T. J., and Fleming, I. (2014) Electrophilic Fatty Acid Species Inhibit 5-Lipoxygenase and Attenuate Sepsis-Induced Pulmonary Inflammation. *Antioxid. Redox Signal.* **20**, 2667–2680

206. Charles, R. L., Rudyk, O., Prysyazhna, O., Kamynina, A., Yang, J., Morisseau, C., Hammock, B. D., Freeman, B. A., and Eaton, P. (2014) Protection from hypertension in mice by the Mediterranean diet is mediated by nitro fatty acid inhibition of soluble epoxide hydrolase. *Proc. Natl. Acad. Sci.* **111**, 8167–8172

207. Weisbord, S. D., Gallagher, M., Jneid, H., Garcia, S., Cass, A., Thwin, S.-S., Conner, T. A., Chertow, G. M., Bhatt, D. L., Shunk, K., Parikh, C. R., McFalls, E. O., Brophy, M., Ferguson, R., Wu, H., Androsenko, M., Myles, J., Kaufman, J., and Palevsky, P. M. (2017) Outcomes after Angiography with Sodium Bicarbonate and Acetylcysteine. *N. Engl. J. Med.* **378**, NEJMoa1710933

208. Ryves, W. J., and Harwood, A. J. (2001) Lithium inhibits glycogen synthase kinase-3 by competition for magnesium. *Biochem. Biophys. Res. Commun.* **280**, 720–725

209. Freland, L., and Beaulieu, J.-M. (2012) Inhibition of GSK3 by lithium, from single molecules to signaling networks. *Front. Mol. Neurosci.* **5**, 14

210. Rojo, A. I., Sagarra, M. R. de, and Cuadrado, A. (2008) GSK-3β down-regulates the transcription factor Nrf2 after oxidant damage: Relevance to exposure of neuronal cells to oxidative stress. *J. Neurochem.* **105**, 192–202

211. Jiang, Y., Bao, H., Ge, Y., Tang, W., Cheng, D., Luo, K., Gong, G., and Gong, R. (2015) Therapeutic targeting of GSK3β enhances the Nrf2 antioxidant response and confers hepatic cytoprotection in hepatitis C. *Gut*. **64**, 168–179

212. Aubert, S., Fauquette, V., Hémon, B., Lepoivre, R., Briez, N., Bernard, D., Van Seuningen,

I., Leroy, X., and Perrais, M. (2009) MUC1, a new hypoxia inducible factor target gene, is an actor in clear renal cell carcinoma tumor progression. *Cancer Res.* **69**, 5707–15

213. Braga, V. M., Pemberton, L. F., Duhig, T., and Gendler, S. J. (1992) Spatial and temporal expression of an epithelial mucin, Muc-1, during mouse development. *Development*. **115**, 427–37

214. Pastor-Soler, N. M., Sutton, T. A., Mang, H. E., Kinlough, C. L., Gendler, S. J., Madsen, C. S., Bastacky, S. I., Ho, J., Al-bataineh, M. M., Hallows, K. R., Singh, S., Monga, S. P., Kobayashi, H., Haase, V. H., and Hughey, R. P. (2015) Muc1 is protective during kidney ischemia-reperfusion injury. *Am. J. Physiol. Physiol.* **308**, F1452–F1462

215. Kalliokoski, O., Jacobsen, K. R., Darusman, H. S., Henriksen, T., Weimann, A., Poulsen, H. E., Hau, J., and Abelson, K. S. P. (2013) Mice Do Not Habituate to Metabolism Cage Housing–A Three Week Study of Male BALB/c Mice. *PLoS One*. **8**, e58460

216. Kosten, T. R., and Forrest, J. N. (1986) Treatment of severe lithium-induced polyuria with amiloride. *Am. J. Psychiatry*. **143**, 1563–1568

217. Kortenoeven, M. L. A., Li, Y., Shaw, S., Gaeggeler, H.-P., Rossier, B. C., Wetzels, J. F. M., and Deen, P. M. T. (2009) Amiloride blocks lithium entry through the sodium channel thereby attenuating the resultant nephrogenic diabetes insipidus. *Kidney Int.* **76**, 44–53

218. Christensen, B. M., Zuber, A. M., Loffing, J., Stehle, J.-C., Deen, P. M. T., Rossier, B. C., and Hummler, E. (2011) ENaC-Mediated Lithium Absorption Promotes Nephrogenic Diabetes Insipidus. *J. Am. Soc. Nephrol.* **22**, 253–261

219. Sinke, A. P., Kortenoeven, M. L. A., de Groot, T., Baumgarten, R., Devuyst, O., Wetzels, J. F. M., Loffing, J., and Deen, P. M. T. (2014) Hydrochlorothiazide attenuates lithium-induced nephrogenic diabetes insipidus independently of the sodium-chloride cotransporter.

Am. J. Physiol. Physiol. **306**, F525–F533

220. Kim, G.-H., Lee, J. W., Oh, Y. K., Chang, H. R., Joo, K. W., Na, K. Y., Earm, J.-H., Knepper, M. A., and Han, J. S. (2004) Antidiuretic Effect of Hydrochlorothiazide in Lithium-Induced Nephrogenic Diabetes Insipidus Is Associated with Upregulation of Aquaporin-2, Na-Cl Co-transporter, and Epithelial Sodium Channel. *J. Am. Soc. Nephrol.* **15**, 2836–2843

221. de Groot, T., Sinke, A. P., Kortenoeven, M. L. A., Alsady, M., Baumgarten, R., Devuyst, O., Loffing, J., Wetzels, J. F., and Deen, P. M. T. (2016) Acetazolamide Attenuates Lithium-Induced Nephrogenic Diabetes Insipidus. *J. Am. Soc. Nephrol.* **27**, 2082–2091

222. de Groot, T., Doornebal, J., Christensen, B. M., Cockx, S., Sinke, A. P., Baumgarten, R., Bedford, J. J., Walker, R. J., Wetzels, J. F. M., and Deen, P. M. T. (2017) Lithium-induced NDI: acetazolamide reduces polyuria but does not improve urine concentrating ability. *Am. J. Physiol. Physiol.* **313**, F669–F676

223. Burke, C., Fulda, G. J., and Castellano, J. (1995) Lithium-induced nephrogenic diabetes insipidus treated with intravenous ketorolac. *Crit. Care Med.* **23**, 1924–1927

224. Lam, S. S., and Kjellstrand, C. (1997) Emergency treatment of lithium-induced diabetes insipidus with nonsteroidal anti-inflammatory drugs. *Ren Fail*. **19**, 183–8.

225. Messerli, F. H., Bangalore, S., Bavishi, C., and Rimoldi, S. F. (2018) Angiotensin-Converting Enzyme Inhibitors in Hypertension: To Use or Not to Use? *J. Am. Coll. Cardiol.* **71**, 1474–1482

226. Weitzberg, E., Hezel, M., and Lundberg, J. O. (2010) Nitrate-Nitrite-Nitric Oxide Pathway. *Anesthesiology*. **113**, 1460–1475

227. Vallance, P., Leone, A., Calver, A., Collier, J., and Moncada, S. (1992) Accumulation of an

endogenous inhibitor of nitric oxide synthesis in chronic renal failure. *Lancet*. **339**, 572–5

228. Pawlak, K., Domaniewski, T., Mysliwiec, M., and Pawlak, D. (2009) The kynurenines are associated with oxidative stress, inflammation and the prevalence of cardiovascular disease in patients with end-stage renal disease. *Atherosclerosis*. **204**, 309–314

229. Wang, Y., Liu, H., McKenzie, G., Witting, P. K., Stasch, J.-P., Hahn, M., Changsirivathanathamrong, D., Wu, B. J., Ball, H. J., Thomas, S. R., Kapoor, V., Celermajer, D. S., Mellor, A. L., Keaney, J. F., Hunt, N. H., Stocker, R., and Stocker, R. (2010) Kynurenine is an endothelium-derived relaxing factor produced during inflammation. *Nat. Med.* **16**, 279–85

230. Yoshida, E., Suzuki, T., Morita, M., Taguchi, K., Tsuchida, K., Motohashi, H., Doita, M., and Yamamoto, M. (2018) Hyperactivation of Nrf2 leads to hypoplasia of bone in vivo. *Genes to Cells*. 10.1111/gtc.12579

231. Curthoys, N. P., and Moe, O. W. (2014) Proximal tubule function and response to acidosis. *Clin. J. Am. Soc. Nephrol.* **9**, 1627–38

232. Lash, L. H., Putt, D. A., and Cai, H. (2006) Membrane transport function in primary cultures of human proximal tubular cells. *Toxicology*. **228**, 200–218

233. Lash, L. H., Putt, D. A., and Cai, H. (2008) Drug metabolism enzyme expression and activity in primary cultures of human proximal tubular cells. *Toxicology*. **244**, 56–65

234. Park, J., Shrestha, R., Qiu, C., Kondo, A., Huang, S., Werth, M., Li, M., Barasch, J., and Susztak, K. (2017) Comprehensive single cell RNAseq analysis of the kidney reveals novel cell types and unexpected cell plasticity. *bioRxiv*. 10.1101/203125

235. Gordon, C. E., Vantzelfde, S., and Francis, J. M. (2016) Acetazolamide in Lithium-Induced Nephrogenic Diabetes Insipidus. *N. Engl. J. Med.* **375**, 2008–2009

236. Bedford, J. J., Weggery, S., Ellis, G., McDonald, F. J., Joyce, P. R., Leader, J. P., and Walker, R. J. (2008) Lithium-induced nephrogenic diabetes insipidus: renal effects of amiloride. *Clin. J. Am. Soc. Nephrol.* **3**, 1324–31

237. Bedford, J. J., Leader, J. P., Jing, R., Walker, L. J., Klein, J. D., Sands, J. M., and Walker, R. J. (2008) Amiloride restores renal medullary osmolytes in lithium-induced nephrogenic diabetes insipidus. *Am. J. Physiol. Physiol.* **294**, F812–F820

238. Finch, C. K., Kelley, K. W., and Williams, R. B. (2003) Treatment of Lithium-Induced Diabetes Insipidus with Amiloride. *Pharmacotherapy*. **23**, 546–550

239. Kalita-De Croft, P., Bedford, J. J., Leader, J. P., and Walker, R. J. (2018) Amiloride modifies the progression of lithium-induced renal interstitial fibrosis. *Nephrology*. **23**, 20–30

240. Michimata, M., Fujita, S., Araki, T., Mizukami, K., Kazama, I., Muramatsu, Y., Suzuki, M., Kimura, T., Sasaki, S., Imai, Y., and Matsubara, M. (2003) Reverse pharmacological effect of loop diuretics and altered rBSC1 expression in rats with lithium nephropathy. *Kidney Int.* **63**, 165–171

241. Konoshita, T., Kuroda, M., Kawane, T., Koni, I., Miyamori, I., Tofuku, Y., Mabuchi, H., and Takeda, R. (2004) Treatment of congenital nephrogenic diabetes insipidus with hydrochlorothiazide and amiloride in an adult patient. *Horm. Res.* **61**, 63–7

242. Walter, S. J., Skinner, J., Laycock, J. F., and Shirley, D. G. (1982) The antidiuretic effect of chronic hydrochlorothiazide treatment in rats with diabetes insipidus: water and electrolyte balance. *Clin. Sci.* **63**, 525–532

243. Shirley, D. G., Walter, S. J., and Laycock, J. F. (1982) The antidiuretic effect of chronic hydrochlorothiazide treatment in rats with diabetes insipidus: Renal mechanisms. *Clin. Sci.*

63, 533–538

244. Magaldi, A. J. (2000) New insights into the paradoxical effect of thiazides in diabetes insipidus therapy. *Nephrol. Dial. Transplant.* **15**, 1903–1905

245. Riendeau, D., Percival, M. D., Boyce, S., Brideau, C., Charleson, S., Cromlish, W., Ethier, D., Evans, J., Falgueyret, J.-P., Ford-Hutchinson, A. W., Gordon, R., Greig, G., Gresser, M., Guay, J., Kargman, S., Léger, S., Mancini, J. A., O'Neill, G., Ouellet, M., Rodger, I. W., Thérien, M., Wang, Z., Webb, J. K., Wong, E., Xu, L., Young, R. N., Zamboni, R., Prasit, P., and Chan, C.-C. (1997) Biochemical and pharmacological profile of a tetrasubstituted furanone as a highly selective COX-2 inhibitor. *Br. J. Pharmacol.* **121**, 105–117

246. Kim, G.-H., Choi, N. W., Jung, J.-Y., Song, J.-H., Lee, C. H., Kang, C. M., and Knepper, M. A. (2008) Treating lithium-induced nephrogenic diabetes insipidus with a COX-2 inhibitor improves polyuria via upregulation of AQP2 and NKCC2. *Am. J. Physiol. Physiol.* **294**, F702–F709

247. Allen, H. M., Jackson, R. L., Winchester, M. D., Deck, L. V., and Allon, M. (1989) Indomethacin in the Treatment of Lithium-Induced Nephrogenic Diabetes Insipidus. *Arch. Intern. Med.* **149**, 1123

248. Lam, S. S., and Kjellstrand, C. (1997) Emergency treatment of lithium-induced diabetes insipidus with nonsteroidal anti-inflammatory drugs. *Ren Fail*. **19**, 183–8.

249. Li, J., Ichikawa, T., Villacorta, L., Janicki, J. S., Brower, G. L., Yamamoto, M., and Cui, T. (2009) Nrf2 protects against maladaptive cardiac responses to hemodynamic stress. *Arterioscler. Thromb. Vasc. Biol.* **29**, 1843–1850

250. Howden, R. (2013) Nrf2 and cardiovascular defense. *Oxid. Med. Cell. Longev.*

10.1155/2013/104308

251. Qin, Q., Qu, C., Niu, T., Zang, H., Qi, L., Lyu, L., Wang, X., Nagarkatti, M., Nagarkatti, P., Janicki, J. S., Wang, X. L., and Cui, T. (2016) Nrf2-Mediated Cardiac Maladaptive Remodeling and Dysfunction in a Setting of Autophagy Insufficiency. *Hypertension*. **67**, 107–117

252. Luo, Z., Aslam, S., Welch, W. J., and Wilcox, C. S. (2015) Activation of nuclear factor erythroid 2-related factor 2 coordinates dimethylarginine dimethylaminohydrolase/PPAR-γ/endothelial nitric oxide synthase pathways that enhance nitric oxide generation in human glomerular endothelial cells. *Hypertension*. **65**, 896–902

253. Ahmed, S. M. U., Luo, L., Namani, A., Wang, X. J., and Tang, X. (2017) Nrf2 signaling pathway: Pivotal roles in inflammation. *Biochim. Biophys. Acta - Mol. Basis Dis.* **1863**, 585–597

254. Kobayashi, E. H., Suzuki, T., Funayama, R., Nagashima, T., Hayashi, M., Sekine, H., Tanaka, N., Moriguchi, T., Motohashi, H., Nakayama, K., and Yamamoto, M. (2016) Nrf2 suppresses macrophage inflammatory response by blocking proinflammatory cytokine transcription. *Nat. Commun.* 10.1038/ncomms11624

255. Morgan, M. J., and Liu, Z. (2011) Crosstalk of reactive oxygen species and NF-κB signaling. *Cell Res.* **21**, 103–15

256. Tran-Van, D., Avargues, P., Labadie, P., Hervé, Y., Dardare, E., and Fontaine, B. (2005) [Intravenous ketoprofen for severe lithium-induced polyuria]. *Presse Med.* **34**, 1137–40

257. Ungprasert, P., Cheungpasitporn, W., Crowson, C. S., and Matteson, E. L. (2015) Individual non-steroidal anti-inflammatory drugs and risk of acute kidney injury: A systematic review and meta-analysis of observational studies. *Eur. J. Intern. Med.* **26**, 285–291

258. Jia, Z., Wang, H., and Yang, T. (2009) Mice lacking mPGES-1 are resistant to lithium-induced polyuria. *Am. J. Physiol. Physiol.* **297**, F1689–F1696

259. Steinhubl, S. R. (2008) Why Have Antioxidants Failed in Clinical Trials? *Am. J. Cardiol.* **101**, S14–S19

260. Xu, R., Tao, A., Bai, Y., Deng, Y., and Chen, G. (2016) Effectiveness of N-Acetylcysteine for the Prevention of Contrast-Induced Nephropathy: A Systematic Review and Meta-Analysis of Randomized Controlled Trials. *J. Am. Heart Assoc.* **5**, e003968

261. Jain, A. K., and Jaiswal, A. K. (2007) GSK-3beta acts upstream of Fyn kinase in regulation of nuclear export and degradation of NF-E2 related factor 2. *J. Biol. Chem.* **282**, 16502–10

262. Gupta, S., and Khastgir, U. (2017) Drug information update. Lithium and chronic kidney disease: debates and dilemmas. *BJPsych Bull.* **41**, 216–220

263. Aiff, H., Attman, P.-O., Aurell, M., Bendz, H., Schön, S., and Svedlund, J. (2014) End-stage renal disease associated with prophylactic lithium treatment. *Eur. Neuropsychopharmacol.* **24**, 540–544

264. Aiff, H., Attman, P.-O., Aurell, M., Bendz, H., Ramsauer, B., Schön, S., and Svedlund, J. (2015) Effects of 10 to 30 years of lithium treatment on kidney function. *J. Psychopharmacol.* **29**, 608–614

265. Sasaki, S., Chiga, M., Kikuchi, E., Rai, T., and Uchida, S. (2013) Hereditary nephrogenic diabetes insipidus in Japanese patients: analysis of 78 families and report of 22 new mutations in AVPR2 and AQP2. *Clin. Exp. Nephrol.* **17**, 338–344

266. Boone, M., and Deen, P. M. T. (2009) Congenital nephrogenic diabetes insipidus: what can we learn from mouse models? *Exp. Physiol.* **94**, 186–190

267. Harris, R. C., and Breyer, M. D. (2001) Physiological regulation of cyclooxygenase-2 in the

kidney. *Am. J. Physiol. Renal Physiol.* **281**, F1-11

268. Brater, D. C., Harris, C., Redfern, J. S., and Gertz, B. J. (2001) Renal effects of COX-2-selective inhibitors. *Am. J. Nephrol.* **21**, 1–15

269. Harris, R. C. (2006) COX-2 and the kidney. *J. Cardiovasc. Pharmacol.* 10.1097/00005344-200605001-00007